PRODUCTION OF ALUMINUM-MAGNESIUM ALLOYS BY ALUMINOTHERMIC REDUCTION METHOD

A Thesis Submitted to
the Graduate School of Engineering and Sciences of
İzmir Institute of Technology
in Partial Fulfilment of the Requirements for the Degree of

MASTER OF SCIENCE

in Materials Science and Engineering

by
Rouman FIRDOUS

July 2025
İZMİR

We approve the thesis of **Rouman FIRDOUS**

Examining Committee Members:

Asst. Prof. Dr. Mertol GÖKELMA
Materials Science & Engineering, Izmir Institute of Technology.

Asst. Prof. Dr. Kemal DAVUT
Materials Science & Engineering, Izmir Institute of Technology.

Asst. Prof. Dr. Murat ALKAN
Metallurgy & Materials Engineering, Dokuz Eylül Üniversitesi.

16 July 2025

Assoc. Prof. Dr. Mertol GÖKELMA
Supervisor, Materials Science & Engineering
Izmir Institute of Technology

Prof. Dr. Yaşar AKDOĞAN
Head of the Materials Science & Engineering Department

Prof. Dr. Mehtap EANES
Dean of the Graduate School of Engineering and Sciences

ACKNOWLEDGMENTS

"اَلْحَمْدُ لِلّٰهِ الَّذِيْ لَهُ مَا فِي السَّمٰوٰتِ وَمَا فِي الْأَرْضِ وَلَهُ الْحَمْدُ فِي الْآخِرَةِ وَهُوَ الْحَكِيْمُ الْخَبِيْرُ"

The following thesis is the result of a two-year master's program at The Izmir Institute of Technology, Izmir, Turkiye, Department of Materials Science and Engineering, written during the spring of 2025.

I express my heartfelt and sincere gratitude to my supervisor, Assoc. Prof. Dr. Mertol Gökelma for his single-handedly precious guidance, constructive suggestions, and encouragement from the start to the last moment of this journey. His unwavering efforts are unimaginable, providing international students like me with an outstanding opportunity to feel and learn at the highest quality. In addition, I thank Prof. Dr. Gabriella Tranell from Norwegian University of Science and Technology (NTNU), Trondheim, Norway where this project commenced, for the insights, guidance, suggestions are highly appreciated since the beginning of this project. And thankful to all professors who taught valuable lessons during these years and IYTE-MAM people for their work with SEM-EDS and XRD analysis and other analysis performed in NTNU.

I would like to thank my parents for their enormous sacrifices in making sure I get the best education to help my community and the world. Their contributions and support toward my education are unwavering from the beginning of my educational journey till now. I would also like to thank my family, especially my mother (Yasmeen Abdullah), Father (Firdous Ahmad), brother, cousins, uncles and aunts for their support and prayers during my studies abroad. Knowing that they are by my side and their calls and messages always gives me heart warmth and strength to foster a better future.

ABSTRACT

PRODUCTION OF ALUMINUM-MAGNESIUM ALLOYS BY ALUMINOTHERMIC REDUCTION METHOD

This study examines an alternative heating and melting process used to produce aluminum-magnesium (Al-Mg) alloys by the 'aluminothermic' reduction method at a temperature higher than the melting point of aluminum, followed by a thorough thermodynamic analysis to identify important features, microstructure changes, and various phase formations. Basic thermodynamic data required for the analysis have been taken from the literature from various experiments and calculated using Thermocalc and FACTSAGE. At normal atmospheric pressure, alloys with varying Mg contents (8–15 wt%) were produced, guaranteeing compositional homogeneity by slow cooling. A key part of this study is to directly produce Al-Mg alloys and discuss the phase formations during solidification.

Comparing the primary Mg production method, the 'Pidgeon process' with an alternative aluminothermic method offers an easy and economical way with zero carbon emissions. Objectives include activity measurements in liquid Pure aluminum and Al-Si alloy, microstructural evolution, comparing various phase formations, and study of the dissolution of Mg in liquid aluminum. Also, to investigate the effects of temperature, holding times, furnace, ratio of raw materials, and furnace atmosphere on the production of Al-Mg alloy, particularly with Mg dissolution, activity, and MgO reduction. It was found that higher temperatures and inert atmospheres lead to higher Mg dissolutions, and the presence of silicon significantly improves the reduction of MgO. FIMC form due to sufficient iron content in Al-Mg alloys with Si as a synthesizer.

ÖZET

ALÜMİNOMAGNEZYUM ALAŞIMLARININ ALÜMİNOTERMİK İNDİRGEME YÖNTEMİYLE ÜRETİMİ

Bu çalışma, alüminyumun erime noktasının üzerindeki sıcaklıklarda uygulanan alternatif bir ısıtma ve eritme süreci ile alüminyum-magnezyum (Al-Mg) alaşımlarının "alüminotermik" indirgeme yöntemiyle üretimini incelemekte; ardından önemli özelliklerin, mikroyapısal değişimlerin ve çeşitli faz oluşumlarının belirlenmesi amacıyla kapsamlı bir termodinamik analiz gerçekleştirmektedir. Analiz için gerekli temel termodinamik veriler, çeşitli deneysel çalışmalardan elde edilen literatür kaynaklarından alınmış ve Thermo-Calc ile FACTSAGE programları kullanılarak hesaplanmıştır. Normal atmosfer basıncında, (8–15 wt%) aralığında değişen Mg içeriklerine sahip alaşımlar üretilmiş ve yavaş soğutma yöntemiyle bileşimsel homojenlik sağlanmıştır. Bu çalışmanın temel amacı, doğrudan Al-Mg alaşımlarının üretilmesi ve katılaşma sırasında oluşan fazların tartışılmasıdır.

Birincil magnezyum üretim yöntemi olan "Pidgeon prosesi" ile alternatif alüminotermik yöntem karşılaştırıldığında, karbon salınımı olmayan, kolay ve ekonomik bir yöntem sunduğu görülmektedir. Bu çalışmanın hedefleri arasında, sıvı saf alüminyum ve Al-Si alaşımında magnezyum aktivitesi ölçümleri, mikroyapı evriminin izlenmesi, farklı faz oluşumlarının karşılaştırılması ve sıvı alüminyumda Mg çözünürlüğünün incelenmesi yer almaktadır. Ayrıca, Al-Mg alaşımı üretiminde sıcaklık, fırında bekletme süresi, hammadde oranları ve fırın atmosferinin etkileri; özellikle Mg çözünürlüğü, aktivitesi ve MgO indirgenmesi açısından araştırılmıştır. Yapılan çalışmalar sonucunda, daha yüksek sıcaklıkların ve inert atmosfer koşullarının Mg çözünürlüğünü artırdığı, ayrıca silisyum varlığının MgO'nun indirgenmesini önemli ölçüde iyileştirdiği belirlenmiştir. Al-Mg alaşımlarında yeterli demir içeriğinin bulunması ve silisyumun sentezleyici olarak rol oynamasıyla FIMC (demir içeren ara metalik bileşik) fazının oluştuğu gözlemlenmiştir.

TABLE OF CONTENTS

LIST OF FIGURES

Figure **Page**

LIST OF TABLES

Table **Page**

CHAPTER 1

INTRODUCTION

The increasing need for lightweight and high-strength materials across various industries and application fields, especially in the automotive and aerospace sectors, has spurred interest in aluminium-magnesium (Al-Mg) alloys due to their good strength-to-weight ratio and low density of about 1.7 g/cm3.[1–3] Magnesium has a very high solubility in aluminium, which enables alloy hardening and increased strength when concentrations are added above 5%. The strength of Al-Mg alloys increases as the Mg content rises, particularly when the Mg content increases from 1% to 6%.[1,4,5] These alloys' unique combination of low density, high mechanical properties, and robust corrosion resistance makes them ideal for applications where weight reduction is crucial. Aluminium and magnesium are conventionally alloyed indirectly, utilizing a variety of steps and stages to form Al-Mg alloys.[1,4,6,7] Paul Héroult in France and Charles Martin Hall in the United States developed the Hall-Héroult method in 1886 to produce aluminium for commercial use. However, it was energy-intensive and resulted in emissions of fluoride and carbon. The Pidgeon process, which was developed in the 1940s by Canadian chemist Lloyd Montgomery Pidgeon, involved heating calcined dolomite with a reducing agent such as ferrosilicon at high temperatures in a closed vacuum machine to extract Mg from ores.[2,8,9] These procedures are still intensive, energy-consuming processes. A resource that is underused but might be used to make these precious alloys more sustainable is the waste that accumulates during the smelting and refining of magnesium and aluminium.

High-purity magnesium metal requires the element to be isolated from its naturally occurring compounds and minerals. A) The molten salt electrolysis method, which separates magnesium and chloride by direct electrolysis of molten magnesium chloride, is one of several methods for producing magnesium. Magnesium is collected at the bottom as a solid. B) The thermal reduction technique, which produces a combination of magnesium oxide (MgO) and calcium oxide (CaO) initially, involves heating dolomite to temperatures exceeding 1200^{o}C to convert MgO into Mg metal.[2,10,11] One promising alternative approach to reclaim magnesium and produce Al-Mg alloys is through the

aluminothermic reduction of MgO. Aluminothermic reduction involves the use of aluminum as a reducing agent to convert metal oxides into their metallic form as shows in Eq. 1.1.[3,8,12]

$$3MgO(s) + 2Al(s) \rightarrow 3Mg(g) + Al_2O_3(s) \quad (1.1)$$
$$\Delta G = 272.5 \text{ kJ/mol } (1000\ ^{O}C).$$

Reaction steps:

$$\text{Oxidation:} \quad 4Al(s) + 3O2\ (g) \rightarrow 2Al_2O_3\ (s) \quad (1.2)$$
$$\Delta G = -2735.513 \text{ kJ/mol } (1000\ ^{O}C)$$
$$\text{Reduction:} \quad 2MgO(s) \rightarrow 2Mg(l) + O_2\ (g) \quad (1.3)$$
$$\Delta G = 927.2 \text{ kJ/mol } (1000\ ^{O}C)$$

An alloy is a mixture of two or more metals, metal, and metalloid mixtures, which forms a completely different material with different properties and characteristics when combined with other techniques. An alloy can be formed between metal-metal, metal-metalloid etc. Their phase, when mixed, can be solid or liquid. However, the solid materials participating in alloy formation need to be melted into liquid phases to dissolve into each other.[7] The crystal structure of the alloy formed can be the same as the primary element or can form another structure depending on the specification and process of alloy formation, e.g., if the primary elements have CCP structure, the alloy formed from them can have CCP, HCP, or another structure.[1,13] The alloy formed typically has better properties than primary elements. Because Mg has a larger atomic radius (13%) than Al, it causes significant distortion of its crystalline dot matrix after dissolving in α(Al) solid solution, which is one of the reasons Mg is recognized as a primary element for solid solution strengthening forming Al-Mg alloys which have superior characteristics such as anti-corrosion, strength, weldability, lightweight etc.[4,13] While forging and rolling work is done on aluminium, more vacancies and dislocations appear in the crystal structure, which prevents atoms from moving about. Some vacancies are replaced by magnesium atoms, improving mechanical properties.[2–4,10] There are various magnesium alloys manufactured using different processes such as AZ91, AM60, AZ31 and 5xxx series of (aluminum-magnesium) alloys.[7]

In this experimental study, aluminium helps to reduce magnesium oxide (MgO) at high temperatures, resulting in magnesium that easily alloys with the aluminium in the reaction mixture (eq. 1.1).[2,6] The recovery of magnesium metal from oxide and the concurrent creation of an Al-Mg alloy with nearly zero carbon emissions are two advantages of this process. The process begins with the collection and preparation of MgO, waste aluminium, whether it is powder, slabs, chunks, etc. of high purity. This mixture is subjected to high temperatures, typically in a controlled environment and with/without gaseous atmosphere in furnace, to facilitate the reduction reaction. The thermodynamic and kinetic aspects of the reduction process are critical to achieving a high yield of magnesium and its effectiveness in alloying with aluminium. Parameters such as temperature, reaction time, and the ratio of reactants are optimized to maximize the efficiency of the process and the quality of the resultant alloy.[6,8,14,15] To investigate the feasibility of producing Al-Mg alloys from aluminium/MgO via aluminothermic reduction, by examining the reaction mechanisms, optimizing process conditions, and evaluating the properties of the produced alloy, this study seeks to provide a sustainable and economically viable method and conditions under which Al-Mg alloy is to be produced.[2,6,8,11,14] The successful implementation of this process could lead to significant environmental and economic benefits, contributing to the circular economy in the metallurgical industry.

The thermodynamic properties were calculated using FACTSAGE (in NTNU) software which indicates the reaction is nonspontaneous under standard conditions and suggests that this reaction requires external energy to drive it forward which will be explained in later sections. With varying the concentrations of MgO in aluminum we expect the formation different phases of alloy with spinel structure in between the temperature range of 900ºC to 1900ºC.[12] The Al and MgO react at 700ºC to form alloy with varying phases + magnesium aluminate, $MgAl_2O_4$ (spinals) during heating above 450ºC and cooling processes. As temperature increases, Mg dissolves further in spinel phase. Addition of aluminum improves the reduction rate of MgO.[13–15]

1.1. Aim of Work

This thesis aims to study an aluminothermic reduction of magnesium oxide to produce aluminum-magnesium alloy and verify the formation of different phases, intermetallics, and chemical structures. The main expectation is to find out various phase transformations and intermetallic phases formed at high temperatures and during cooling in different experiments under varying parameters and the effect of alloying elements solubility and activity of Mg. This is a versatile method to produce the Al-Mg alloy at high temperatures in a lab environment. The reaction of raw materials will be studied and analysed to see if the Al-Mg has been formed, if the aluminothermic reduction of MgO has occurred or not, and under which conditions, atmosphere, and alloying elements new phases have formed. Also, we expect to see the effect of parameters and some trace impurities on intermetallic formation with changing parameters. The amount of added Magnesium and forging temperatures will be varied, to examine how this affects the resulting alloy. How temperature and holding time effect the solubility, diffusion, and activity of Mg in Aluminum matrix. The processes occurring on the interface of MgO-Al will be observed and studied their phenomena. Different characterization techniques will be used, which include SEM, EDS, EPMA, and XRD to analyse the numbers and quantify the results using ImageJ software.

CHAPTER 2

THEORY AND LITERATURE

2.1. Magnesium and Its Usage Areas

Magnesium is a silvery-white, lightweight metal with extensive application in various sectors, such as electronics, construction, automotive, and aerospace, Table 1.1. Natural sources such as seawater, dolomite and magnesite are primary ways to obtain Magnesium in natural form.[16–21] Currently regarded as crucial material of the twenty-first century is 'magnesium (Mg)', modern technology, and sustainable development. Magnesium alloys have exceptional physical and chemical characteristics, including reduced density, elevated specific strength and stiffness, superior damping capabilities, favourable biocompatibility, substantial hydrogen storage capacity, and elevated theoretical specific capacity for batteries.[1,4,13,15,17] Primary Sources of Magnesium include A) seawater: Seawater is one of the biggest sources of magnesium with a magnesium content of around 0.13% by weight. Electrolysis is the method used to extract magnesium from it. B) Brine Deposits: magnesium salts are abundant in naturally occurring brine deposits, such as those found underground or in salt lakes. C) Magnesite and Dolomite Ores: Dolomite and magnesium are extracted from sedimentary rocks to make magnesium oxide (MgO) and magnesium metal.[4,22,23] These ores are frequently found in countries like Australia, Russia, China, and Türkiye. It can also be found in several common silicates, such as talc, olivine, and most forms of asbestos, as well as natural minerals like carbonates. Moreover, it can be found as a sulphate (kieserite), hydroxide (brucite), and chloride (carnallite, KMgCl36H2O).[8,13,16,17] It can be found in other minerals including meerschaum, chrysolite, and serpentine. Seawater gets its distinct bitter taste primarily from the dissolved chloride that makes up approximately 0.13 % of the magnesium content. It is the third most common structural metal, after iron and aluminium, and the 8th most abundant element in the crust of the Earth (approximately 2.1 %).[1,3,17,24] On a scale where the abundance of silicon equals 106 atoms, its cosmic abundance is calculated to be 9.1 x10^5 atoms.

Table 1.1. Application of the alloy in different fields.[16]

Industry	Application
Automotive industry	Engines, car body, brake housings and drive shafts
Aerospace	Bodies, rockets, satellites, astronaut suits, air tanks
Medical fields	Implants, prosthetics, exoskeleton
Sports	Skies, snowboards, skates, tennis rackets

As shown in Table 1.2 below, Mg has higher strength than vastly used aluminium and consumes low energy for production, but it yields very low density when used in pure form. The processing energy and production emission of Mg are lesser than that of Aluminum. Magnesium production has greatly increased across different countries of world since 1900s.

Table 1.2. Strength, processing energy, emissions, and density for Al-Mg.[12]

Property	Al	Mg
Emissions ($kg(co_2)\cdot kg^{-1}$)	22	6.9
Processing energy ($kw\cdot h\cdot kg^{-1}$)	56	43
Strength-to-weight ratio ($kn\cdot m\cdot kg^{-1}$)	130	158
Density ($kg\cdot m^{-3}$)	2700	1738

The analysis of Table 1.3 leads to the conclusion that any attempt to lower the price of Mg must concentrate on two distinct areas: (i) developing a process that is less expensive than the one that is currently in use and/or (ii) creating or refining low-cost methods for the fabrication of final components.

Table 1.3. Production cost US$ per pound of magnesium, a comparison with the production cost of steel, aluminum, titanium.[16]

	Steel	Aluminum	Magnesium	Titanium
Ore	0.02	0.10	0.01	0.30
Metal	0.10	0.68	0.54	2.00
Ingot	0.15	0.70	0.60	4.50
Sheet	0.30-0.60	1.00-5.00	4.00-9.00	8.00-50.00

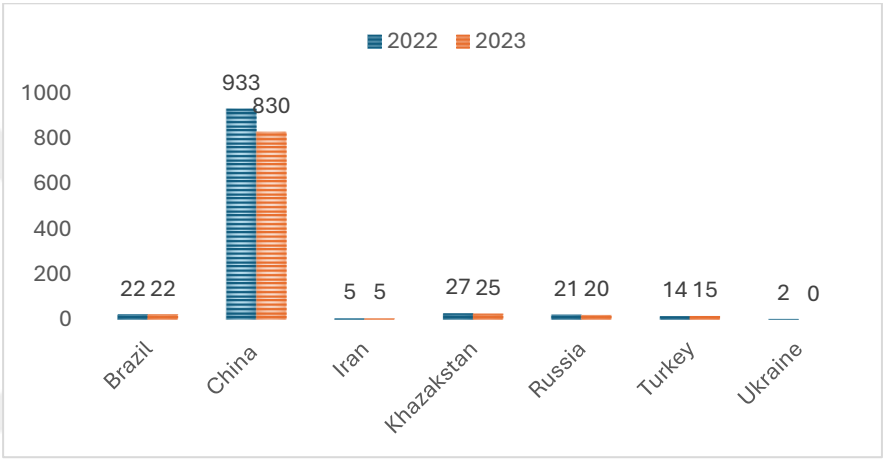

Figure 2.1. World Mg production in 2022-2023 in thousand metric tons.[25]

The commercial production of magnesium involves the electrolysis of molten magnesium chloride ($MgCl_2$), primarily obtained from seawater. Fig 2.1 and 2.2 bar graphs, shows the production of Mg comparison between different countries. In 2022, China produced 933 thousand tons of magnesium. Refractory materials accounted for over 69% of China's magnesium production. In 2021, China's net magnesium exports totaled 1.8 megatons.[26] During the research period, China's recycled magnesium content varied from 5% to 14%. China ought to expand their magnesium production network to include additional luxury goods.

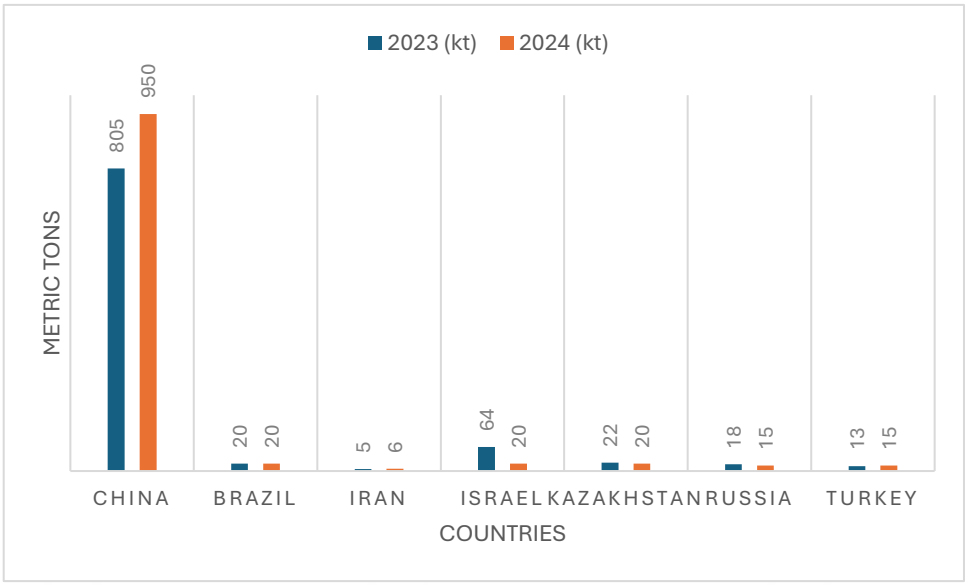

Figure 2.2. Various countries' Mg production in kilotons for year 2023 and 2024.[18]

In 2023 China being leading Mg producing country estimated 830,000 metric tons of metal production. In 2024 China produced 950,000 metric tons of magnesium ~ 90% of total world production.[25,27]

For decades, metals forming alloys with magnesium used in different applications have shown outstanding properties and results owing to the ideal properties of magnesium. Various benefits depend on the type of application the alloy is used in:

1. Lightweight: elements forming alloys with magnesium are found to be 76 % lighter than steel, suited for applications where weight is a constraint, such as in airplanes. Lightweight alloy will considerably reduce the weight of the whole object and increase its performance.[1,3,4]

2. Strength-to-weight ratio: Magnesium alloys are lightweight materials with excellent strength-to-weight ratios. Because of this, they can be used in situations where high strength and low weight are essential.[1,2]

3. Damping capacity: Magnesium has a high damping capacity, which enables it to absorb vibrations efficiently. Because of this, magnesium alloys are beneficial in applications like electronic housings and automotive components, which are crucial to reducing vibration and noise.[2–4,24]

4. Corrosion Resistance: Because of their excellent corrosion resistance when treated properly, certain magnesium alloys can last longer in outdoor and marine applications.[5]
5 Recycling: When compared to certain other materials, magnesium alloys are recyclable environmentally friendly and low carbon emissions.[1,12]
6. Heat Dissipation: Ideal for heat sink as Mg alloys show excellent heat conduction and dissipation.[13,16]

Magnesium has continuously been used in multiple industrial areas, including aerospace, in making components and parts of aircraft, satellites, automotive engine blocks, transmission, wheels, etc, to reduce weight and increase fuel efficiency.[1,5,26,28] In consumer electronics, Mg is used to make lightweight casing, blocks, and shields of laptops and mobile phones. Computers, and home appliances, etc. The Mg alloy products have been on rise since 1990s. AZ being the dominant variant of the alloy such as AZ31, AZ61, and AZ80 series have been used as an alternative to polymer materials such as polycarbonate due to benefits provided by Mg alloys stated above. Mg alloys finds its benefits in heat dissipation, RF shielding of electronic components, strong body feel, light weight and durable have made the items better in many ways such as portability. In automotive sector, Global trends are forcing the auto industry to create more compact, cleaner, eco-friendly, and cost-effective automobiles.[21] Due to consumer and governmental demands for cleaner, healthier automobiles, the top automakers focus on cutting exhaust emissions and car weight. Car mass has become a crucial factor in assessing design efficiency, as carbon dioxide emissions are directly correlated with fuel consumption.[18,19] Research is moving toward these aspects by improving power trains and aerodynamic designs, using alternative fuels, and developing weight reduction techniques. Using different materials is the simplest and most economical way to reduce a vehicle's weight. The majority of castings are composed of steel and cast iron, although researchers are looking into other materials like magnesium and aluminum due to engine weight concerns. The use of aluminum has grown by more than 80% in the last ten years. Aluminum alloys have been utilized for many years in automotive components, including the vehicle's body, cylinder heads, pistons, etc.[29] However, magnesium has a 1/4th density of zinc, 3/4th of aluminum, and 1/5th of steel, making it a strong choice for weight reduction.[30] Because magnesium has a density that is 35.6% lighter than aluminum and 78.5% smaller than steel, it is now one of the most popular weight-saving materials.[2,10,15] Mg has been used in various components in vehicles; Magnesium AZ31 alloy is used by

Hyundai and Kia Motors Corporation (HKMC) for several interior parts, including the driver airbag housing, steering wheelbase, control column housing, lock assembly, and seat frame. Body weight is around 29% and can be as much as decreased. Numerous chances exist for researchers to conduct surveys and studies about using magnesium material in seat frames, exteriors, and interiors. The chassis' components are unique and display a variety of behaviors, with wheels being the first structures to be replaced by magnesium. Numerous well-known companies, like Land Rover and Range Rover, employ magnesium alloys.[20,29] Magnesium alloys are used to construct the front-end carrier range rover Velar, while the Land Rover has a magnesium cross beam to support the instrument panel. Compared to previous versions, the Jaguar-F style's pressure die-cast magnesium alloy reduces weight.

In construction, compounds such as MgO, Magnesium hydroxide, are being used as shields from fire hazards, mixed in cement and concretes for strength. In energy storage products, the heavy limitation of lithium-ion batteries of dendrite formation causes energy storage failures and hazards; magnesium batteries are a trending field to improve density and capacity in a smaller volume. Magnesium alloys are used as biodegradable implants and prosthetics in medical fields due to high corrosion resistance and low weight. [29,30] Because they are a successful way to replace hard tissue and restore human bony abnormalities, bone repair materials are changing course and becoming a hot topic in the biomedical materials industry.[4,10,31] Over the past several decades, several biomaterials have been established to replace bone tissue. Because of their combination of mechanical, metallurgical, and load-bearing properties, metallic materials are considered appropriate biomaterials in contrast to ceramic or polymeric materials. Implant materials like plates, screws, and pins are applied in vivo and are removed by second surgery once the tissue has healed. This leaves the patient unwell and incurs further surgical expenses. It is evident from earlier research that metallic materials degrade with time, leading to either bone tissue loss or a lack of biocompatibility. Stress creation and implant instability may arise from the mismatched characteristics of natural bone and implant materials. Due to their in-situ presence in the body and capacity to favorably promote the formation of new bones, magnesium (Mg) alloys can be utilized in bone reworks since they are favorable osteo-conductive metallic materials that are also biodegradable and compatible.[31] Because of their biodegradability in the environment,

magnesium alloys have recently attracted the attention of as many biodegradable materials as possible for bone implants.[4,10,13]

2.2. Magnesium Production Methods

Magnesium being the 8th most abundant metal in earth by mass, it is readily available in natural oxide or carbonate forms in rocks and sea water as well as biological systems, dead sea in Jordan has highest concentration of dissolved magnesium (Mg^{2+}).[16,17] Magnesium is extracted and refined using various techniques, each with unique benefits and difficulties. Traditional methods can be categorized into 3 groups: Electrolytic by electrolysis of Magnesium chloride, Thermal reduction of dolomite or Magnesia and metallothermic reduction methods.[8,11]

2.2.1. Pidgeon Process

Used as primary and most common production method of Mg metal, a thermal reduction process of magnesium smelting includes four major steps: 1) Calcination, 2) Pelleting, 3) Vacuum thermal reduction, and 4) Refining. Canadian metallurgist Dr. Lloyd Montgomery Pidgeon created the Pidgeon process in the 1940s.[8] The fact it offered a more economical and efficient way than previous techniques like the electrolytic process and magnatherm process, it was a significant improvement in the extraction of magnesium. During World War II, when magnesium was in great demand for military uses (such as lightweight airplane alloys), the technique gained widespread adoption. The Pidgeon process has several advantages over the electrolytic magnesium smelting method, including a straightforward and well-established process flow, low construction costs, a short construction time, multiple heat sources, high-quality magnesium, low power consumption, and efficient use of coal, natural gas, heavy oil, gas, and other resources.[3,8,32] The Pidgeon process serves as the major basis for the magnesium smelting sector in China, which is the world's largest producer of primary magnesium. The Pidgeon method of magnesium smelting involves feeding dolomite, the raw material, into

a reduction tank that is heated externally by a reduction furnace. The calcined dolomite is then thermally reduced to metallic magnesium in a vacuum using 75% ferrosilicon as a reducing agent.

Furthermore, China possesses the most fabulous dolomite reserves in the world, which have been mined for over a millennium.[17,27] This produces favourable resource circumstances for the Pidgeon process's long-term growth. The Pidgeon method does, however, have many drawbacks, including the use of a tiny reduction tank, poor filling capacity of a single tank, low thermal efficiency, intermittent production, high labor effort, high energy consumption, and significant environmental contamination.[33,34] Calcination of dolomite ($CaCO_3$ + Mg CO_3) takes place in a rotatory kiln at around 1200°C. Then, the dolomite is crushed into small particles 10-40 mm in size. The dolomite undergoes decomposition at high temperatures and is converted into MgO and CaO. Pidgeon Process is categorized into thermal reduction methods of Mg extraction. Using ferrosilicon as reducing agent, MgO, extracted from dolomite or magnesite, is reduced to separate Magnesium and Oxygen. By heating it to high temperatures, dolomite ($CaMg(CO_3)_2$) or magnesite ($MgCO_3$) is calcined to yield calcium oxide (CaO) and magnesium oxide (MgO). As a reducing agent, silicon (Si) is combined with the resultant MgO.[2,11,24] A high-temperature vacuum furnace, between 1200°C and 1400°C temperature, is used to hold and calcine the mixture. In these circumstances, silicon and magnesium oxide react to form silica (SiO_2) and magnesium vapor. In a colder section of the furnace, the magnesium vapor is collected and condenses into solid magnesium metal. After purification, the magnesium metal is cast into shapes that may be used. This process consumes heavy energy due to two or three steps of process and reactions are involved. Silicon dioxide is generated as by product which must be further managed properly.[2,8,24] The reactions occur as;

$$MgCO_3 \rightarrow MgO + CO2\ (g) \quad (2.1)$$

$$2MgO + Si \rightarrow 2Mg(g) + SiO_2 \quad (2.2)$$

$$\Delta G = 282\ kJ/mol\ ,\ T = 900^oC$$

The fundamental method and primary technological procedure for producing magnesium and magnesium alloys using the Pidgeon process are the same domestically and internationally. The degree of mechanization and automation, variances in fuel and

energy usage, and differences in the equipment used in each segment are the primary factors that contribute to differences in technical developments and clean production levels across businesses.

2.3. Processes Occurring in Pidgeon Method

In pidgeon process, 4 main processes take place during extraction of Mg metal as stated earlier, 1) Calcination, 2) pelleting, 3) vacuum thermal reduction, and 4) refining.

Calcined dolomite is created by heating dolomite to 1100–1200 °C in a shaft kiln or rotary furnace. Here is the precise procedure: following crushing and screening, dolomite with a particle size range of 10–40 mm is transported by a sizable inclination belt conveyor to the top silo of a vertical preheater. The preheater's preheating box receives the ingredients from the silo via a feeding pipe. The kiln's tail hot gas, which is around 1000–1100°C, preheats the dolomite to roughly 900 °C as the materials progressively descend into the preheating box. A burner mounted within the rotating kiln supplies the kiln with a high-temperature heat source. The materials are cooled in a fanned vessel to 700°C using a cooling air. The air is provided by surrounding fan. This cooling air provided by secondary fan helps to reduce the high temperature of the dolomite below 100°C. and in order to employ the cooling air as supplementary combustion air for the combustion system, it is heated to a temperature of more than 700°C. A vibrating unloader at the bottom of the vertical cooler releases the cooled calcined dolomite, which is then moved to a storage warehouse using a bucket elevator and plate conveyor.

$$CaCO_3 \cdot MgCO_3 \rightarrow MgO + CaO + 2CO_2\,(g) \qquad (2.3)$$

Guo, J et al. [35], studied the effect of calcination temperature and time in pidgeon process using X-ray diffraction. They found higher is the calcination temperature, faster is the material mass loss and vice-versa. Hence it can be recommended to maintain moderate temperature during calcination of raw materials.

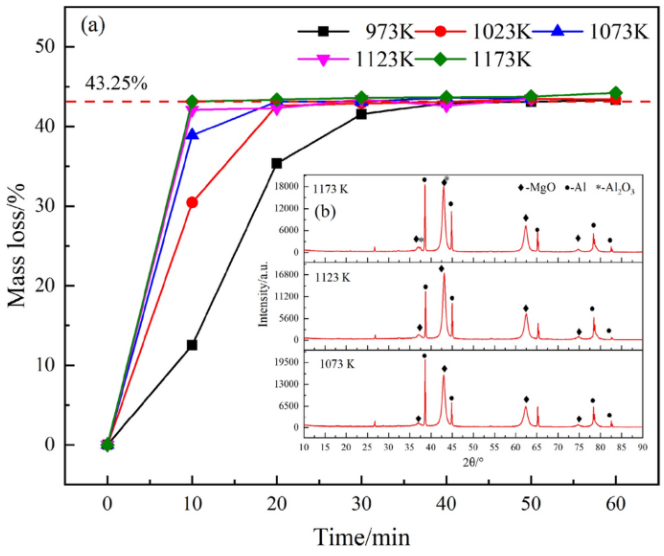

Figure 2.3. a) Effect of calcination temperature and time on mass loss; b) XRD patterns of calcined products at different temperatures.[35]

By the specifications of the pelleting process calcined dolomite, ferrosilicon powder, and fluorite powder, as catalysts are mixed in the right proportion for further reduction process in the ratio of 100:7.8:0.06, respectively, are weighed, batched, ground, and compressed at a pressure of 9.8 to 29.4 Mpa. The pellet preparation aims to get the raw materials ready for the reduction process. The stock's bottom unloading gear transports the calcined dolomite to pre-crushing machinery. Examples of unloading devices are a vibrating feeder belt conveyor and a rod valve. Next, the silo receives the crushed calcined dolomite. Fluorite is utilized straight in the batching process, and the crushed ferrosilicon powder is also supplied to the silo.[2,8,33,34] After being combined in the batching machine in the proper amounts, the three components are fed into a ball mill for grinding via a belt conveyor before being compressed into pellets.

The process of reduction occurs sporadically. The reduction tanks used by various magnesium manufacturers have varying requirements. As a result, the reduction cycle, magnesium production, and feeding material quantity vary. The typical cycle lasts eight to twelve hours. Large tanks with a 24-hour reduction cycle are also available. The pellets are initially positioned in the reduction tank, which is the location for the reduction reaction, at the start of a reduction cycle. After installing a magnesium crystallizer and an alkali metal trap, a heat shield is utilized to prevent the pellets' heat radiation.[2,6,8]

Finally, the system is emptied, and the end cover is fastened. These pellets are heated to 1200°C in a reduction tank, which is under a vacuum level of 13.3 Pa or higher, as shown in Fig. 2.3.[2,11] For about 8 to 10 hours, MgO is reduced at this temperature, is vaporized, and gets cooled and stuck to the walls of the cooling chamber on top of the reduction tank, under the effect of external cool water. Up to 1200°C heating, the mixture pellets melt. With the catalysis of fluorite, silicon atoms reduce the MgO through bonding with oxygen, readily forming silicon dioxide, due to the reason MgO has more negative free energy at higher temperatures than silicon dioxide. Sublimation of Mg occurs at such high temperatures, the vapours are cooled down in the top tank and collected as crude magnesium. After 12 hours, Mg is fully reduced and ready to be taken out of the tank for cooling.[11,32] Higher the reduction temperature, better quality of Mg is obtained but this consumes higher energy and exhumes more carbon gasses than other processes. The main chemical reaction in reduction process is:

$$2MgO + 2CaO + 2Si(Fe) \rightarrow 2CaO.\ SiO2 + 2Mg\ (g) \qquad (2.4)$$

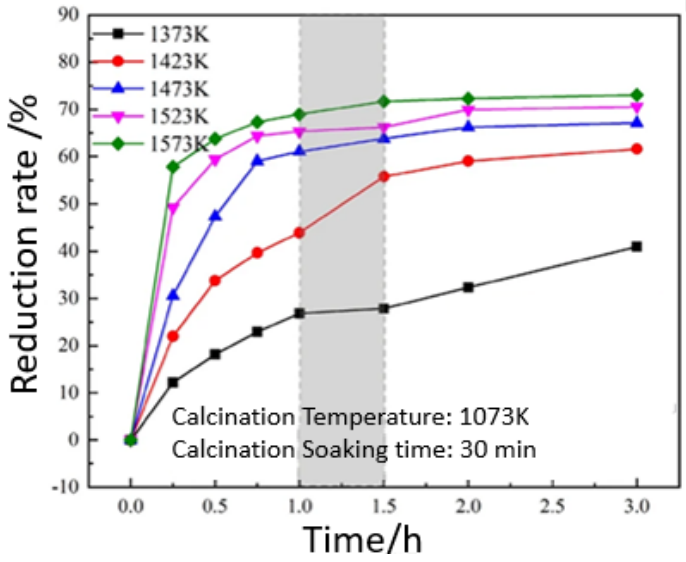

Figure 2.4. Effect of reduction temperature and time on reduction percentage of MgO in $MgCO_3$–Al pellets.[35]

As seen in Fig. 2.4, Guo, J. et al. [35] experimented that with higher reduction temperature results in faster reduction of MgO pellets. The reduction percentage of MgO first rose quickly at 1573 K. The MgO reduction percentage was 57.87% at 15 minutes and 72.28% at 2 hours when the period was extended. There was no noticeable loss of the evaporated phase in the reduction process other than magnesium vapor, as evidenced by the experiment's recorded reduction percentage of magnesium oxide not exceeding the theoretical maximum reduction percentage of 75%. When the temperature dropped, the MgO reduction percentages were 12.23%, 21.97%, 30.58%, and 49.26% at 1373 K to 1523 K and 15 minutes, respectively. After three hours of operation, the MgO reduction percentages were 40.96%, 61.62%, 67.16%, and 70.57%, respectively. The findings demonstrated that the MgO reduction yield slowed when the temperature dropped. Furthermore, Fig. 2.4 showed that the change in the reduction rate of magnesium oxide at 1373 K differed from temperature changes at other temperatures.[35] The MgO reduction yield rose when the reduction duration was extended within 1 hour and after 1.5 hours, although it varied extremely slowly between 1 and 1.5 hours.

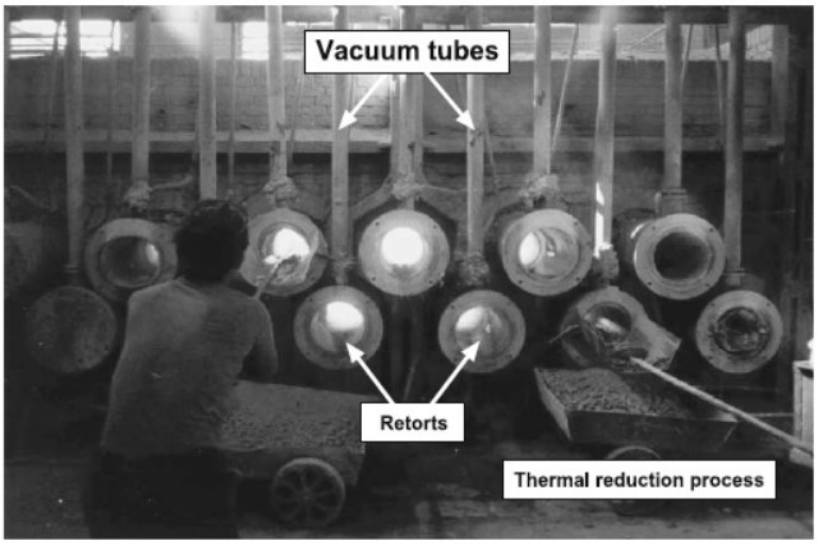

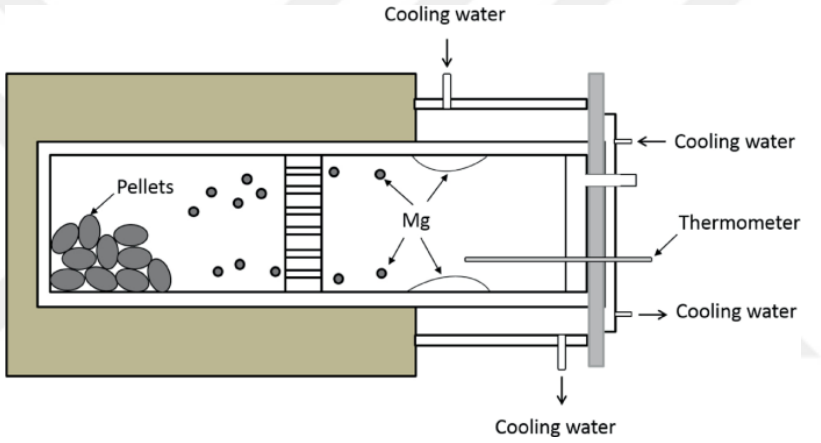

Figure 2.5. Factory image and schematic diagram of Pidgeon process, reduction tank.[2]

The reduction is preferred at a vacuum lower than 10 Pa to produce dense crystalline magnesium. At around 1473 K, the temperature in the reduction reaction area is kept steady because at this temperature, silicon in ferrosilicon reduces the MgO and calcium oxide (CaO) in the pellets to metallic magnesium. Some part of Mg escapes in the form of vapours from the tank to crystallizer, where it solidifies. Tank is brought back to atmospheric pressure and opened to collect the mg metal slag (crude Mg) and is cleaned and sent for further refining.[2,15] Then further heat is applied to melt crude magnesium illustrated in Fig. 2.5. The refined magnesium is then cast into ingot after being refined via flux at a high temperature of around 710°C forming magnesium ingots.

Table 2.1. Comparison of different methods.[6,10,12,32]

Method	Raw materials	Energy consumption	Purity of Mg	Environmental impact
Pidgeon process	Dolomite, Ferrosilicon	High	Moderate	High CO_2 emissions
Electrolytic process	Magnesium Chloride	High	High	Moderate
Magnetherm process	Dolomite, Aluminum	Very High	High	Moderate
Carbothermic reduction	Magnesium Oxide, Carbon	Moderate (potential)	High	Low (if developed)

Such as mixing aluminum with different metals, which include copper, zinc, silicon, manganese, zirconium, and rare earths, among others, magnesium alloys are favoured due to their exceptional structural and mechanical properties, making them suitable for various fields of applications. Every 1% rise in Mg content added to aluminum causes an approximate 35MPa increase in the tensile strength of the alloy.[3,8,10,15] Hence, the Mg content must be contained within 6 wt% in the alloy. Table 2.1 gives comparison data of various Mg production methods.

2.4. Alternative Industrial Production Methods

Carbothermal method is not metallothermic process but is also used in some fields as it uses carbon to directly reduce MgO at temperatures above 1700^{o}C. The process consumes high amount of energy and is not stable for production of magnesium at this high temperature as evaporation causes losses and require more techniques to retrieve magnesium gas. Magnesium is collected in vapour form and allowed to cool to obtain solid metal of high purity. This method consumes very high energy around 35kWh per kg of magnesium and exhumes huge amount of carbon gasses.[32]

The reaction is as:

$$MgO(s) + C \rightarrow Mg + CO\ (g). \quad \Delta G = 579.4\ kJ/mol.\ at\ RT. \tag{2.5}$$

High-purity magnesium is produced by the Magnatherm process, a thermal reduction technique that employs aluminum to decrease magnesium oxide. Although it uses a lot of energy, it is helpful in treating lower-grade raw materials.[33] The solid-state silicothermic magnesium reduction method was enhanced by developing and using the magnatherm process. For more than 35 years, this procedure was employed in commerce. The equipment and operations of the reduction plant are explained as they were during the industry-wide restriction. The goal was to work with fewer personnel and achieve greater thermal efficiency while using the raw materials directly without the need to create a briquette. Aluminum is used as a reducing agent with calcined dolomite, a combination of calcium oxide (CaO) and magnesium oxide (MgO). Aluminum is used because it can efficiently decrease magnesium oxide and has a high affinity for oxygen. Under vacuum or an inert environment, the mixture is heated in a furnace to temperatures of around 1550°C. While calcium oxide and aluminum oxide combine to produce a slag, magnesium oxide is reduced to magnesium vapor by the aluminum.[13,32] Then Mg vapours are cooled in a chamber and slag is collected. This process is known to produce high purity Mg metal. Drawbacks being it consumes more power and energy than pidgeon and carbothermic processes and has very complex equipment in process.

Electrolysis is another production way; in this process, an electric current is generated in a cell-like container, and the aqueous solution is radicalized and separated into ions. The magnesium extraction process is regarded as a significant method because of the involvement of brine or seawater in producing Mg, as it is available in huge quantities and at cheap costs. Molten magnesium chloride ($MgCl_2$) is reduced electrolytically in this process. High-purity magnesium is produced by the technique, which is frequently employed in industrial settings. From Seawater or Brine: By reacting seawater with lime (CaO), magnesium hydroxide ($Mg(OH)_2$) is produced: Magnesium chloride is then created by reacting the precipitated $Mg(OH)_2$ with hydrochloric acid (HCl). Water can disrupt the electrolysis process; hence, magnesium chloride needs to be anhydrous (water-free). By heating $MgCl_2$, water is removed, resulting in dehydration.[34] In a specifically constructed electrolytic cell, the molten magnesium chloride is electrolyzed. When $MgCl_2$ is molten, the cell functions typically at temperatures between

700 and 750°C. In the cell, Mg^{2+} gains two electrons to form Mg metal, while chlorine loses two electrons and oxidizes. Forming Mg metal and Cl gas separately. Magnesium produced by this method has low impurities. However, the process requires heavy external energy and is a complicated process. Requires precise measurement and control. The cell components should sustain high temperatures and corrosion. Chlorine gas produced at the end must be appropriately utilized.

$$Mg_2{+} + Ca(OH)_2 \rightarrow Mg(OH)_{2^+} + Ca_2{}^+ \quad (2.6)$$

$$Mg(OH)_2 + 2HCl \rightarrow MgCl_2 + 2H_2O \quad (2.7)$$

$$MgCl_2 \rightarrow Mg + 2Cl \quad (2.8)$$

2.5. Oxide-Metal Interfacial Reactions

Magnesium oxide being used widely as a refractory material. MgO, mainly used in steel and iron production processes, utilizes the reactions occurring at the interface. Liquid aluminum and solid MgO reactions have been studied in practice in aluminum alloy-producing industries.[36,37] Some theories suggest that at the interface of liquid aluminum and solid MgO, they react to form spinel $MgAl_2O_4$ first, as Al alone cannot wet MgO at this temperature of below 1000°C.[36,38] However, this spinel formation reaction reduces the interfacial energy and surface tension and improves wetting. As the temperature slowly rises and with longer holding times, spinel formation improves the kinetics and wetting.[39] The more the spinel layer thickens, the more surface tension cracks form through it, and slag infiltration starts. The initial reaction starts with the formation of a continuous spinel/oxide layer between the Al-MgO interface, inhibiting particle diffusion.[38,39] Some studies suggest that Alumina also keeps forming. This reaction is controlled by diffusion of solid particles of Mg and oxygen, through the cracks formed on surface and aluminum dissolves the MgO locally and reacting with oxygen releasing Mg which leads to nucleation of alumina and magnesium aluminate spinel regions due to redox reaction occurring at the interface. Various chemical reactions occurring on the interface reduces the contact angle between oxide and molten metal. Silicon slags help in considerable reduction of contact angle and improving slag MgO wetting.[36,38] In some

slag/metal interfaces, metal ions diffuse from slag into liquid metal due to electrochemical processes, magnesium acting as cathode and Al as anode, and Mg^{2+} ions transport through liquid metal, completing a circuit due to electric potential variations. Taishi Matsushita et al.[40] studied the effects of slag/metal interface and Marangoni convection flow and found that surface tension gradients are driven by temperature and concentration, and some interfaces enhance mass transfer by inducing convection through the liquid metal. Marangoni flow defines that when two states of matter, primarily liquid-gas or liquid-solid, are in contact, surface tension gradients act in between. These gradients depend on external factors, including temperature, capillary effect, concentration of surface-active species, and electric potential. The viscosity of slag highly reduces diffusion of ions to liquid, and presence of nitrogen atmosphere helps more from interface into liquid bulk. Hence, low viscosity of slag is preferred to improve wetting and diffusion of metal into molten aluminum.[40] Viscosity of Mg is found to be 1.3×10^3 Pa.s at melting temperature.[37] In some aluminum-iron-silicon systems, high oxygen affinity of elements results turbulence in interfacial contacts which lead to emulsification (droplets) creating high contact area, reaction increases and more oxides such as spinels and alumina or iron oxides accumulate around the contact point. Interfacial reactions with oxygen presence in MgO and liquid aluminum are highly influenced reason being strong affinity for oxygen. MgO-Al decreases interfacial tension by absorption of oxygen molecules at the contact points, enhancing the wettability of MgO by liquid aluminum and promoting better dispersion of MgO particles in the melt consequently Marangoni's flow is induced segregating the Mg particles at a nucleation site. Excess oxygen promotes oxidation of elements creating more and more dross which degrades the mechanical and refractory property of the alloy.[40,41] Mg atoms are released after dissolution and mass transfer through the oxide layer into aluminum melt, more transfer of atoms means increase in driving forward the reaction. Diffusion occurs primarily from MgO into liquid Al as it is easy for atoms to diffuse into liquid rather than solid. Mg activity determines the reduction of MgO in liquid aluminum. More mass diffusion faster will be the reaction which creates more spinel layers, at high Mg activity.[38,42] In solid-solid Al-Mg alloys, at interface during annealing to moderate temperature, γ-phase ($Mg_{17}Al_{12}$) and thick β-phase (Mg_2Al_3) were seen to form caused by diffusion of atoms across the interface. β-phase has low activation energy than other causing it to form readily near the host alloy, and thicker due to its higher interdiffusion coefficients approximately 10 times higher

than γ-phase. The lower is the activation energy, reducing the interfacial energy, such as in Al alloy host, diffusion of mixed metal is enhanced. Addition of MgO in liquid Al alloy creates grain boundaries and defects which form main point of nucleation of phases.[40,43]

2.6. Aluminothermic Reaction Method

Aluminum is used as a reducing agent in a chemical reaction called the aluminothermic reduction technique, sometimes called the thermite process, which separates metals from their oxides. This exothermic reduction method is frequently employed in metallurgy to produce alloys, pure metals, and welding applications. The idea behind the process is that a more reactive metal, aluminum, may push a less reactive metal out of its oxide.[1,2] The reaction produces a huge amount of heat, making it efficient and self-sustaining for a range of industrial uses. By reducing primarily refractory metal oxides or ores, aluminothermic methods are often used to create master alloys for the steel and superalloy industries, providing a carbon-free production technique.[2,8] Thermal reduction and electrolysis were the primary processes used to extract magnesium. The Pidgeon process, a well-known procedure, is the most developed technology for smelting magnesium in China. Its benefits include lower capital requirements for plant construction, a flexible production scale, and a higher level of magnesium purity. However, the Pidgeon process's drawbacks of high energy consumption and environmental contamination have presented a significant obstacle to the advancement of the economy and society.[10,11] Because aluminothermy uses less energy and produces magnesium more efficiently than the Pidgeon method of smelting magnesium and reduces carbon gas emissions, this method also has a lot of potential applications if the issue of the reverse reaction between magnesium vapor and CO is successfully managed.

$$\text{Metal Oxide} + \text{Al} \rightarrow \text{Metal} + \text{Al}_2\text{O}_3$$

Aluminothermic reduction is a metallothermic method to directly prepare and produce Aluminum-Magnesium alloy at high temperatures consuming less energy and raw materials exhuming least toxic gasses which is the primary objective of this study. This

process offers high potential to replace industrial methods such as carbothermic, silicothermic, electrolytic processes of Mg extraction and purification and is least expensive method.[12,32] However, the slag produced contains parts of Mg hence purity of Mg is compromised by presence of small traces of oxygen. In this process, Fig. 2.6, Magnesium oxide (metal oxide) is reduced in presence of aluminum, which gets oxidized. At high temperatures above 1500°C aluminum reacts with MgO to form different phases of aluminum oxide, Al_2O_3, separates magnesium in vapor phase to form an alloy.[8,24] According to 2nd law of thermodynamics, entropy of system always increases over time for its spontaneity. More is the entropy change; the more reaction stability shifts from reactants to products. Formation of products is easy and requires less energy at this point the equilibrium position goes toward products. This entropy change will cause more phase changes in the alloy formation over higher temperatures above 900 K.[44] The possible chemical reactions involved during the aluminothermic reduction of MgO:

$$3MgO + 2Al(l) \rightarrow 3Mg\,(g) + Al_2O_3(s) \quad \Delta G = +272.5\ kJ/mol \quad T = 700K \qquad (2.9)$$

$$4MgO + 2Al \rightarrow 3Mg + MgO.Al_2O_3 \qquad (2.10)$$

$$\Delta G = 479600 - 296.81T$$

$$MgO + Al_2O_3 \rightarrow MgAl_2O_4 \qquad (2.11)$$

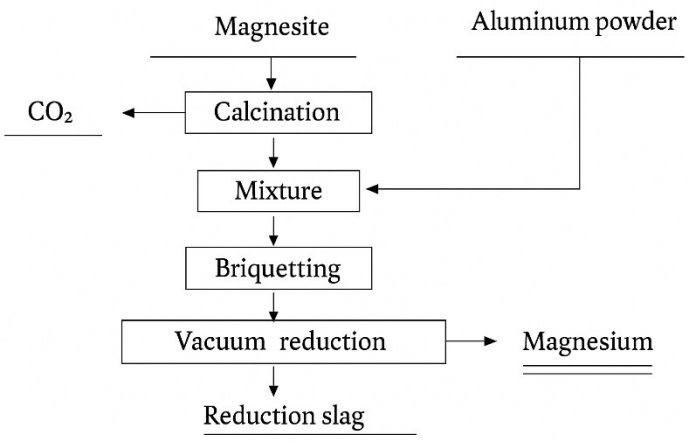

Figure 2.6. General flowchart of the vacuum aluminothermic reduction process.[2]

Yaowu Wang et,al, studied the production of magnesium by aluminothermic reduction process it was concluded that in the aluminothermic process, raw material consumption is reduced by 50%, and calcination energy consumption is reduced by more than 70% reduction procedure. The ratio of raw materials shows significant decrease, less than 50% compared to pidgeon process, indication reduction in energy consumption. The aluminothermic reduction process is conducted at a lower temperature, which helps to prolong the reduction pot's useful life and minimize repair costs. Teng Zhang et, al.[2] performed experiments to produce Mg-Al alloys by aluminothermic reaction using microwave heating furnace, they concluded by employing the closed microwave aluminothermic process, magnesium-aluminium alloy is readily produced microwaves high heating rates promote reduction of MgO when the raw material size is small of 10mm radius, reaction time is also reduced to 30 minutes. Moreover, at very high temperature magnesium vapour and aluminum metal react favourably in a confined, high-pressure reaction environment to generate Mg_2Al_3 and Mg-Al alloy.[26]

Wang et, al.[11] studied and examined using the magnesium silicate mineral serpentine as a raw material to make magnesium. The process was conducted under vacuum to reduce magnesium oxidation. The maximum yield was obtained at 1350°C, indicating that adding CaF_2 enhanced the separation of magnesium from the silicate slag.[11]

Overall, the aluminothermic reduction method of magnesium manufacturing may reduce energy by more than 50%, enhance productivity by 100%, and save materials by up to 50% compared to the Pidgeon process. Additionally, it may achieve zero waste residue discharge and a 60% reduction in CO_2 emissions.

2.7. Thermodynamics of Reaction

The importance of thermodynamics in aluminothermic reduction is because it establishes whether a reaction is possible under specific circumstances. Magnesia (MgO) is aluminothermically reduced by aluminum (Al) according to the following reaction:

$$3MgO + 2\ Al \rightarrow 3Mg + Al_2O_3\ (s) \qquad (2.12)$$

Using Aluminum as reductant, oxygen atoms are removed from Mg at high temperature forms alumina and extracts Mg, releasing huge amount of heat which sustains the process further.[2,26] Al has very high affinity for oxygen as specified in Ellingham diagram. After the reaction begins it doesn't require external energy to proceed upto end. The Gibbs free energy change (ΔG) shows negative value for the reaction at temperature above 1600^{O}C. More negative ΔG more stable are the products formed, reaction favours towards products.[45]

$$3MgO + 2Al\ (l) \rightarrow 3Mg\ (g) + Al_2O_3(s) \qquad (2.13)$$

$$\Delta G = 515200 - 294.73T(K)\ J/Mol$$

Mg can evaporate immediately if the reaction generates enough heat, which affects the separation process of Mg; the high temperature may also cause side reactions that result in the formation of spinels (Mg-Al-O phases).

The Ellingham diagram shows ΔG vs. Temperature for different metal oxides.

Aluminum's oxidation reaction:

$$4Al + 3O_2\ (g) \rightarrow 2Al_2O_3\ (s) \qquad (2.14)$$

Shows less negative ΔG than magnesium's oxidation:

$$2Mg + O_2\ (g) \rightarrow 2MgO\ (s) \qquad (2.15)$$

Hence Al can be used to reduce MgO according to these thermodynamics at very high temperature 1600^{O}C as MgO is more stable oxide than alumina. At high temperatures, ΔG for Al_2O_3 remains less than MgO, making possible that aluminum can efficiently remove oxygen from MgO. High temperature favors the reaction and Mg yield from MgO. However, the rate of reaction is affected by activation energy requirement which may be needed in high amount in the beginning. Diffusion limitation of Mg through the aluminum bath and reaction zone. Partial pressure of Mg vapor, according to Le Chatelier's Principle, vacuum conditions or low pressure of Mg gas shifts the equilibrium to right side of reaction. How we should maintain the partial pressure of Mg gas must be taken into consideration.

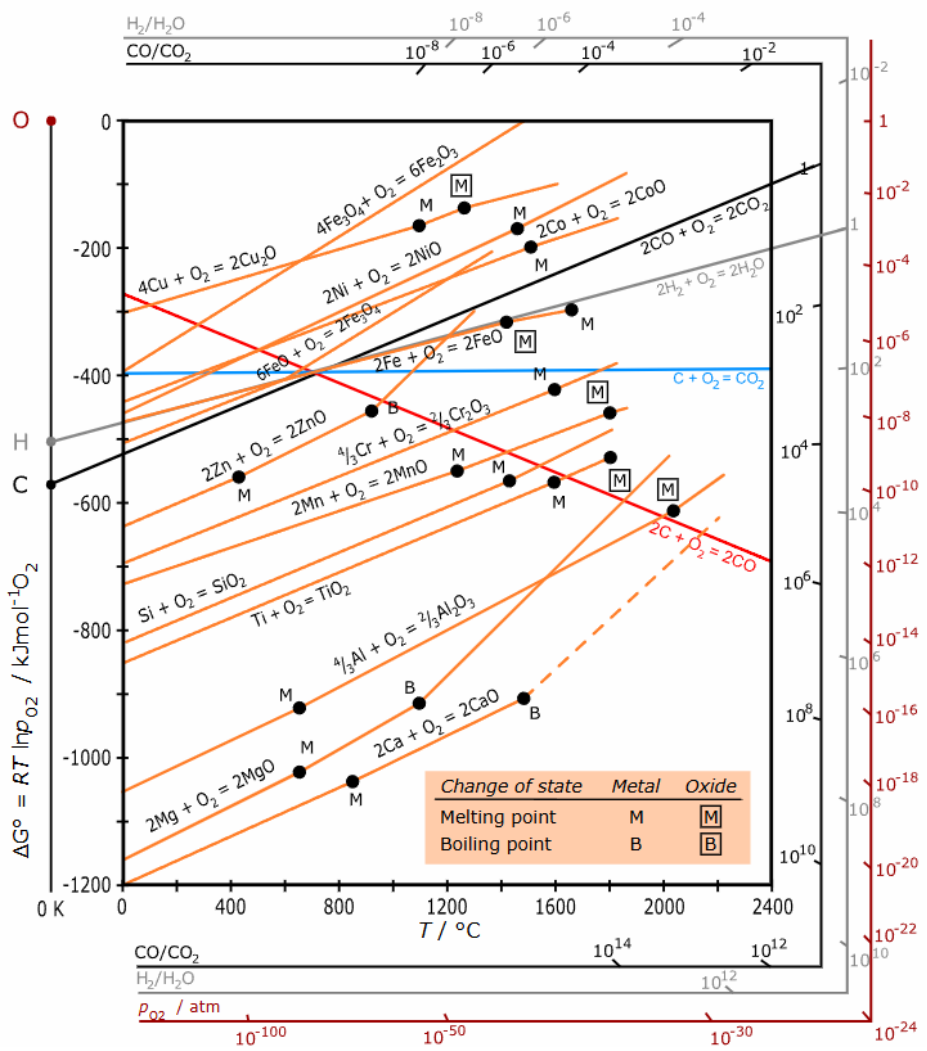

Figure 2.7. Ellingham diagram.

Hence the reaction proceeds to make stable products with different phases and structures. The data was taken from literature indicating that thermodynamically it is possible for the reaction to take place and Magnesia reduction in presence of Aluminum reductant is achieved. Fig. 2.7 shows the Ellingham diagram for various oxide reactions which shows free energy associated with various metal oxides the more negative energy for an oxide, more it has stability in this phase. The thermodynamic energy barrier that a system must cross for a certain reaction to occur is shown by ΔG^{O} in the diagram. Here we see MgO graph line is way below alumina and silicon which indicated MgO can be reduced by metals such as Al, Si etc. provided the temperature is high above $1400^{O}C$. This means aluminum requires high energy to reduce MgO and form a stable phase.

However, in presence of a catalyst reductant such as Aluminum and specific inert atmosphere, the reduction temperature could be reduced. Temperature and composition are the main factors influencing the variety of solid solutions and intermetallic compounds found in the Al-Mg binary system. β (Al_3Mg_2) and γ ($Al_{12}Mg_{17}$) are the main intermetallic phases that influence the alloy's mechanical characteristics. Free energies, entropies, and enthalpies of formation for these phases are calculated by evaluating the electromotive force of reversible galvanic cells. The results show that the solid solution rich in aluminum have a low positive heat of formation, indicating that magnesium is not very soluble in aluminum. A more stable structure with a high magnesium content is indicated by the terminal solution that is rich in magnesium, which shows negative temperatures and entropies of formation. Indicating highly ordered stoichiometric circumstances, the intermediate β and γ phases exhibit considerable negative excess entropies of formation and moderate negative heats, with noticeable minima at specific compositions.[37,45]

CHAPTER 3

EXPERIMENTAL WORK

3.1. Materials and Methods

The materials used in this study are commercial fine powdered MgO with purity ≥ 98%, fine Aluminum Powder with purity ≥ 94% (Fig. 3.1), Aluminum –Silicon, 'trade name: Silumin' (Al-11Si) alloy shows bulk purity > 92% contains 0.131% of Mg traces. Pure Aluminum solid bulk (from RUSAL) with purity 99.7%. Si- 0.15%.

In this study 4 different experiment approaches are conducted, 1) Resistance furnace, 2) Muffle Furnace 3) Tube furnace, 3) Induction furnace with different parameters, raw materials ratio. All reacted Al-Mg alloy samples from the approaches performed were taken out from crucibles, cut, grinded into small cubic shapes and polished from coarse surface upto 3 microns diamond polishing solvent.

The resulting samples were subjected to SEM, EDS and XRD analysis and analyzed.

The SEM analysis is performed using the ZEISS evo10 having SE Detector BSE Detector EDX Detector (at IYTE-MAM), with accelerating voltage ranging from 5kV to 20 kV, probe current ranging in pico and nano amperes. Micrographs are captured at 100x to 1000x range magnification. EDS point ID scan were taken at certain points of interest shown in SEM images in later sections, to detect elemental phase compositions in all experiments. XRD (X-Ray Diffractometer) made by Bruker Da Vinci D8 is used to analyze the phases and elemental composition in the sample, with radiation Monochromatic CuKα, wavelength of 1.5406Å was applied for a scattering angle 2θ covering a range of 20 - 80 degrees, and an X-Ray generator of 40.0 kV. The results were then visualized by the EVA software.

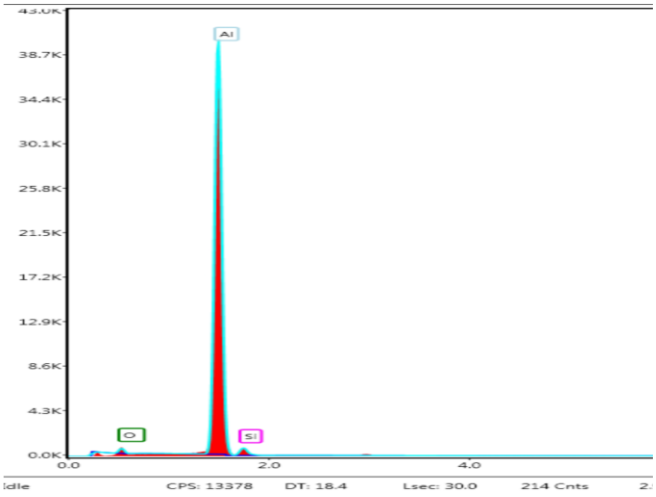

Figure 3.1. EDS scan of pure aluminum

ImageJ software was used to calculate the area fractions of various phases in an alloy using the SEM image shown in Fig. 3.2. Which is further used along with the EDS analysis to calculate Mg content in individual phases in SEM images.

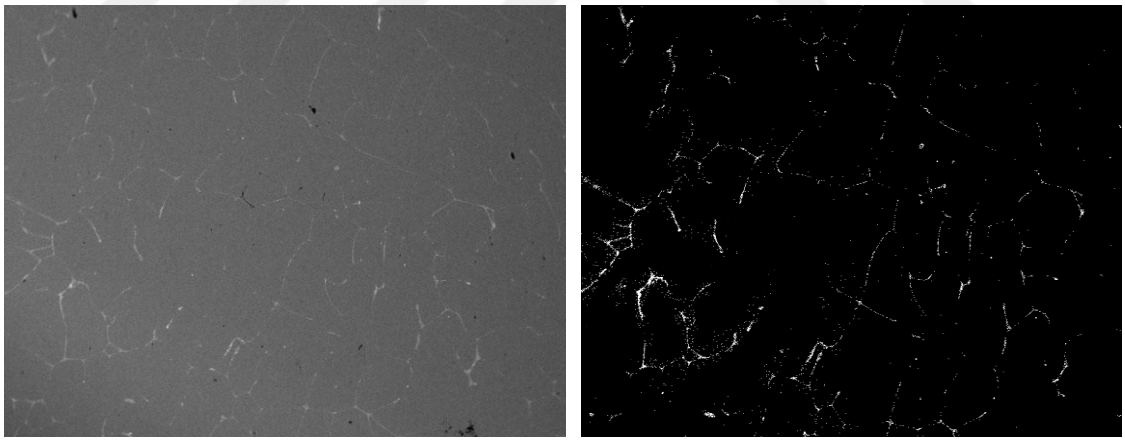

Figure 3.2. Mg phase content area (white/bright area) from ImageJ analysis.

Fig. 3.3 shows the alloy samples alloy after experiment is fully completed. The As-cast sample taken out of sample after cooling the material slowly to room temperature is cut into cubic shape, grinded and polished to 3 microns on top surface then sent for SEM analysis.

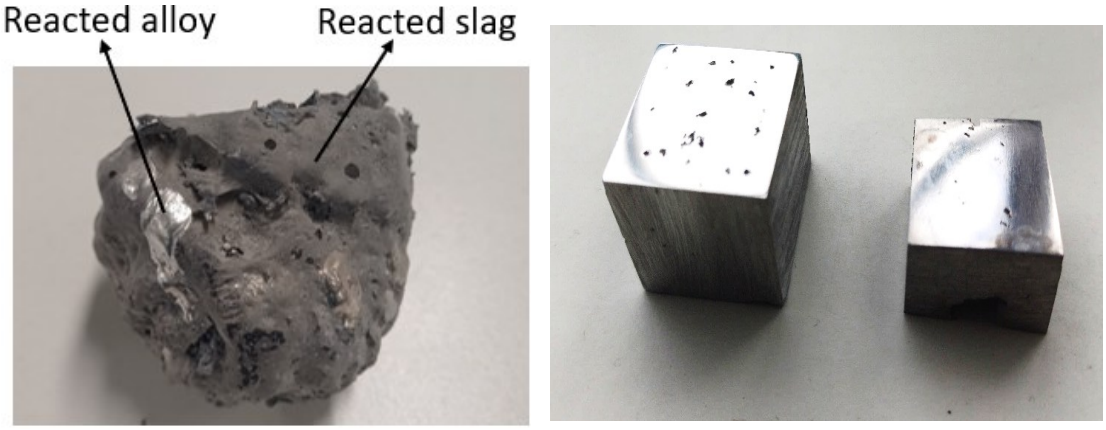

Figure 3.3. As-cast produced alloy (left), Polished metal alloy cubes (Right).

3.2. Experimental Procedure

Different experiments were performed in different furnaces at varying parameters are given matrix Table 3.1.

Table 3.1. Full experimental matrix.

Exp #	Pure Al (g)	Al-Si (g)	MgO (g)	Atm.	Max Temp oC	Dwell Time. (h)	Metal-oxide Ratio
1	200	0	12.5	Air	800	0.5	1:15
2	200	0	20	Air	800	0.5	1:10
3	0	150	10	Air	800	0.5	1:15
4	0	150	15	Air	800	0.5	1:10
5	184	0	12.26	Air	800	4	1:15
6	0	206	13.7	Air	800	4	1:15
7	0	258	25.8	Air	800	4	1:10
8	5 (powder)	0	0.33	Nitrogen	800	0.5	1:15
9	5 (powder)	0	0.5	Nitrogen	800	0.5	1:10

(cont. on next page)

Table 3.1 (Cont.)

10	0	275	18.33	Air	800	0.5	1:15
11	40	0	5	Argon	1200	0.5	1:8
12	50	0	5	Argon	1200	0.5	1:10
13	40	0	2.5	Argon	1200	0.5	1:15
14	30	0	2	Argon	1200	0.75	1:15
15	5	0	1	Argon	1200	0.5	1:20
16	30	0	5	Argon	1200	0.5	1:6

3.2.1. Experiments in Resistance Heating Furnace

First the aluminothermic reduction experiments were performed using pure solid aluminum and Al-Si alloy individually is melted in A2 cylindrical graphite crucible of dimensions: outer diameter = 9.5 cm, Inner diameter = 7.5 cm, height = 11.3 cm, in Protherm [PLF Series 140-160] chamber resistance furnace, shown in Fig. 3.4 up to temp. ~800^{O}C. MgO powder is preheated to 100^{o}C prior to adding in Al bath. Mg is available as MgO and is added individually and mixture is stirred thoroughly, the mixture is heated again at same temperature for 30 minutes/4 hours in different trails, illustrated in Fig. 3.5. Experiments are performed with materials content and parameters as shown in Table 3.1, exp. 1 to 7. Further the liquid mixture is allowed to cool down slowly to room temperature or casted into a mould.

In experiments 3, 4, 6, 7 and 10, the raw material used is Al-Si alloy contrary to pure aluminum used in remaining experiments, and MgO content is varied according to ratios 1:10 and 1:15. Their SEM, and EDS measurements are shown in Figures and tables below individually. To analyse the effect of holding times on solubility and mass transfer the holding time of two experiment 6 and 7 was set at 4 hours. Different Phases in the reacted metal alloy are seen in SEM EDS analysis.

Same experiment trials are repeated using different reactant as Aluminum-silicon bulk alloy molten in the same crucible and MgO powder is added at melting temperature of aluminum and mixture is stirred. Further all the samples produced are sent for analysis SEM/EDS, XRD, and XRF.

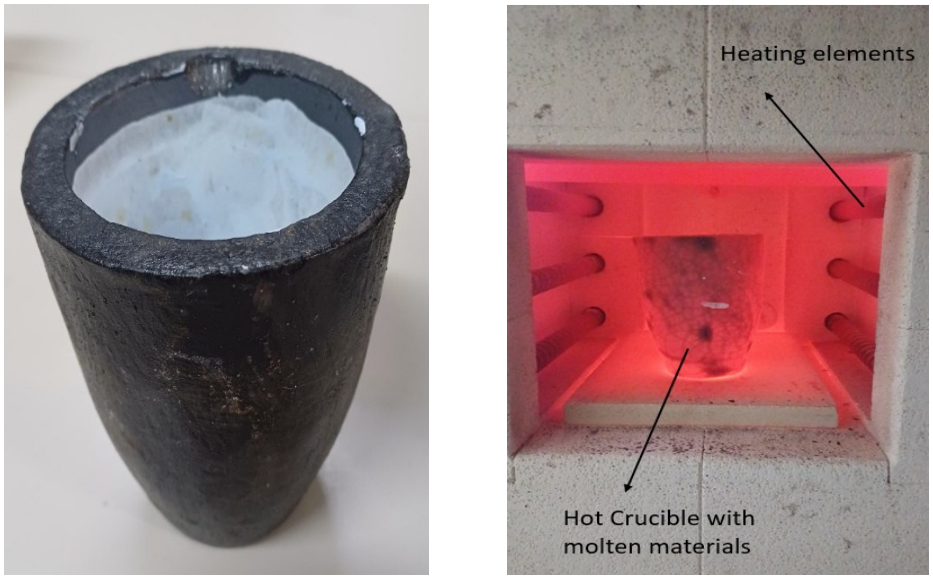

Figure 3.4. Crucible A2 (left) and Resistance Furnace with crucible (right) at high-temperature.

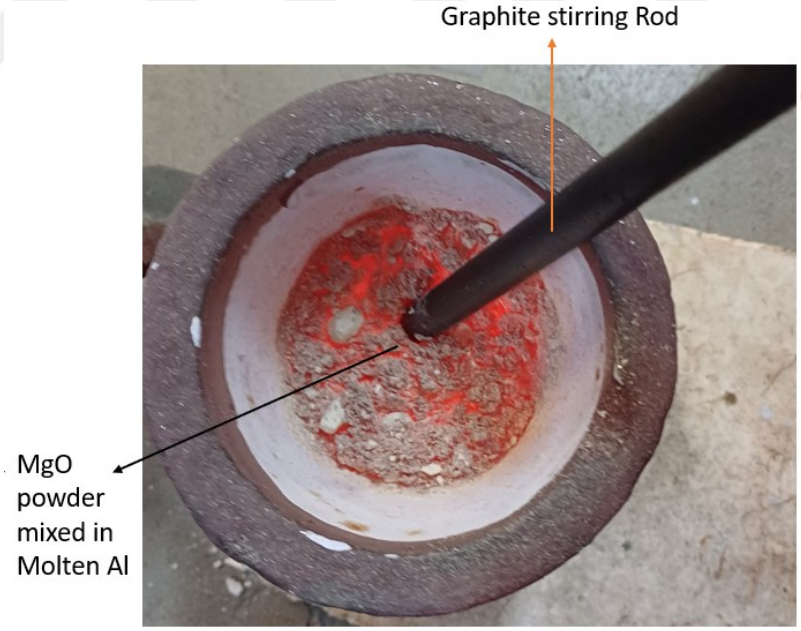

Figure 3.5. Molten Al in crucible with added MgO powder.

Further some more experiments were performed in another resistance furnace called as muffle furnace with brick insulation made by Nabertherm GmbH, Germany, Fig. 3.6, where inter gas atmosphere is used. Experiments were performed in cylindrical alumina crucibles having 2 inches diameter heated to maximum temperature of 1200 ^{o}C. MgO was added manually after melting pure aluminum pieces and stirred for a minute with alumina rod. Here the quantity of raw materials and holding temperature was less compared to resistance furnace trials as shows in matrix Table 3.1, Exp. number 10 to16.

Figure 3.6. Muffle furnace with alumina crucibles containing raw materials.

3.2.2. Experiments in Induction Furnace

An induction furnace is used and preheated MgO powder is added to a molten Aluminum-silicon alloy bath, melted in A2 crucible in induction furnace and placed between helical copper coil, cooled continuously by water flow at room temperature. At around 800 ^{o}C in a graphite crucible, the mixture is stirred vigorously, intermittently, three times after every five-minute gap illustrated in Fig. 3.7 and parameters given in Table 3.1, “Exp 10 (0-275-18.22-Air-800-0.30)”. Afterwards, crucible in the furnace is held for an extra 15 minutes at 800 ^{o}C. The sample is allowed to cool slowly to room temperature and then removed. Experiment is finished, sample is polished and sent for analysis described in later sections.

Figure 3.7. Induction furnace production process melting, mixing, and stirring of Al MgO.

3.2.3. Experiments in Tube Furnace

In this approach, the powder-form raw materials aluminum and MgO are mixed in proportion and then pressed in a manual compression machine in a coin shape Fig. 3.8 (left). The two raw compressed materials shaped as small cylinders in boat crucibles shown in the Fig. 3.8 (right) having diameter 1.5 cm and heigh 1 cm, below are individually taken and placed in the tube furnace, manufactured by 'Protherm Germany', for sintering with continuous nitrogen gas flow of 1 liter/min rate throughout the process at atmospheric pressure. The samples are heated upto 800 ^{o}C and held for 30 minutes, then slowly allowed to cool and samples are pulled out from the long alumina tube using a long horizontal steel rod. Two experiments are performed with ratio, content of raw materials and parameters are shown in the Table 3.1 "Exp. 8 (5p-0-0.33-N-800-0.5)" & "Exp 9 (5p-0-0.5-N-800-0.5)".

Figure 3.8. Manual compression device with raw materials (left) and Compressed Al-MgO powder into coins in boat crucibles.

CHAPTER 4

RESULTS AND DISCUSSION

In this chapter, we compare the effect of varying MgO concentration and holding time on solubility, activity, and mass transfer from slag to liquid metal. SEM images with elemental composition of different phases in the samples produced after various experiments, the calculated results from SEM analysis, Thermodynamics and activity of Mg are presented, as well as ImageJ quantification data and FactSage analysis. SEM analysis, EDS elemental calculations are shown and factsage calculations are presented in later sections. The EDS analysis graphs from SEM scans are included in Appendix A.

4.1. Results from Experiments 1, 2, and 5

The three experiments are performed using raw material, pure aluminum liquid melt, with constant concentration while MgO is added at varying ratios of 1:10 and 1:15 of Al:Mg. From the Resistance furnace experiments, the BSEI SEM image and measurements are presented below for experiments named 1, 2, and 5, whose raw material content and parameters are written in Tables with SEM image at two points. The contrast in the SEM images shows different phases for their elemental composition measurements. SEM micrograph for Experiment 1 is seen in Fig. 4.1 with elemental measurements. The reacted metal is homogeneous and white lines and spots indicate as grain boundaries and are Al rich containing small amount of Mg, O and Si indicating the oxide and spinel phases $MgAl_2O_4$ are observed.

Fig. 4.1 illustrates the SEM micrograph of "Exp.1 (200-0-12.5-Air-800-0.5)" with BSE imaging and with EDS elemental details given in tables for two phases.

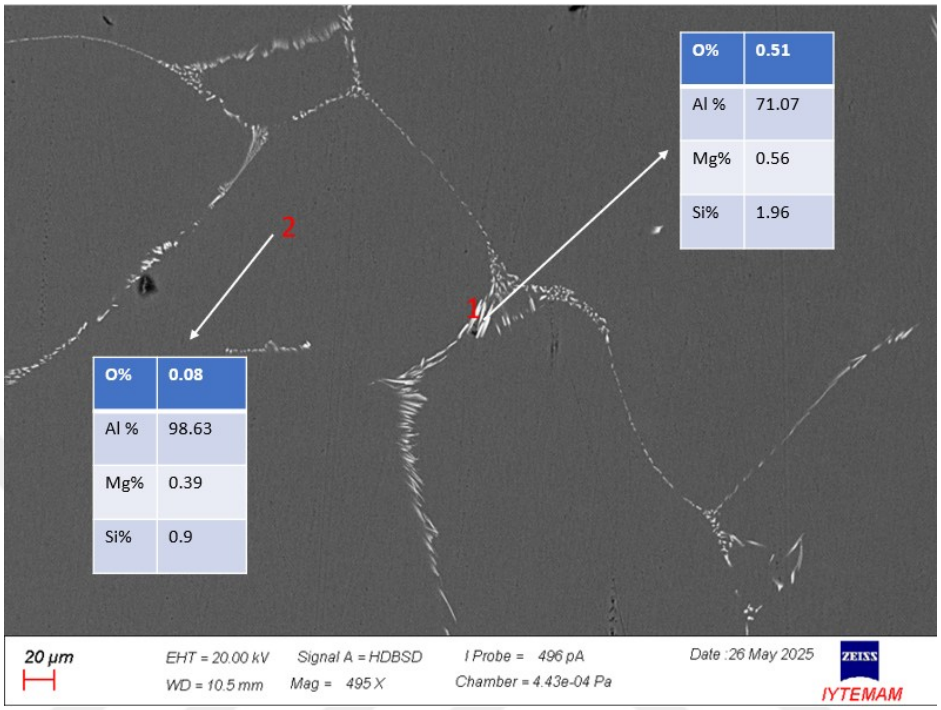

Figure 4.1. SEM image of experiment 1 with point EDS elemental measurement.

Different phases are seen in SEM image with elemental content Fig. 4.1. The grey area is rich aluminum metal matrix phase with traces of Mg metal uniformly dissolved in it. Same phases and dissolved elements are seen in other pure aluminum raw material used experiments shown below. The flake like structure seen in the brighter phase is formed due to iron content present in it. Iron content must be strictly limited in Al-Mg alloys as it decreases the strength-to-weight ratio and corrosion resistance of the alloy.

Fig. 4.2 displays the SEM micrograph for “Exp.2 (200-0-20-Air-800-0.5)”, with tables provides the EDS elements data using the. Grain boundaries are indicated by white lines and dots in the homogenous reacting metal, which is rich in Al with trace amounts of Mg, O, and Si, suggesting the oxide and spinel phases $MgAl_2O_4$.

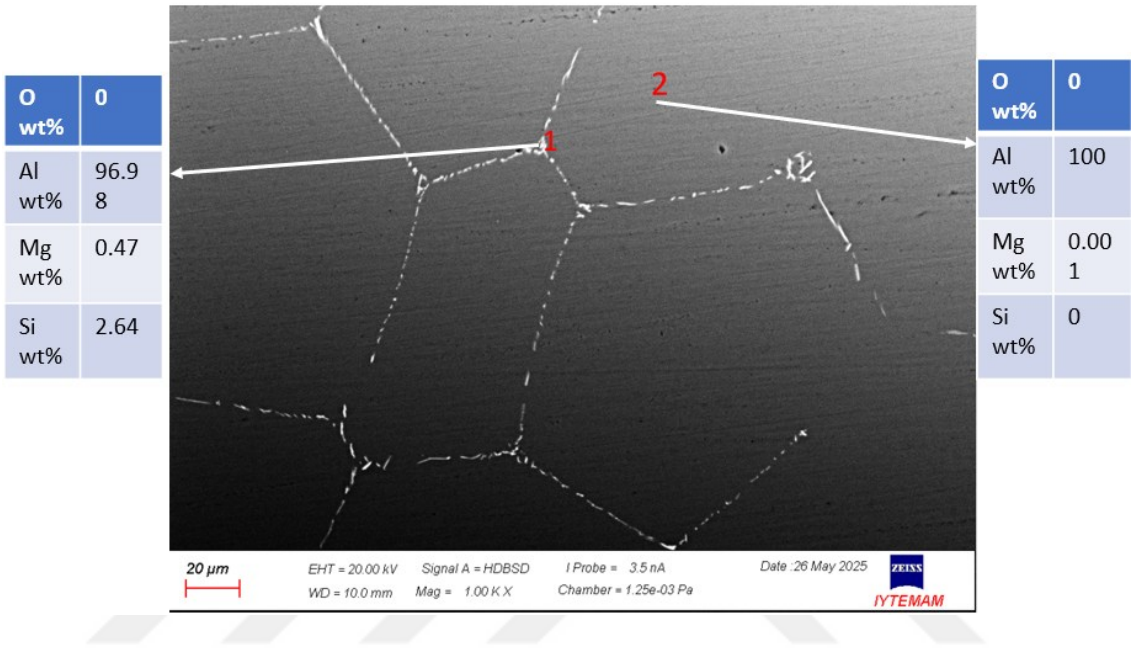

Figure 4.2. SEM image of experiment 2 with point EDS elemental measurement.

Since GBs are the central location for phase nucleation, we see very fine, mostly hexagon-shaped grains produced in the matrix. The SEM picture shows many phases; the grey region is a rich aluminum metal matrix with evenly distributed traces of magnesium metal. Comparing SEM images of Exp. 1(200-0-12.5-Air-800-0.5) & 2 (200-0-*20*-Air-800-0.5) we observe with increasing Mg content, grain size increases. However more Mg content makes the alloy brittle due to rich intermetallic formation and reduce its corrosion resistance. Hence, it is necessary to limit the Mg composition in the alloy.

SEM image shown in Fig. 4.3 for "Exp.5 (184-0-12.26-Air-800-4)" with EDS analysis in tables respectively, the same tendency is for Al rich areas and oxides found around grain boundaries.

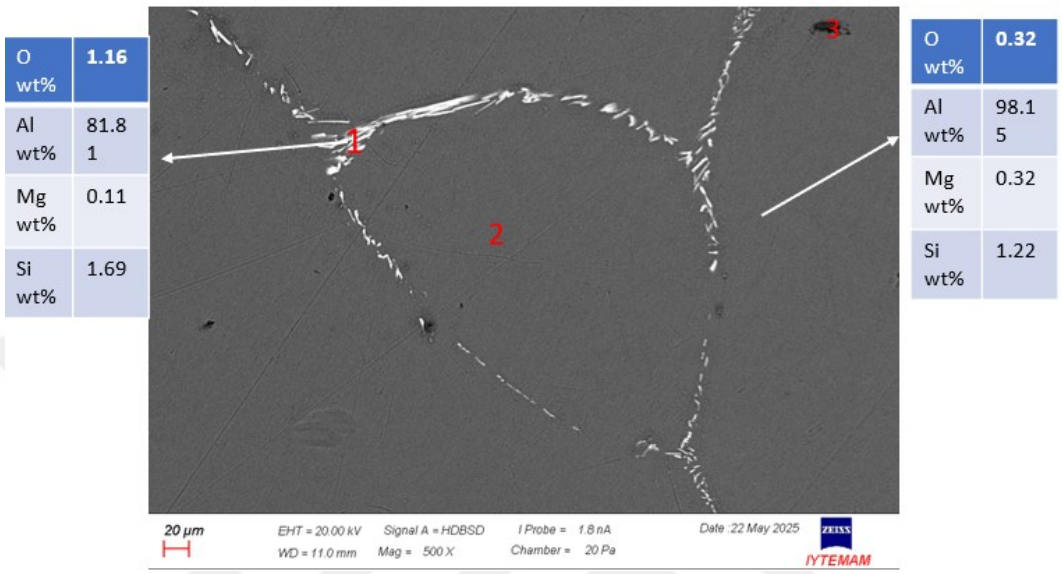

Figure 4.3. SEM image of experiment 5 with point EDS elemental measurement.

Different shapes of grain boundaries are which depend on the solidification phenomena of the alloy while the whole metal matrix is homogeneous. The thin flake like structure seen in above SEM matches the oxide films of Al and Mg spinel.

The reacted metal is homogeneous in the above Resistance furnace trails with pure aluminum and MgO raw materials. We find two phases in all SEM BSEI shown: 1) brighter regions along and within grain boundaries that are aluminum-rich, containing oxygen and Mg in low content. It is also assumed that spinels (magnesium aluminate) form at the interface when MgO encounters molten aluminum; the stability of oxide phases is high. This acts as the driving force for creating a thin spinel layer over the interface, reducing the surface tension of liquid aluminum, and further reducing the mass transfer from slag to liquid metal[38]. However, as the temperature increases above 1000°C, these oxide layers formed at interface are broken, allowing more Mg transfer, and readily forming various Al-Mg phases and intermetallics in the matrix, as studied in literature[36,38]. Mg mass transfer occurs due to diffusion across the interface, and as

interfacial compound alumina is formed. A homogeneous Al-rich matrix is dominant (point 2). Compared to other experiments, pure aluminum trails show fine hexagonal regions or grains surrounded and separated by fine grain boundaries, as depicted in SEM image Fig. 4.2, “Exp.2 (200-0-20-Air-800-0.5)”. The thin flakes in SEM are particularly formed when the alloy undergoes slow cooling and solidification, the tension breaks, and folds occur and settle in the liquid. MgO contact forms the nucleation site of oxides, allowing diffusion of Mg metal across the interface into the metal matrix. The atomic size of Al and Mg is almost the same; hence, Mg replaces the Al atom on the face sides, preferably.

4.2. Results from Experiment 3, 4, 6, and 7

We observe a bright region non-uniform are Al rich iron containing (Al-Mg-Fe) phase along with oxides. The long needle like shapes is found as silicon dominant phases Mg_2Si (point 3). These alloys don’t form the visible grain boundaries in SEM image Fig. 4.4.

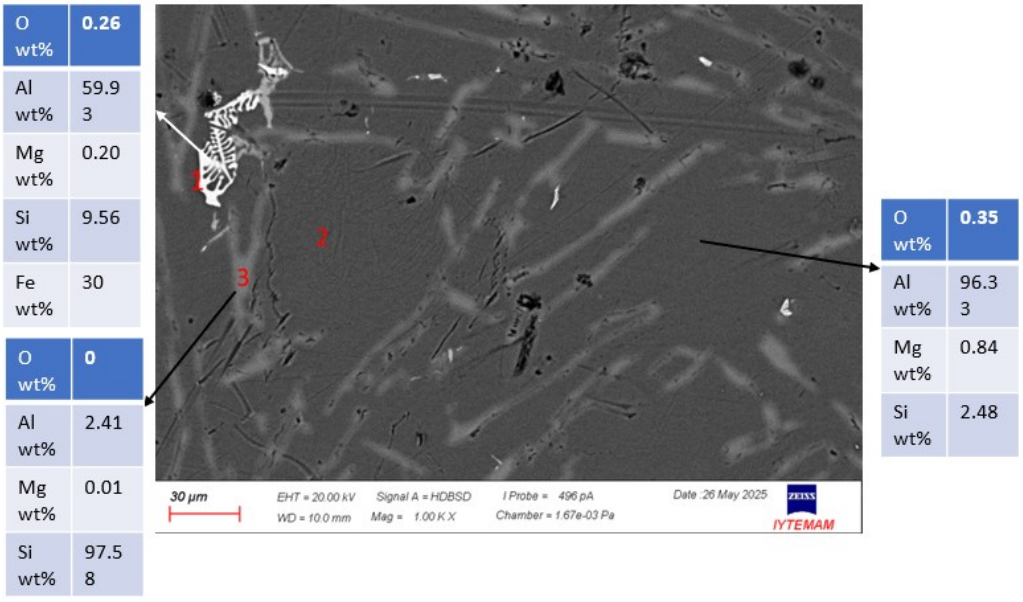

Figure 4.4. SEM image of experiment 3 with point EDS elemental measurement

In the “Exp.3 (0-150-10-Air-800-0.5)”, SEM, three different phases are observed, the script (bright white) like phase consists of iron phases forming β phases of Al-Mg-Si-Fe with compositions at eutectic points, seen in EDS point ID measurement given in the SEM image. Point 3 the precipitate phase is Si-rich with traces of Mg, forming Si-Mg and Al-Si-Mg phases. Silicon slags help in considerable reduction of contact angle and improving slag MgO wetting. The point 2 dark phase is Al- rich however it should be observed that this phase consists of more Mg dissolved than the silicon rich phase.

SEM analysis of “Exp.4 (0-150-15-Air-800-0.5), Fig. 4.5 illustrates variety of shapes of Chinese-script phases containing Al-rich β-Al-Fe-Si phases in the matrix. It is observed that this phase nucleates close to Si rich precipitates.

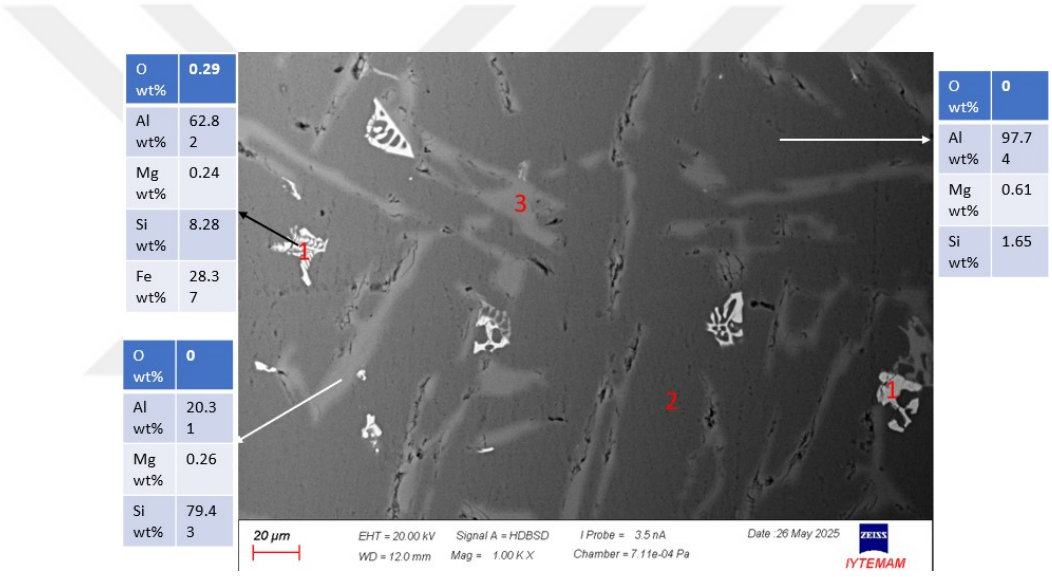

Figure 4.5. SEM image of experiment 4 with point EDS elemental measurement.

This phase is considered as orthorhombic intermetallic compound, containing moderate quantity of Fe with Si acting as a synthesizer.[46] It can be seen this phase in 3,4,6,7 experiments show irregular spreading and non-planner growth. This occurs due to anisotropic growth preferred more in a direction and extends as branched arms. The EDS composition are shown in Fig. 4.5 tables for 3 phases.

The “Exp.6 (0-206-13.7-Air-800-4)” SEM micrograph in Fig. 4.6 displays three morphology phases with varying element compositions in all three phases bright white, grey and dark black at three points. The brighter phase is little to observe clearly. Since Al has a greater affinity for Mg than Si and atoms may readily swap places without significantly altering the lattice structure during diffusion, the Al-rich dark phase (point 3) has more Mg than the other two alumina (bright) and Si-rich phase(grey).

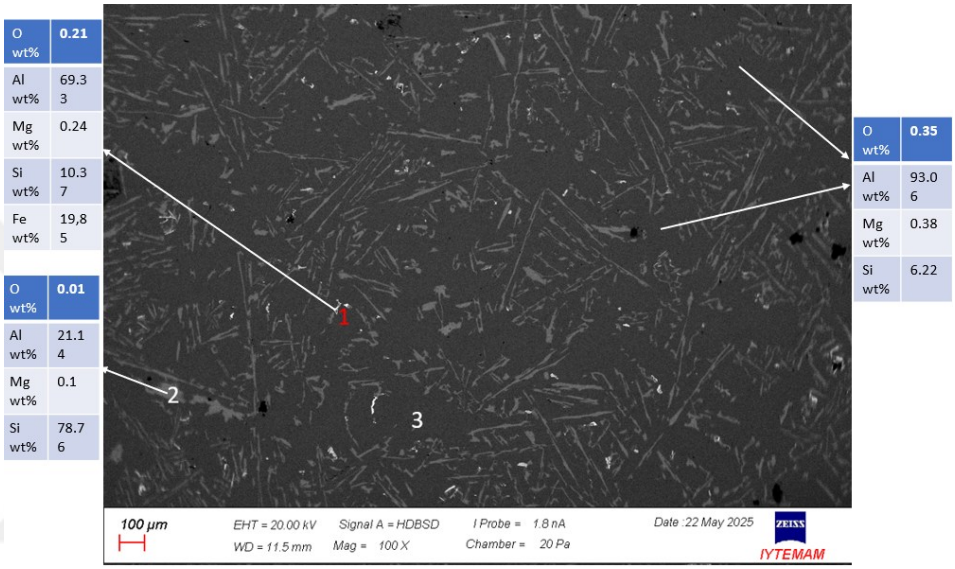

Figure 4.6. SEM image of experiment 6 with point EDS elemental measurement.

The Mg_2Si phase is called Magnesium silicide intermetallic phase, it provides age hardening in the alloy and helps in improving strength. This phase primarily forms during solidification or is created with artificial aging. Si content in alloy helps in improving wear resistance but may reduce ductility. The microstructure and mechanical characteristics of alloy may also be influenced by trace elements, including iron, manganese, titanium, and strontium, which may be present purposefully or as impurities.

The SEM image Fig. 4.7 is for the “Exp.7 (0-258-25.8-Air-800-4)” showing three phases the Al rich β-phase at high magnification (point1) and with-it grey needle and plate shaped Si-rich precipitate (point 2) in vast homogeneous Al rich matrix, darker area.

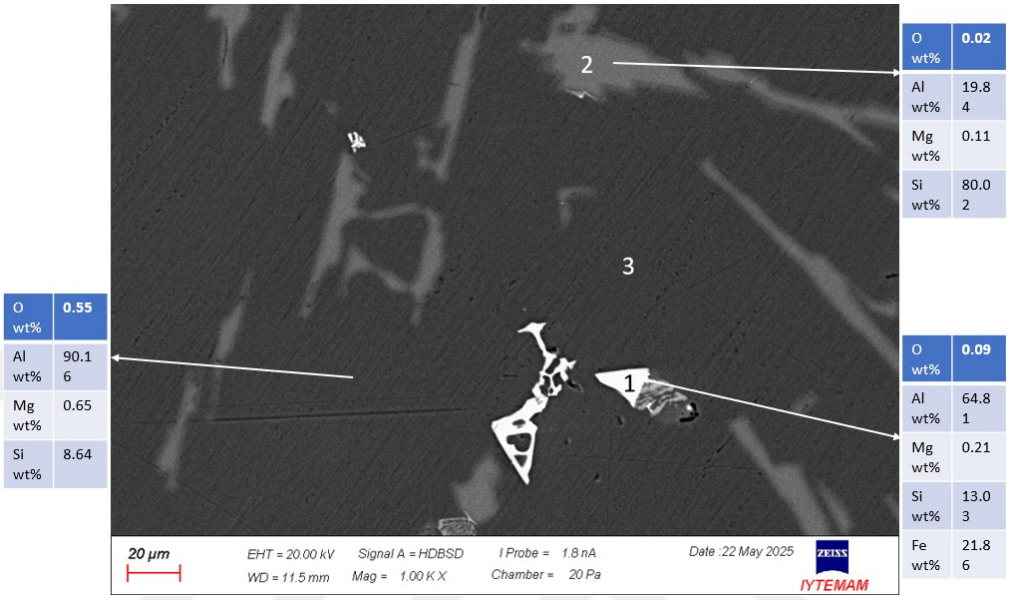

Figure 4.7. SEM image of experiment 7 with point EDS elemental measurement.

In this trial we observe high quantity, 0.65 wt% of Mg compared to other two phases, dispersed across Al matrix. EDS point ID shows the elements composition present in the three phases. Elemental composition is written in tables with the SEM micrograph. Here also high content of Fe is seen at point 1, bright phase which creates the orthorhombic morphology as observed in former experiments.

4.3. Results from Experiment 8 and 10

In SEM micrograph, Fig. 4.8, We find 2 phases: bright 1 (point 1 and light grey (point 2). The bright phase is observed as an Al-rich phase with mixed Si, Fe, and Mg in good quantity. It contains spinel phases and intermetallic phases segregated around the grain boundaries specifically. When the MgO comes in contact with liquid metal, the stable oxides are shown here to be formed first, such as spinels and alumina layers covering the interface to reduce the system's instability and maintain equilibrium at the interface. The S-S diffusion occurs as the activity of Mg increases on the interface. Mg mass transfer occurs in small amounts as low activity further decreases the reaction's Gibbs free energy of formation, making the reaction more exothermic and causes more Mg to dissolve in the Al matrix.

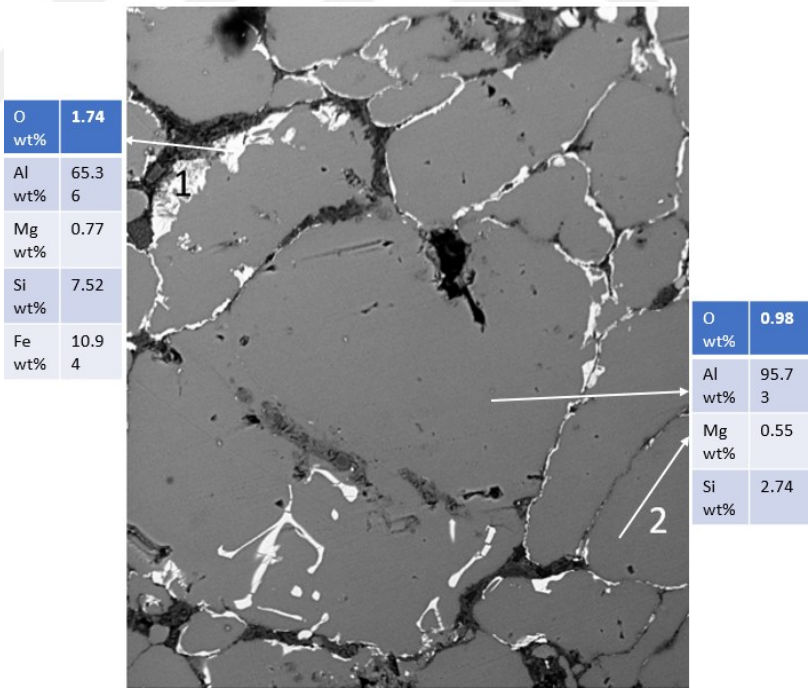

Figure 4.8. SEM image for experiment 8 with point EDS elemental measurement.

Where induction furnace is used instead of resistance chamber furnace, raw materials include Al-Si alloy and fine powder MgO added and stirred. SEM image shown in Fig. 4.9 “Exp.10 (0-275-18.33-Air-800-0.5)”, identifies 3 different phases the white regions, the script like structure (point 1) forms the oxides and spinel with high aluminum content and moderate Silicon and iron shown in SEM image EDS analysis elemental composition. It is assumed that iron is responsible for formation of shapes like this and with stirring in furnace the folded structure is seen. Point 2, light grey regions the needle like shape are the Si rich phases and intermetallics, Mg_2Si precipitate which forms during aging of alloy. This morphology is formed due to mismatch in nucleation and growth speed of the FIMC and matrix phases.

Figure 4.9. SEM image for experiment 10 with point EDS elemental measurement.

FIMCs are very directional growth phases, they begin to grow in one direction and matrix phase grows uniformly. Aluminum phase during growth, fuses between the dendrites of FIMC and locks their shape resulting in skeletal or script shaped phase. FIMCs are brittle but have high hardness than the surrounding matrix and crack easily. Addition of Mn can make FIMC more compact and stable structure. [47]

BSEI images in Fig. 4.10 represent SEM micrographs of resistance furnace experiment with base Al-Si alloy mixed with MgO at 800ºC.

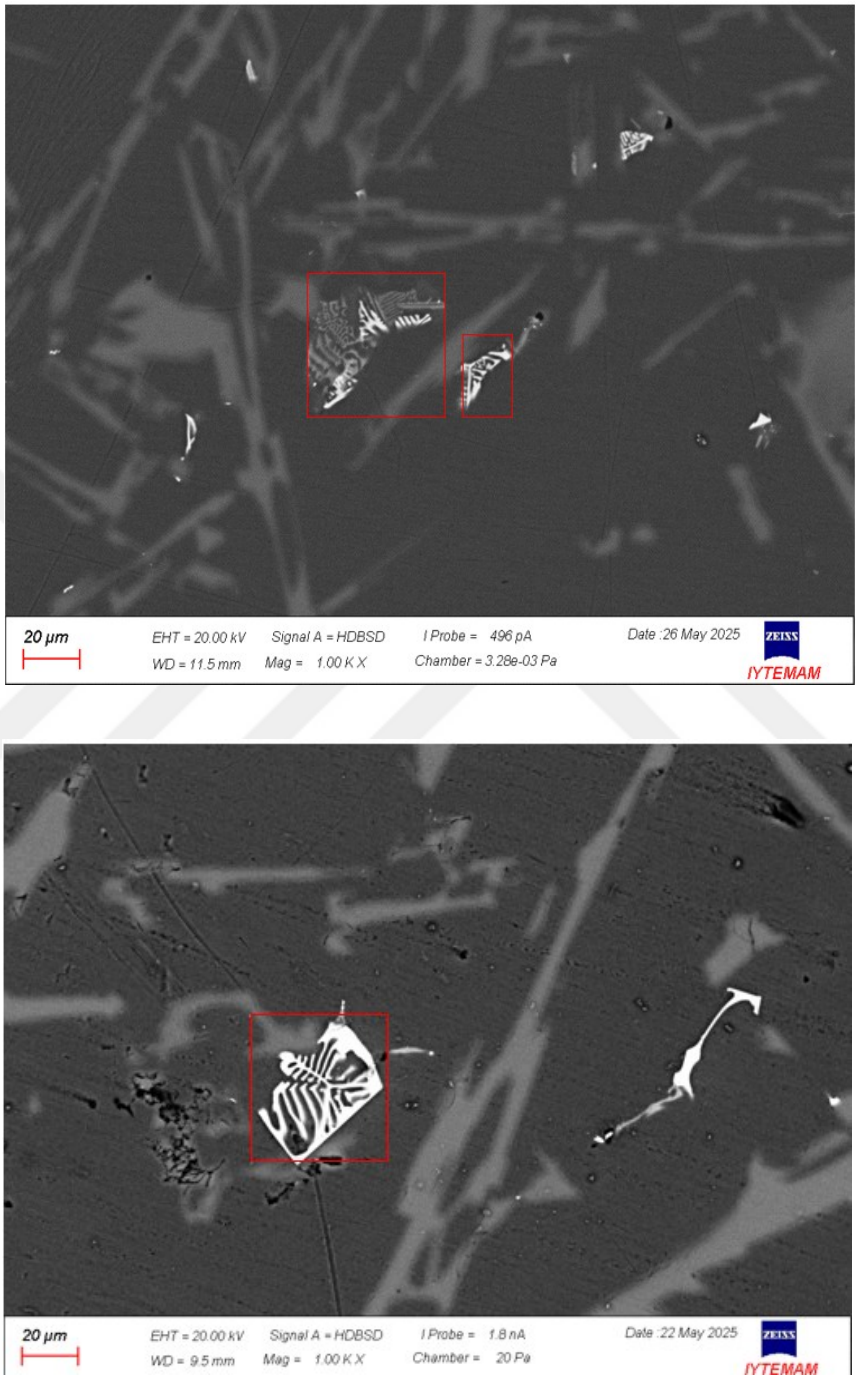

Figure 4.10. SEM image of experiment 10 & 4 showing script like phase in matrix formed due to high Fe content (red box)).

The script like structure phase is beta and gamma alloy phases Fe-containing intermetallic compounds Al(MgSi,Fe), formed at eutectic reactions around 450ºC in Al-Mg system. Some particles remain unreacted and dissolve in the matrix and form stable phases over time.

EDS scan of Fig. 4.10 shows presence of small amount of Fe in which could form α- AlMgFe or β-Al(MgFe) phase where Si acts as stabilizer in same script phase, This specific type of phase is not seen in pure aluminum containing experiments, we conclude this phase occurs due to presence of Si and Fe in the mixture. Fe forms such as intermetallics and co-exist with Al-Mg system. The β-Al(MgFe) phase grows with low crystallography structure, and interface energy. More such prominent shapes are observed in alloys with very low Manganese content. This phenomenon is seen in experiments 3, 4, 7, 6, and 10 where Al-Si alloy is used as raw material indicating role of Si and Fe in formation of these phases and with slow cooling the particles form orthorhombic intermetallic compounds [FIMC] in irregular shape and promotes its 3D structure. This morphology is studied to play a crucial role in improving alloy toughness corrosion resistance and reducing internal stress. With increasing Mg content in the alloy, the Chinese script phase becomes more prominent and sharper, and its area increases [47].

4.4. Results from Muffle Furnace Experiments

Different ratio of raw materials, pure aluminum shards and MgO fine powder and T_{max} = 1200ºC. We don't see any dendritic or Chinese script like phases due to absence of Fe and Si impurities which proves our statement regarding its formation due to Fe element. The alloy samples produced were analyzed using SEM, XRD and EPMA.

SEM Analysis: Accelerating voltage set ranging from 5kV to 20 kV for different experiments performed. The higher the voltage, the higher the brightness and resolution of the image. The aperture that controls the number of electrons striking the sample was kept between 1-0. The probe current range was set at 40 to 72 mA for practical imaging of scans for different experiments. Images were generated for both the secondary

electrons and backscattered electron BSE (shown below). BSE images display the sample's brighter and dark regions, which indicate the presence of different phases on the sample topography. Fig. 4.11 (left) SE topography image of "Exp.12 (50-0-5-Ar-1200-0.5)" shows different phases, regions at high magnification. The grey regions show separate alloy regions and phases, grains, boundaries, and surface structure, with EDS elemental content given in tables.

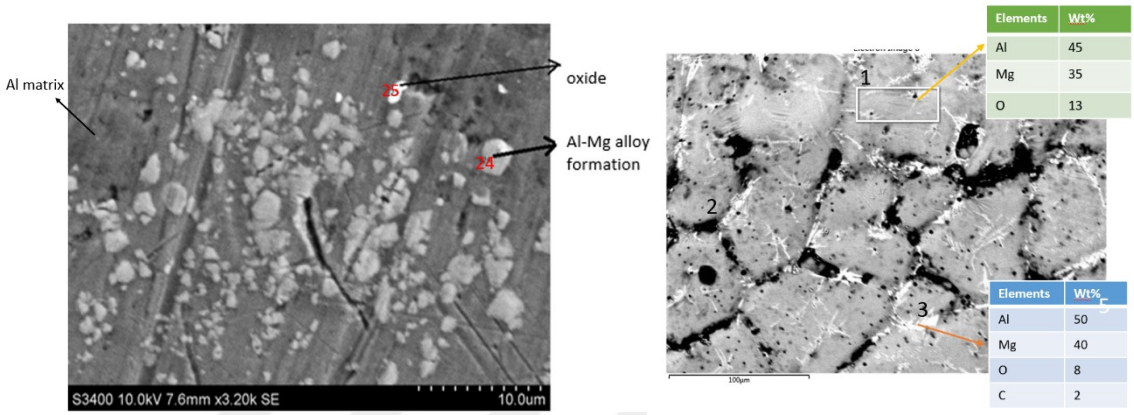

Figure 4.11. SEM micrograph: left, Exp. 12 SEI and right, Exp.11 BSEI.

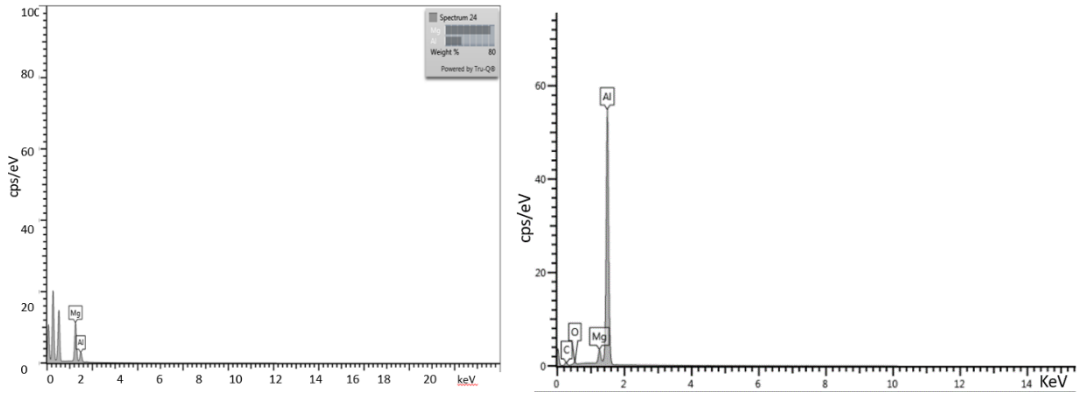

Figure 4.12. Point ID EDS analysis of Exp. 12 (left), 11 (right).

The darker/black areas are the aluminum matrix in which we observe some plate like structure as reacted Al-Mg alloy, Fig. 4.12 (left) shows the EDS plots of elemental composition for the same. The reacted alloy is homogenous with a uniform distribution

of Mg, as seen by mapping analysis Fig. 4.14**.** We can see the EDS point ID analysis of the experiment where the peaks of Mg and Al are seen having almost 80 wt% of magnesium and 20 wt% of aluminum along with some impurities (not identified).

"Exp.14 (30-0-2-Ar-1200-0.75)" SEM SE & EDS analysis is shown in Fig. 4.13, taken after fully polishing the surface of sample., with EDS elemental details given in tables for two phases.

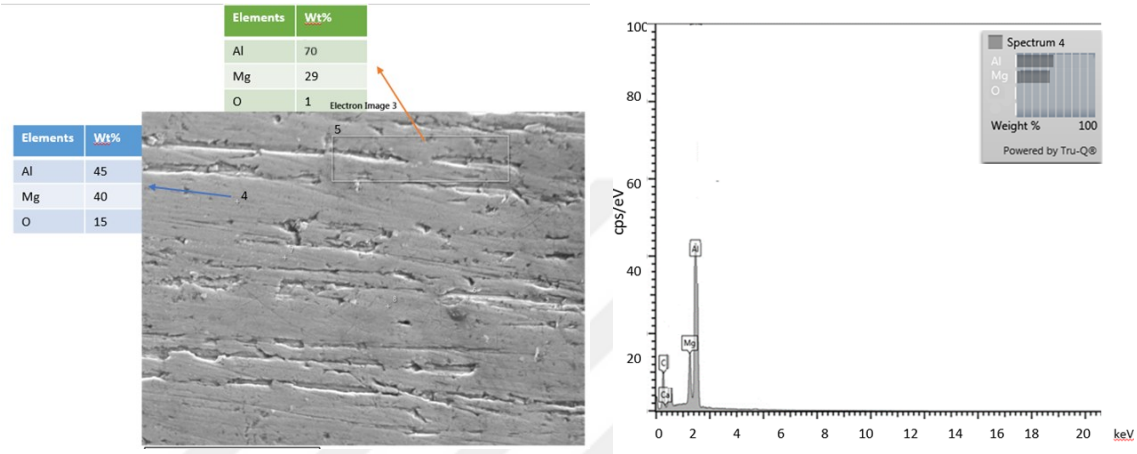

Figure 4.13. SEM micrograph left, SEI and right, EDS of exp. 14.

This image shows the sample topography micrograph on left where we see some thin cracks like shapes within which we observe higher quantity of Mg compared to the matrix which is having more α-Al phase. The reduced Mg from MgO is collected and segregated around the GBs and cracks. This Mg forms intermetallics with aluminum having more content of Mg than Al. This phase is very brittle and degrades the strength of the alloy, for this reason Mg must be contained within 6% limit in Al-Mg 5XXX series of alloys.

Mapping analysis to find the distribution of materials was performed in the same way after EDS analysis. Below images, Fig. 4.14, show the mapping of different experiments with uniform distribution of magnesium in samples with aluminum. Magnesium (red map below) is reduced from MgO during the reaction and thoroughly spread across the sample in the area under investigation.

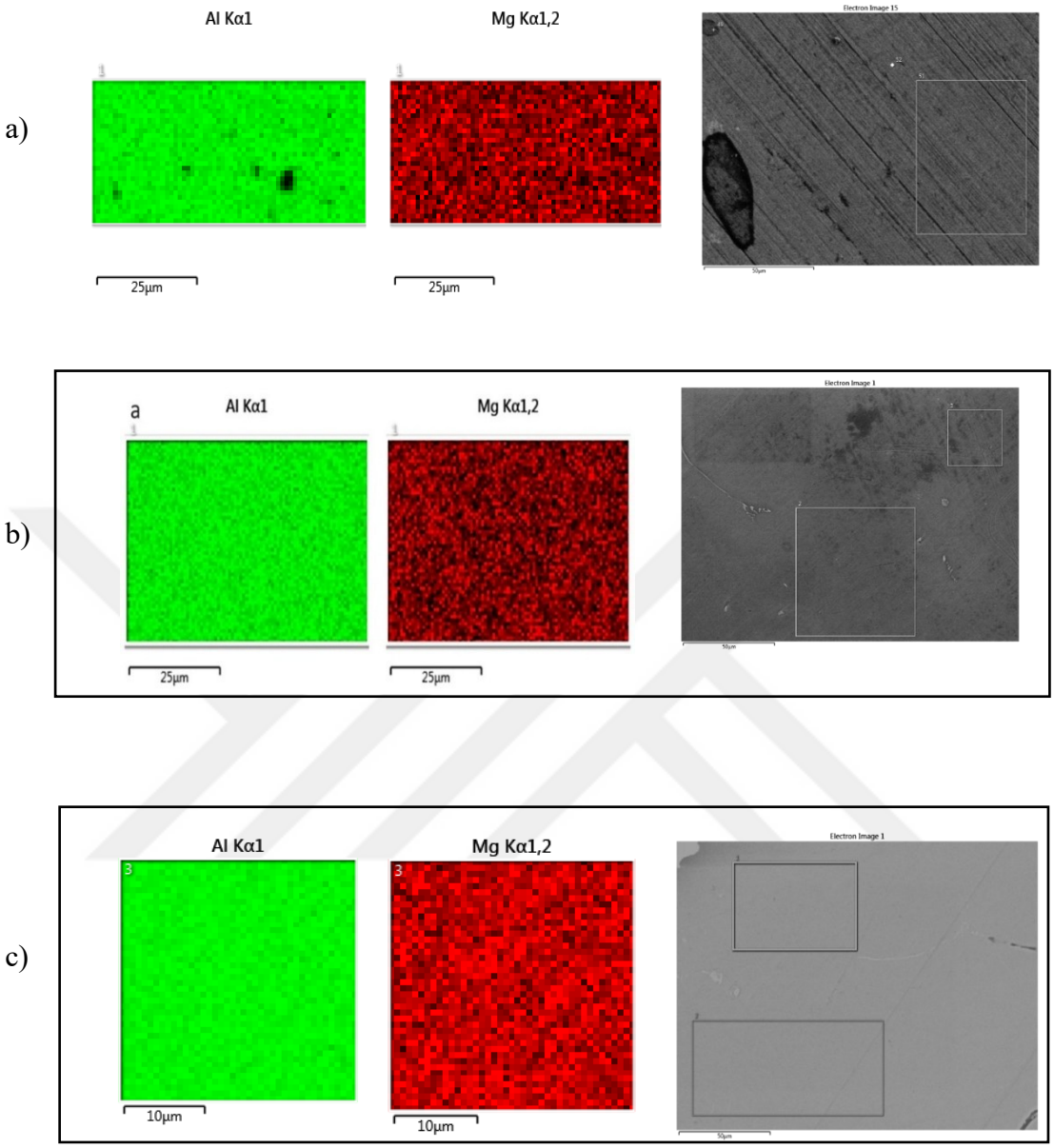

Figure 4.14. Mapping analysis of different experiments a) experiment 16 b) experiment 2 C) experiment 14. The red map gives the distribution of magnesium while green map illustrates the Aluminum distribution uniformly.

XRD Analysis: We studied the intensities of the alloy compared with the ICDD standard PDF (powder diffraction file). We found that both peaks and intensities are almost 90% match, showing the existence of an Al-Mg alloy with adjacent intermetallics and phases. XRD of various phases in a single experiment is shown, such as $Mg_{0.05}Al_{0.95}$ (Al-Mg) is a Low-Mg solid solution primary matrix phase, and their intensities are related to JCPD. Fig. 4.15 a, b, c, below shows the XRD analysis of experiments 11, 16, 14, respectively. At around 1200°C, we can see $A_{l11}Mg_2O_4$, $Mg_{17}Al_{12}$ (β-phase), $Al_{7.33}Mg_{4.36}$ intermetallic phase with rich Mg content, $Al_{1.23}Mg_{2.77}$ also Mg-AlO, $Mg_{0.734}Al_{2.177}O_4$ spinel (Magnesium Aluminate) and intermetallic phases while Al-Mg solid solution (low-Mg FCC) being the primary phase in reacted alloy illustrated above.

a)

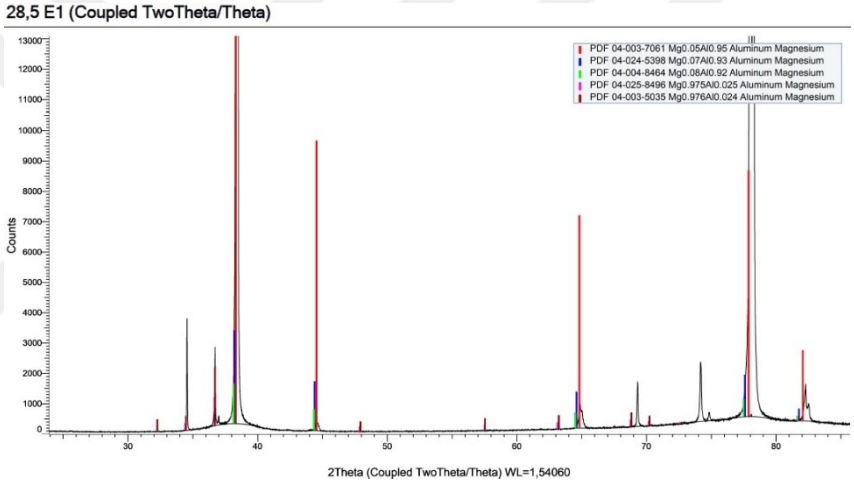

b)

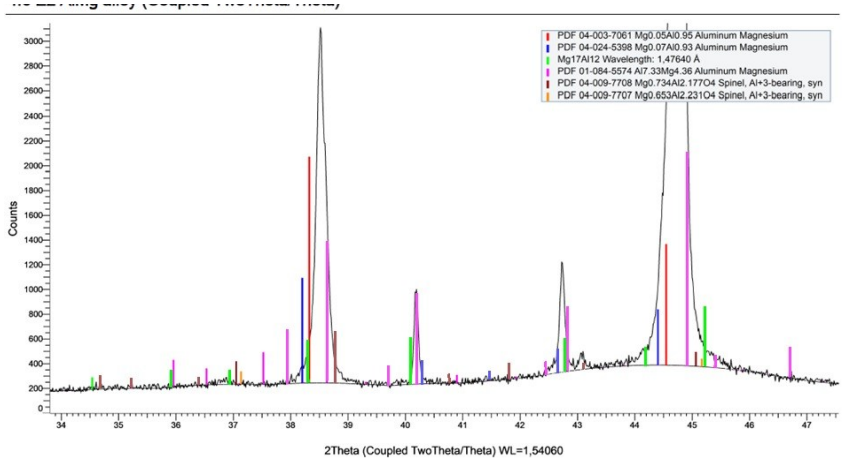

c)

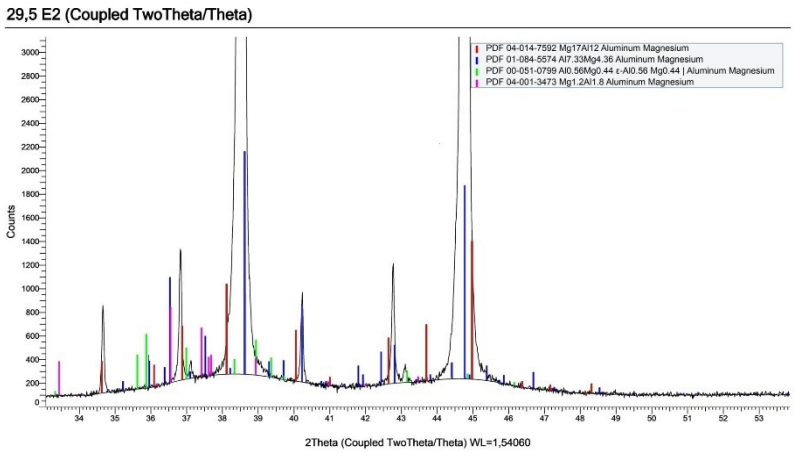

Figure 4.15. XRD analysis of experiment a) 11, b) 16, c) 14.

Sharp peaks of narrow width are obtained that are closely related to the ICDD, which depicts that the alloy obtained is purely crystalline and minimum amorphous, with analysis showing different structures of Al-Mg alloy with changes in structure. Different intermetallic phases with HCP and spinels were also found. We can observe the same tendency and details from the SEM/EDS phase study of experiments 1, 2, 4, and 10, and we conclude that the phases are in correlation. The expected phases of spinel and the formation of thin oxide layers around the grain boundaries and interface of Al and MgO coincide with our calculations and some theoretical models.

EPMA Analysis: To compare and extend our study further, the EPMA BSE image and mapping analysis was done on four alloys produced at T_{max} = 1200ºC. EPMA is a non-destructive technique to detect trace elements in a metal, alloy, or natural minerals. EPMA can create 2D morphology of surface with scanning scale upto 1 micron. Parameters of EPMA were set as 15KV Acc. Voltage, dwell time 10ms. We can see a high concentration of Mg around grain boundaries with Al metal indication formation of alloy and Al-Mg oxide phases, which were expected from the theoretical calculations of the alloy.

Figures 4.16 through 4.19 below show the EPMA BSE image and elemental distribution map of four experiments. BSE image was taken from the top polished surface showing different morphology.

The EPMA BSE image and element Map of “Exp.14 (30-0-2-Ar-1200-0.75)”, shown in Fig. 4.16**,** three phases are seen in the reacted metal, the α-Al white bright phase flake like structure containing intermetallics and dominant Al-Mg-Fe phase segregated along grain boundaries. We can see fine GB in metal matrix grey phase as solid solution which makes upto around 90% of area of sample image. Some pores dark black area is also visible but extremely low in area.

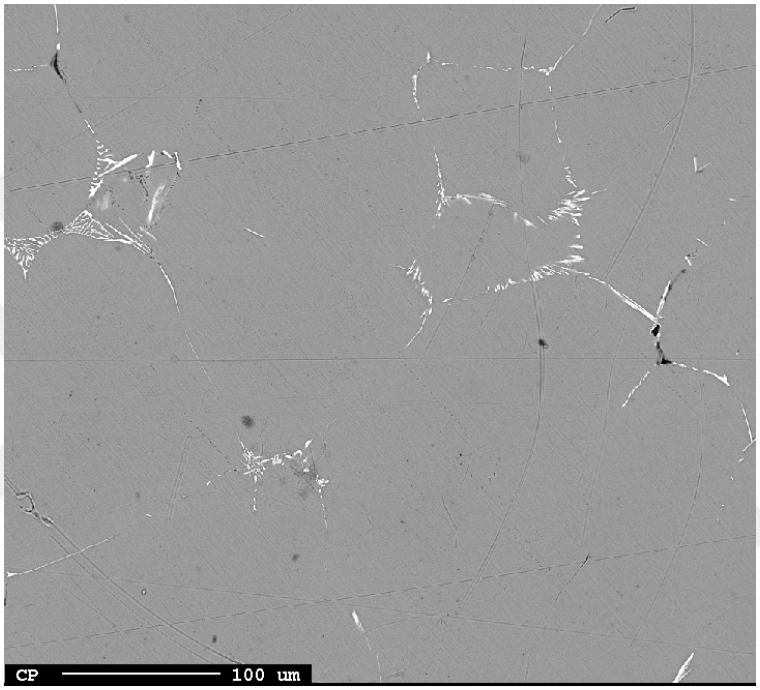

I.

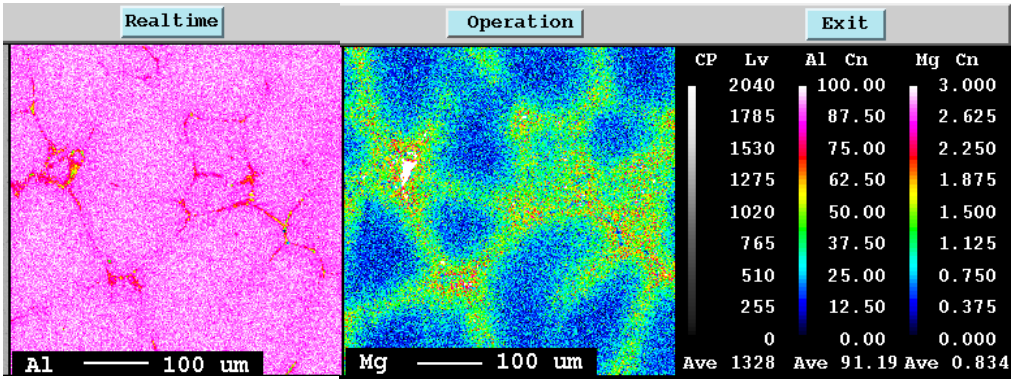

II.

Figure 4.16. EPMA analysis I) BSE image and II) composition map of Exp. 14.

Fig. 4.17, EPMA BSE image and element Map of Exp.16 (30-0-5-Ar-1200-0.5)", shows the mapping of distribution of Al and Mg in the matrix, high quantity of Mg is seen around GB compared to matrix which is having more Aluminum. Mg is a dilute solute in the main α-Al matrix at low concentrations, but significant Si is present forming Al-Mg-Si phases and other second phases with Mg. This also indicates that alloy formation occurs around GB in beginning and GB form primary nucleation site for the Al-Mg alloy.

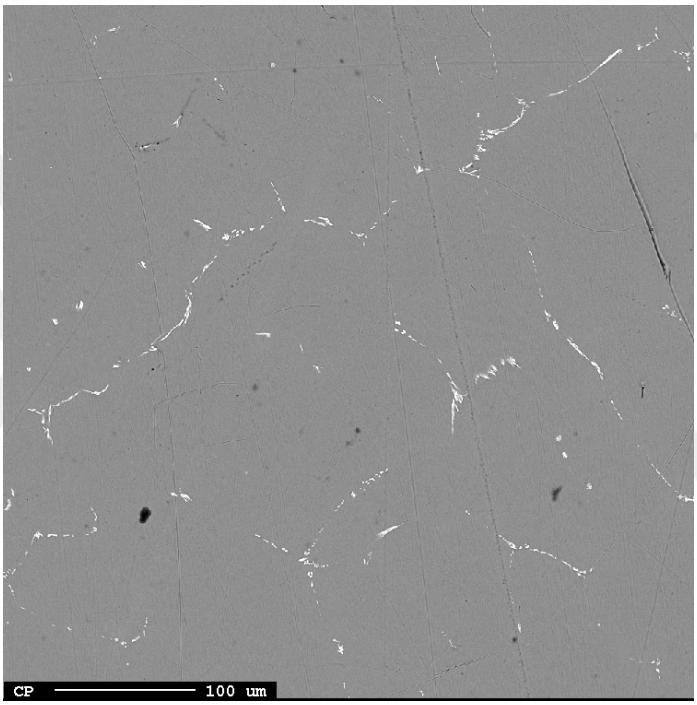

I.

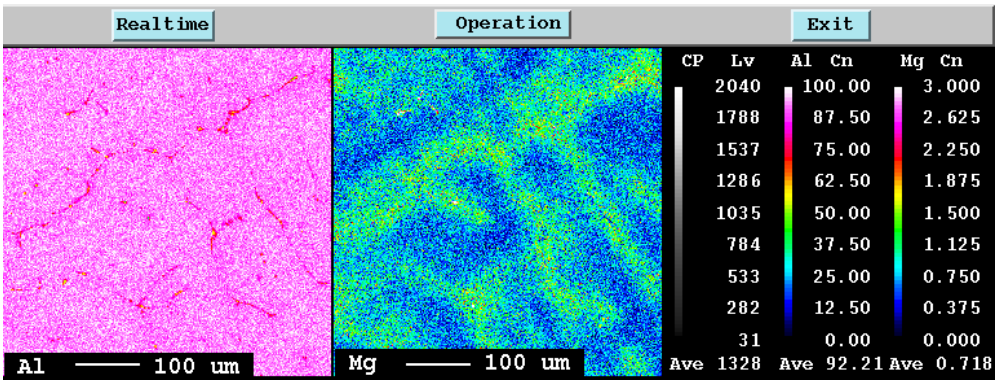

II.

Figure 4.17. EPMA analysis I) BSE image and II) composition map of Exp. 16.

The same process and phenomena are seen in EPMA BSE images Fig. 4.18, EPMA BSE image and element Map of “Exp.11 (40-0-5-Ar-1200-0.5)”, Grey matrix phase is more are than bright alloy phase.

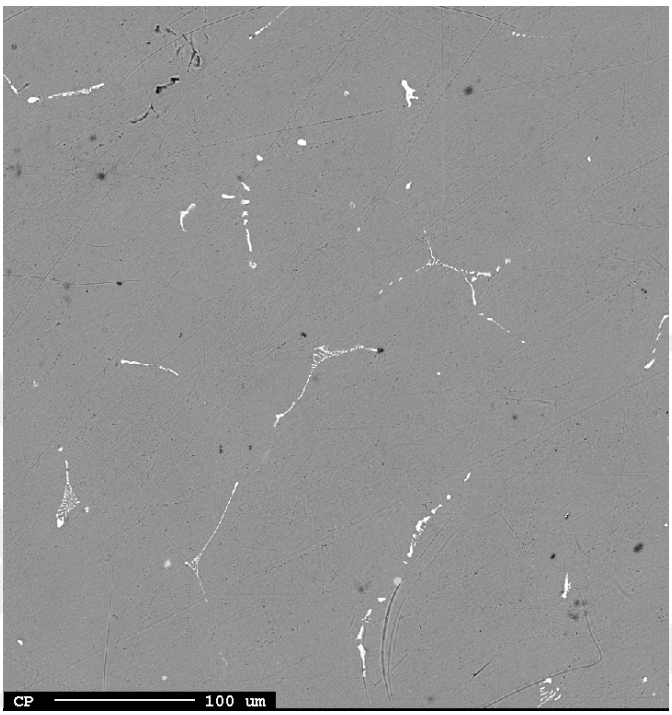

I.

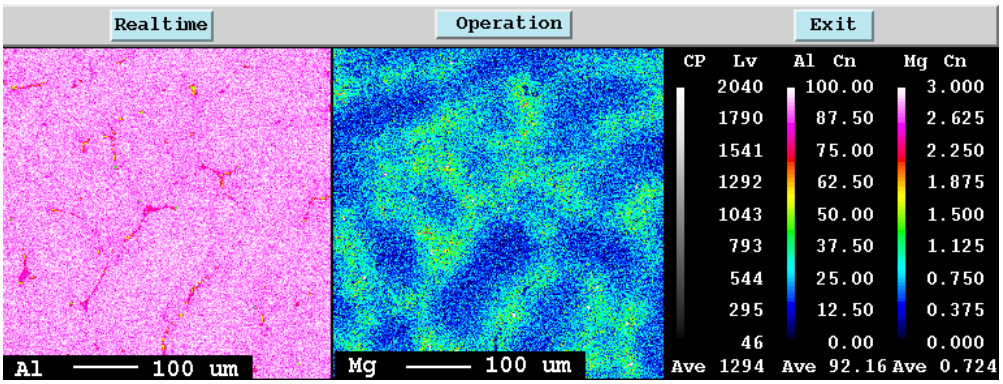

II.

Figure 4.18. EPMA analysis I) BSE and II) composition map of Exp. 11.

Diffusion of Mg is seen in matrix in composition map images Fig. 4.19 EPMA BSE image and element map of “Exp.15 (5-0-1-Ar-1200-0.5)”, higher quantity around GBs ranging ~0.75 wt% → 2–2.25 wt% → 3.0 wt%. Dark black spots are seen in the images which relate to the material's open pores or fissures.

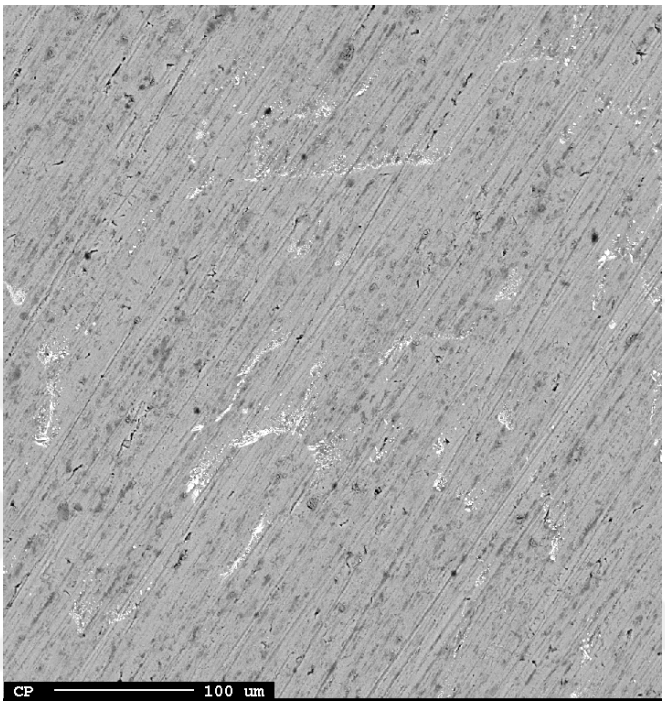

I.

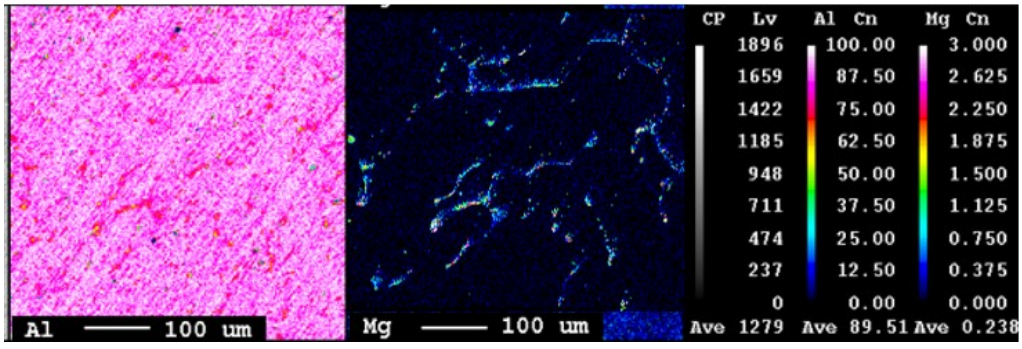

II.

Figure 4.19**.** EPMA analysis I) BSE and II) composition map of Exp. 15.

With EPMA elemental analysis, we found very few trace impurities of Fe and silicon, contradicting the results from this study. The Chinese script (dendrite-shaped) is formed but with a high Fe >18 wt% content in the alloy with Si acting as synthesizer and in this EPMA analysis we don't find such orthorhombic, 3D dendritic phase formation. Various phases seen in EPMA are shown in Table 4.1, which relate to earlier experiments' SEM and EDS results.

Table 4.1. EPMA elemental and phase distribution in EPMA images.

Si	Al	Mg	Ca	Fe	Phase
0.000	99.357	0.758	0.011	0.005	Al-Mg-Ca
0.000	99.132	0.861	0.000	0.007	Al-Mg
0.084	99.585	0.289	0.013	0.029	Al-Mg-Si
0.044	99.577	0.290	0.000	0.089	Al-Mg-Fe
0.000	99.445	0.526	0.025	0.004	Al-Mg-Ca
0.166	99,360	0.777	0.009	0.020	Al-Mg-Fe-Si
0.195	98.425	1.369	0.009	0.002	Al-Mg-Si

4.5. Analysis of Thermodynamic System

4.5.1. Aluminum-Magnesium (Al-Mg)

Is a system that defines all the phases and interactions in binary Al-Mg mixtures. It acts as a cornerstone of binary alloys in designing for specific applications, corrosion resistance, strength-to-weight ratio, ductility etc. The exact regulation of phase formation during solidification and heat treatment is made possible by the thermodynamic characterization of this system, which is essential for maximizing mechanical qualities particularly in the aerospace, automotive and marine sectors. The system features phase equilibria explaining solid-state solutions and intermetallics with Mg solubility in Al and how it affects the behaviour of the alloy. Some of the features are as:

A) Phase Diagram: Complete solubility in the liquid state and restricted solubility in the solid state are seen in the Al-Mg binary phase diagram. The system contains a eutectic reaction of about 450 °C and around 33 wt% magnesium Fig. 4.20. The diagram's main stages are as follows:

- α-Al (Face-Centred Cubic): A solid solution rich in aluminum that has a restricted solubility in magnesium. Maximum Mg solubility of 14.9 wt% at eutectic temperature.
- β-Mg (Hexagonal Close-Packed): A solid solution rich in magnesium that has minimal solubility in aluminum. Al solubility of 12.3 wt% is stable below 452C but is very brittle.
- The eutectic point is where the eutectic mixture (α + β) forms.

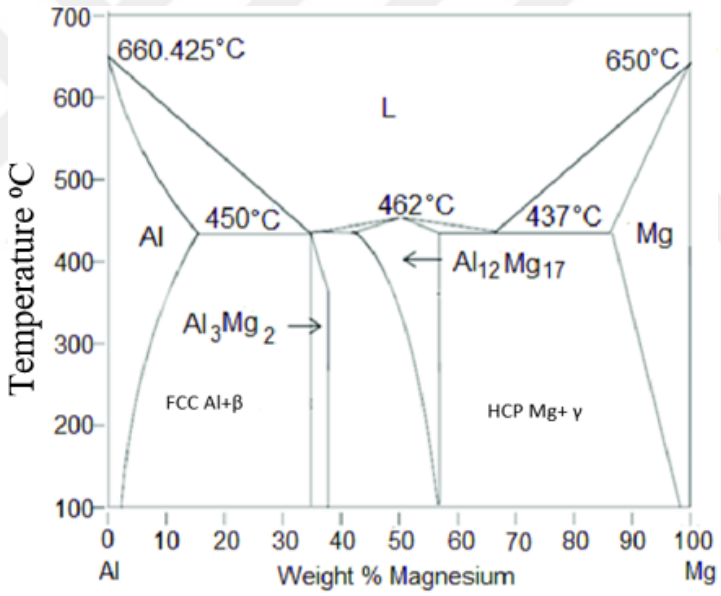

Figure 4.20. Al-Mg binary phase diagram.

- Intermetallic phases: In the Mg-rich area, they include Al_3Mg_2 (β-phase) and $Al_{12}Mg_{17}$ (γ-phase) are not much stable and tend to quickly dissipate into stable phases.

These characteristics show that although the elements are mutually soluble in the liquid state, depending on the content and temperature, their interaction in the solid-state causes phase separation or intermetallic production.

B) Activity and Solubility: Liquids exhibit high activity and negative deviation from ideality because the intermolecular attraction is higher than gasses increasing fugacity and solids exhibit more than liquids, hence Mg activity is higher in liquid Al. This forms one of the reasons for Mg involvement in readily making multiple component systems such as Al-Mg-Si, Mg_2Si precipitates, Al-Mg-Fe, Al-Mg-Mn phases.

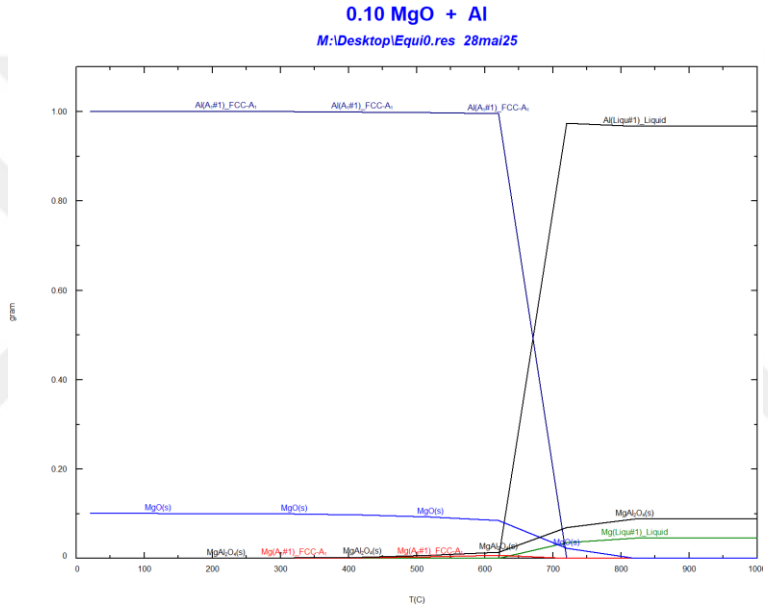

Figure 4.21. FACTSAGE predictions of alloy at 0.10 MgO content.

The products of this aluminothermic reduction are not pure Mg and alumina as expected since Mg forms intermediate and intermetallic phases, or aluminates and oxides, so pure alumina and Mg cannot coexist except at very high temperatures where Mg evaporates and is collected in the separate cooling chambers. As shown in the Fig. 4.21, for 10wt% Mg, the expected phases are formed at a temperature above the eutectic point, the spinels, and the alumina. According to the phase diagram at 800, the alloy should be in a liquid state, but that is not the case, as we see in the experiment. Al is liquid with powder Mg dispersed in it. Then, comparing with the SEM/EDS analysis in our study,

we find various phases matching the FACTSAGE calculation and theoretical expectations, which help us determine the interfacial reactions from the oxide and spinels at the point of contact between the raw materials. The same is seen in the Pure aluminum experiments in this study. At interface, the Al and MgO react creating new interfacial phases along the layers such as spinels and alumina the reactions are as:

$$4MgO + 2Al = MgAl_2O_4 + 3Mg \quad (4.1)$$

$$\Delta G^\circ = 66.7kJ, T = 1000\,^oC$$

$$4Al_2O_3 + 3Mg = 3MgAl_2O_4 + 2Al \quad (4.2)$$

$$\Delta G^\circ = -258.3kJ \quad T = 1000\,^oC$$

4.6. Enthalpy of Mixing and Activity

Enthalpies of mixing in liquid Al-Mg alloys have been measured by Moser et al.[48] by drop calorimetry at around 1025K. The enthalpies are in the negative and process is exothermic and consistent illustrated in Fig. 4.22. ΔH_{mix} values ranging from approximately –1 up to –10 kJ/mol in multiple studies done in many experiments, depending on composition and temperature. Another method used was with galvanic cells with solid electrolytes. CaF_2 electrolyte single crystal rod was used 921 to 1093 K at Mg mole fractions ranging between 0.05 to 0.90 also related to Moser et al.[48] showed negative enthalpies. Another few trails performed by Agarwal and Sommer (1974), using calorimetric methods for temperature around 973 K found exothermic enthalpy around -5 to -8 Kj/mol.[48,49]

Activities were calculated by using Galvanic cells with liquid electrolytes and found at X_{Mg} = 0.1 to 0.7 at temperature 910 to 1070K found Slight negative deviations from ideal and activity coefficient less than 1 across all compositions.[50] Tiwari et al.[50] studied the TD properties using EMF method. The activities of Mg alloy from 0 to 12 wt% concentration follow Henry's law. And shows low deviation from ideality raoult's law at 1073K. and activity is given by.

$$\alpha_{Mg} = 0.88\ X_{Mg} \text{ at } 1073\ K.$$

K = 0.88 Henry's constant.

For concentration of Mg >0.12, there follows a good relation between this study and Tsyplakova and Strelets study in the low concentration range.

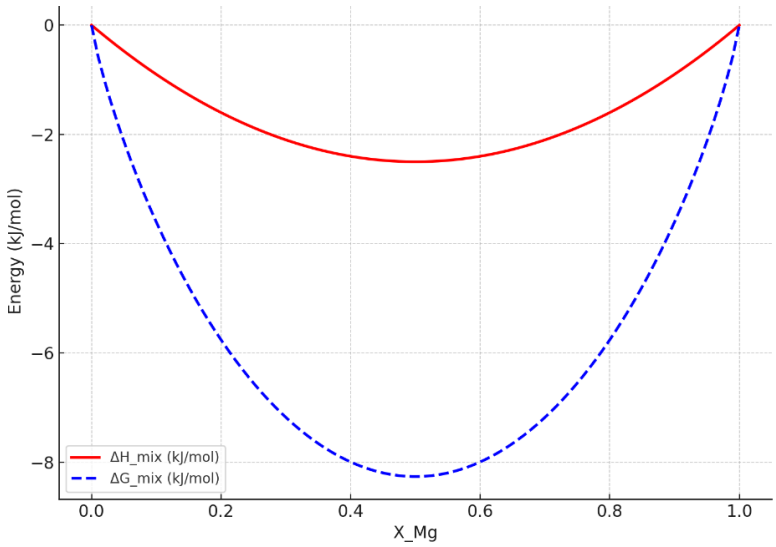

Figure 4.22. Enthalpy and Gibbs free energies of mixing vs Mg mole fraction T = 1000 °C.[44]

The reactions 14 and 15 are spontaneous and favour the Mg diffusion through the interface. Spinel layer is formed after Mg diffuses into Al melt and reacts with Alumina near the interface. Furthermore, these oxide layers reduce the vaporization of Mg, stabilizing the system. The activity of Mg in aluminum melt is vanishingly small. The Gibbs free energy driving force acts only in nucleation of new phases but for dissolution of Mg and its diffusion. Here the non-standard Gibbs free energy (ΔG^{o}) plays a crucial role in driving the reaction, such as,

$$\Delta G = \Delta G^{o} + RT\ln Q, \qquad \text{where } Q = \frac{aMg^{3}}{aAl^{2}} \tag{4.3}$$

The solubility limit of Mg in Al is ~14 wt%., activity of Mg in Al-Si alloy is very low = 0.130 at the beginning, Therefore, lnQ comes out to be -9.35. Hence RTlnQ = - 83.114 KJ/mol. T = 1073.15K

At equilibrium $\Delta G = 0$. So even if $\Delta G^0 = 50$ for the reaction at 800°C, the reaction still has standard ΔG negative making it a spontaneous reaction. Thus, the mass transfer from slag to melt is feasible and activity plays a good role in solubility of Mg in aluminum at moderate temperatures, until Mg content tends to reach an equilibrium, the percentage of Mg mass transferred in different experiments is given in quantification Table 4.2, 4.3 below.

4.7. Quantitative Analysis of Phases

In order to figure out the actual numbers of mass transfer from slag, the SEM images are quantified using ImageJ software, their phase composition is calculated mathematically, and quantity of elements and phases is determined as given in Table 4.2**.** The weight fraction is given by:

$$\text{Mass fraction of Mg} = \frac{(\text{VMg} \cdot \rho\text{Mg})}{\text{VAl}\cdot\rho\text{Al}+\text{VMg}\cdot\rho\text{Mg}} \qquad (4.4)$$

Where V_{Mg} = volume fraction of Mg, ρ_{Mg} = density of Mg metal, V_{Al} = volume fraction of Al, ρ_{Al} = density of Al. The data shows low concentration of (whiter) Mg phases in experiment where raw material is Al-Si. This is due to the reason that Mg after reduction into Al matrix forms different types of precipitates and phases. Resulting in less uniform distribution of Mg. This explains the reducibility of MgO in different redundants. In pure aluminum experiments (Exp. 1,2,5), Mg forms alloy phases, intermetallics as expected on the interface, and segregates along the grain boundaries in high amount. Weighting each phase with density, Al-Si is denser than Mg (1.738g/cm^3) this reduces the Mg relative mass transfer because Al-Si contributes more mass than pure Al in the same volume. Here we observe highest area fraction of 1 where pure aluminum and 15 wt% of MgO is used.

ImageJ quantitative data revealed that Mg phase mass fraction range from 1.2 to 2.4 in alloys containing Al-Si raw material due to their low visibility phase coverage in SEM images and for pure Al rage is higher. Area fraction of Al-Si-Mg phases and

precipitates is seen significantly higher than pure aluminum. The Table 4.2 below gives the quantitative data of only Al-Si-Mg phases in the resistance furnace (RF) and IF experiments.

To figure out how much magnesium is in each experiment's BSE SEM micrograph: Area fraction of Al matrix in all the experiment is given in table by subtracting the area fraction of bright phases with light grey (Si rich phase) in some experiments where available.

Al matrix area % = 100- (Mg area% + Si rich area%.) for experiments containing Si phase.

Al matrix area % = 100 – Area %, for experiments having only two bright and dark phases.

Table 4.2. Quantification data of Mg phase composition

Exp. No.	Alloy Area%	Si Rich Area %	Al Matrix Area %
1	3.134	--	96.866
2	0.882	--	99.118
3	0.463	15.251	84.286
4	0.391	6.658	92.951
5	0.975	--	99.75
6	0.422	13.252	86.326
7	0.359	14.25	86.386
8	16.845	---	83.854
10	0.4050	8.11	91.622

Table 4.3. Overall Mg concentration in various alloy experiments.

Experiment No.	Magnesium Content
1	0.3950
2	0.0017
3	0.8494
4	0.5943
5	0.3183
6	0.4422
7	0.5779
8	0.5908
10	0.7736
11	1.4
14	1.7
15	1.12
16	1.5

The overall Mg content available in all three phases in a sample SEM image observed with ImageJ line graph in Fig. 4.23.

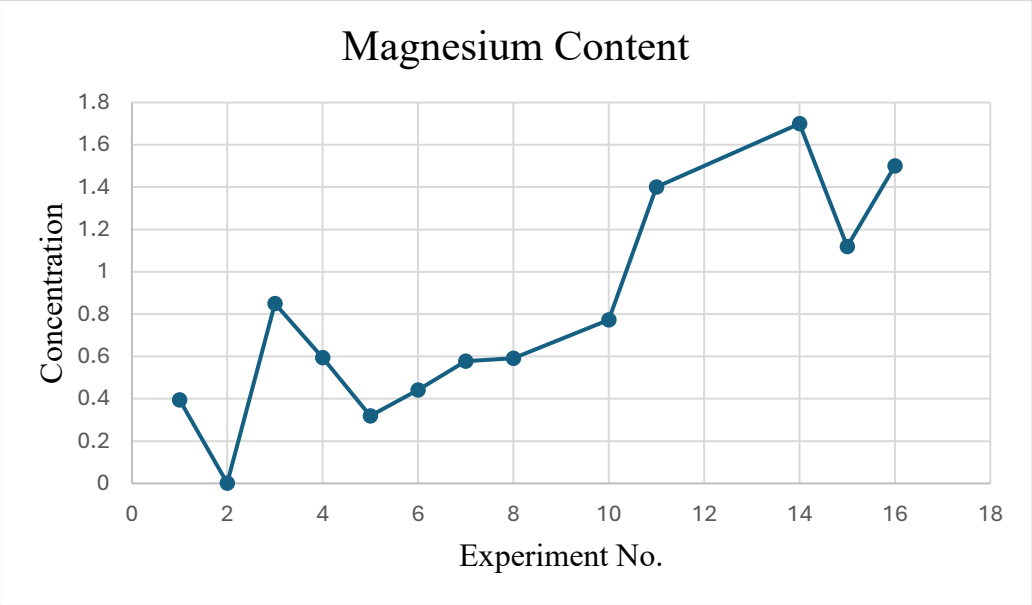

Figure 4.23. Total Mg wt% content in each experiment.

The exact numbers are presented in Table 4.3 above. We observe more combined Mg content is dissolved in Al-Si based experiments compared to pure Al based experiments highest Mg content is present in "Exp. 3 (0-150-10-Air-800-0.5)" where Al-Si raw material was used and for pure aluminum trails significantly less Mg is present.

This indicated that Si behaves as a catalyst in this reduction process and dissolution of Mg into liquid aluminum as well forming stable phases which aid in strength and tolerance of alloy. Pure Al solid raw material has 0.02% of Mg content. The Al-Si alloy has low tolerance to Mg diffusion and behaves as additive to other intermetallic formation in alloy.

Shown in bar graph Fig. 4.24, in both pure aluminum and Al-Si and based experiment, the difference in Mg content before and after alloy production is calculated mathematically. For Al-Si raw material the average Si wt%. content is calculated from OES analysis = 0.130. Pure aluminum has 0.02% Mg content. observing the graph, we see high content of residual Mg in Exp. 3, 4, 7 and 10, these experiments are Al-Si alloy based again proving our hypothesis. Experiments 11, 14, 15 & 16 were performed in muffle furnace at very high temperature, and we observe highest Mg solubility in these four trails.

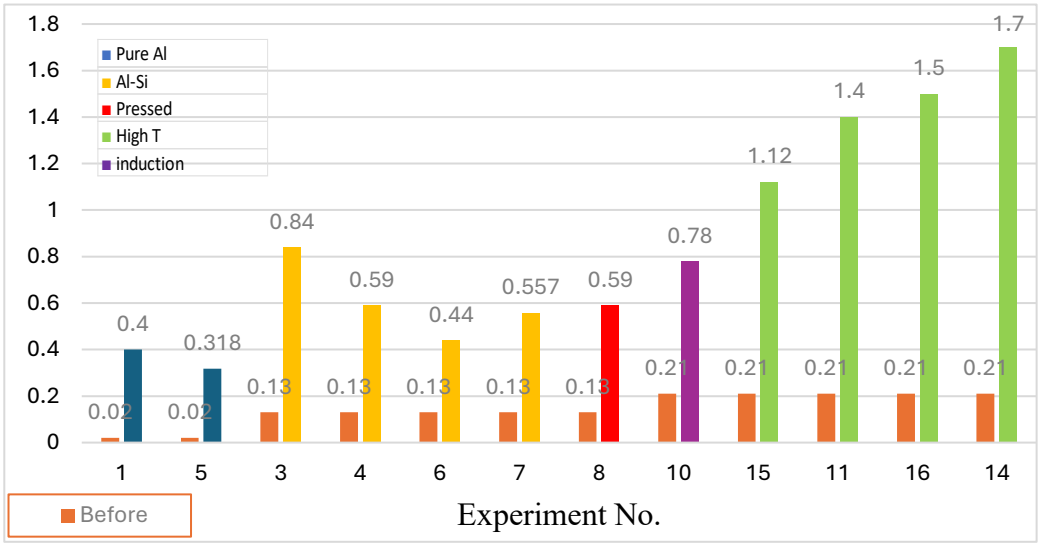

Figure 4.24. Mg wt% combined from all phases in all experiments after production.

To determine the residual Mg content in every sample, calculations are performed. In Table 4.4 below, we can see the final residual Mg content derived from the EDS analysis of all phases of the experiments. We observe a higher content of Mg in the matrix phase (phase 2) compared to the other two phases.

Table 4.4. Residual Mg content in different phases of different experiments.

Exp.	Raw Material	Phase 1 Mg Wt%	Phase 2 Mg Wt%	Phase 3 Mg Wt%	Final Mg Content	Oxide-metal Ratio
1	Pure Al	0.56	0.39	--	0.3950	1:15
2	Pure Al	0.47	0.001	---	0.0017	1:10
3	Al-Si	0.20	0.84	0.01	0.8494	1:15
4	Al-Si	0.24	0.61	0.26	0.5943	1:10
5	Pure Al	0.11	0.32	--	0.3183	1:15
6	Al-Si	0.24	0.38	0.1	0.4422	1:15
7	Al-Si	0.21	0.65	0.11	0.5779	1:10
8	Pure Al (powder)	0.77	0.55	--	0.5908	1:15
9	Al-Si	0.35	0.84	0.03	0.7736	1:15
11	Pure Al	40	35	--	1.4	1:8
14	Pure Al	29	40	--	1.7	1:15

Experiments 1,3,5, and 8 have only 2 phases, alloy, and matrix, due to the non-availability of Si raw material. “Exp.8 (5p-0-0.33-N-800-0.5)”, where the aluminum powder is compactly pressured before sintering in a tube furnace, shows high residual Mg in phase one because that high pressure reduces the porosity between the powder

particles and reduces the interaction distance between Al and MgO particles; hence, improving the reduction of MgO.

4.8 Grain Boundary Phenomena

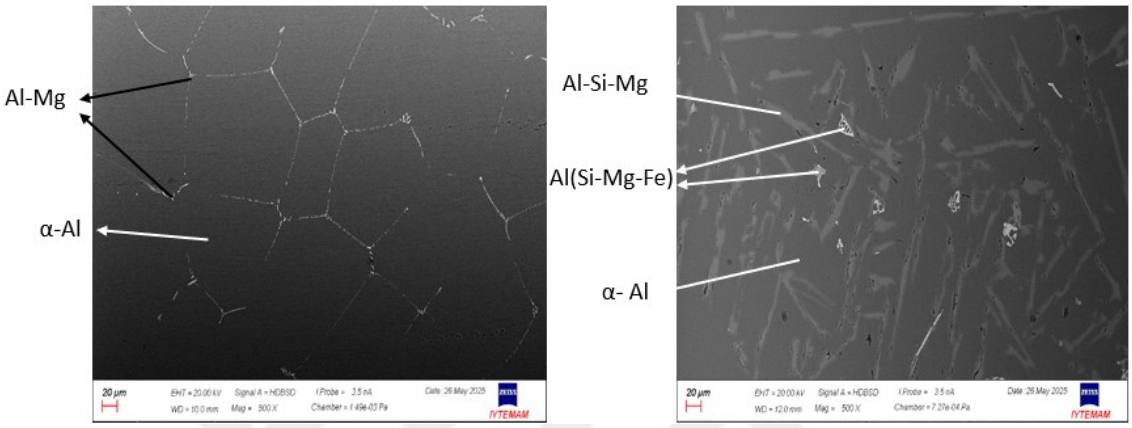

I) II)

Figure 4.25. SEM BSE images I) uses the pure aluminum shows prominent polygonal GB. II) uses the Al-alloy as raw materials nil or negligible GB are seen at very high magnification.

Pure aluminum produces a distinct spinel layer and Al particles at the interface upon reaction with oxide. Spinel has a better crystalline structure and allows clean grain boundary visibility. Bader's model predicted that charge transfer occurs between atoms at the interface of liquid Al-solid MgO. The ionic nature of MgO consists of O and Mg charges -1.3e and +1.3e, maintaining net zero; however, it is still less than the pure ionic charge of Mg (2e). Thus, charge transfer occurs, and nucleation occurs across the grain boundary. This results in the visibility of more prominent grain boundaries.

In Al-Si alloy, it enhances the reduction and reduces the viscosity of Al, forming thick spinels and more precipitates as it ages. Si also forms Mg-silicate phases around 594°C precipitates and segregates along the boundaries as a coating[51]. Non-stoichiometric Al or Mg-rich alloy phase is not well oriented, hence degrading the grain's prominent shape. Furthermore, the eutectic reactions of the Al-Si system create fine

grains of various phases in microstructure at around 450ºC. Fig. 4.25 two SEM topography micrographs are shown, it is also clear that prominent grain boundaries are visible in pure aluminum alloy with Mg segregation mostly along grain boundaries.

CHAPTER 5

CONCLUSION

In this study, the aluminothermic reduction process of MgO was studied in presence of Aluminum as reductant in pure form and Al-Si alloy form. Trials were conducted at two holding temperatures a) 15-30 min and b) 4 hours with max temperature of 800ºC and compared with muffle furnace experiments performed at 1200ºC with HT less than 30 min and less raw material content, to study the effect on phase formations and solubility of MgO. The effect of MgO wt% and holding time was investigated to determine the solubility of MgO around melting point of Aluminum.

The overall conclusion that is drawn from these results is that the aluminothermic reduction of MgO in presence of Aluminum resulted in formation of various phases of Al-Mg alloy. Mg solubility in Al, mass transfer and deposition along the grain boundaries in the aluminum matrix could be seen. In some areas MgO reduction has Mg segregated across the GB leading to formation of $Al_{12}Mg_{17}$ and into different phases, Chinese-script morphology in some experiments.

Results summarized:

- The reacted alloy had a high content of Al and Mg in dark regions; SEM images indicate a partial reduction of MgO in the matrix as more Mg is dissolved in the matrix phase in all experiments compared to other Si phases (grey). However, Mg shows relative solubility, and the content observed is dispersed non uniformly. It was clear that homogenous and partial reduction of MgO resulted in Mg dissolution in liquid Al at a slow dissolution rate.

- Various microstructures are seen in the SEM micrographs; pure aluminum containing trails show well-defined grain boundaries and only two phases in a homogeneous matrix (Fig. 3.9,3.10,3.11). The substitutional solid solution is observed, leading to Mg diffusion in the matrix. The Mg segregated along the grain boundaries to reduce the internal stress, which is proven by EPMA analysis. The Al-Si raw material containing samples shows three different phases

with no prominent grain boundaries, but the phases appear distinct in color, texture, and shape. The grey color phase is a rich precipitate formed during the hardening of the alloy. The grain size is non-unform and of different shapes.

- Diffusion of solute in liquid metal and their nucleation leads to the formation of different phases depending on the parameters, conditions, and internal dynamics. Three phases are formed in this study throughout all experiments viz, bright, light grey, and dark. The bright region is the Al-Mg phase with a small impurity of Si and O2. The same is seen in EPMA analysis, which is rich in α-Al and Al_3Mg_2 intermetallic phases, and spinels as well during the interfacial reaction. The light grey phase long needle shaped, is formed only in experiments containing Al-Si alloy as raw materials indication eutectic Mg_2Si phase. This Si has played a key role in Mg reduction and diffusion. Forming a precipitate (Si-rich) phase in the matrix as MgSi2, AlMg. The dark Al matrix also has the highest quantity of Al and Mg content, implying that Mg is widely dispersed and soluble through the matrix due to its activity.

- At interface of MgO and Liquid aluminum, ist reaction occurred is formation of Al oxide and Mg aluminate spinel due to the reason that oxides are most stable compounds and upon contact with Oxygen from MgO, aluminum readily forms thin layer of Aluminum to dissipate the interfacial energy and reducing further formation of the passive layer. Hence, higher temperature is required to further dissolve the MgO into liquid aluminum.

- Eutectic reactions resulted in formation of β- and γ- Phases of Al-Mg-Si, FIMCs in A6XXX alloy which is nonstable intermetallic but is stabilized by Si in mixture.

- Formation of binary eutectic (AlMgFeSi) FIMCs, non-planner, non-uniform Chinese script-like shaped β-phases in the matrix in 3, 4, 6, 7, and 10 experiments due to high iron content > 18wt% Fig. 4.10. Which according to literature is shown to improve the tensile strength of the alloy significantly, however iron content could reduce the corrosion resistance property. These phases increased in volume with increasing Mg concentration in α-Al phases. They start to get coarser and thicker, and these phases are strengthened by a small amount of Si acting as

synthesizers of this odd shape and assisting stability. Mg segregates on the Al-Fe alloy during its growth and enhances the heterogeneous nucleation, and more Mg content makes more potent MgAl2O4, improving 3D Chinese-script morphology. This morphology grows due to its anisotropic growth, leading to branches in different low-energy planes [110] direction. The α-Al and Chinese-script phases grow at different speeds, allowing α-Al to fill the gaps between the branches and lock the matrix strictly.

- Quantification analysis revealed that grey intermetallic phases (Al-Si) have more area fraction than pure aluminum phases, comparing Tables 7 and 8. Using EDS analysis, we calculated that more solubility of Mg (Table 4.3, figure 4.23) was found in experiments containing Si as a raw material graph and more in the Al-rich (dark phases) matrix than others, shown in EDS scans. The highest overall Mg content was observed in the 3 experiment and the least in 2; this is because Al-Si alloy forms different metallic precipitates and phases with Mg, and a uniform distribution is limited in the matrix. Comparing the graphs in Figures 4.22 and 4.23, we can see an increase in residual Mg quantity and a higher number is seen from Al-alloy-based experiments compared to pure aluminum alloys. This indicates that Si plays a significant role in the solubility of Mg across the interface and the formation of Al-Mg alloy.

- The longer holding temperature is found not to affect Mg dissolution in the matrix significantly. However, the involvement of Si in the system has considerably improved the MgO reduction and solubility of Mg at a moderate temperature of $800^{O}C$. Nevertheless, observing the FIMCs, we find that longer holding times help the formation of coarser, vivid, and larger volumes compared to resistance furnace experiment SEM images with muffle furnace SEM images. With phase shape changing from sharp to 3D and Chinese script with increasing Mg content

5.1. Final Conclusions

1. Silicon content present raw materials positively improves the solubility of Mg in liquid aluminum.
2. High temperature leads to more Mg diffusion across the interface between oxide and metal.
3. Rapid uniform heating of induction furnace has no significant effect on phase formations and solubility of Mg unless currents induce Lorentz force causing magneto-stirring.
4. In tube furnace experiment where Compact pressured raw materials show higher Mg content Fig. 4.8, indicates the close interaction of raw materials particles resulted in more reduction of MgO compared to pure aluminum experiments.
5. Si helps in synthesis of FIMCs with Al-Mg-Fe phase, forming Chinese-script morphology.

Future Work

- Deeper analysis of phases which are formed at different production processes using other various analysis techniques.
- Exploring the possibility of lowering the reduction temperature of MgO using some methods or addition of catalysts to make the process more energy efficient and economical.
- Exploring different compositions to investigate effects of minor alloying elements such as Mn, Si, Zn, Cu on microstructure, phase formations and how varying their content affects phase stability and mechanical properties.
- With Optical Emission Spectroscopy can gain more detailed information from structure and elemental composition.
- Conduct aging studies over a lengthy period of time to assess phase stability at high temperatures.
- Could be possible to add Nickel in the production and form a supper alloy. Study the Thermo-Mechanical fatigue (TMF) resistance in the alloys.

BIBLIOGRAPHY

1. Kainer, K. U.; Von Buch, F. The Current State of Technology and Potential for Further of Magnesium Applications. *Magnesium-Alloys and Technology* **2003**, 1–22.
2. Zhang, T.; Wang, M.; Niu, L.; Zhang, J.; Zhang, H.; Zhang, M. Novel Approach to Prepare Magnesium and Mg-Al Alloy from Magnesia by Using the Closed Microwave Aluminothermic Method. *Metals* **2023**, *13*, 905.
3. Belov, N.A.; Naumova, E.A.; Akopyan, T.K.; Doroshenko, V.V. Phase Diagram of Al-Ca-Mg-Si System and Its Application for the Design of Aluminum Alloys with High Magnesium Content. *Metals* **2017**, *7*, 429.
4. Zolotorevskiy, V. S.; Belov, N. A.; Glazoff, M. V. Casting Aluminum Alloys; *Elsevier:* Amsterdam, Netherlands, 2007.
5. Mondolfo, L. F. *Aluminium Alloys: Structure and Properties*; Butterworths: London, UK, 1976.
6. Salas Avilés, J. A.; Flores Valdés, A.; Torres Torres, J.; Ochoa Palacios, R. M.; Flores Saldívar, A. *A.* A Kinetic Study on the Preparation of Al-Mn Alloys by Aluminothermic Reduction of Mn_3O_4 and MnO Powders. *Metals* **2023**, *13* (9).
7. Snopiński, P.; Tański, T. Thermal Stability and Microstructure Evolution of Ultra-Fine Grained Al-Mg Alloy. *IOP Conf. Ser. Mater. Sci. Eng.* **2018**, *461*, 012085.
8. Xing, Z.; Lu, J.; Ji, X. A Brief Review of Metallothermic Reduction Reactions for Materials. *Small Methods* **2018**, *2* (12).
9. Maqbool, A.; Khan, N. Z.; Siddiquee, A. N. Towards Mg Based Light Materials of Future: Properties, Applications, Problems, and Their Mitigation. *J. Manuf. Sci. Eng.* **2022**, *144* (3), 803–815.
10. Song, C.-R. Recent Progress of Al-Mg Alloys: Forming and Preparation, Microstructure Manipulation and Application. *J. Mater. Res. Technol.* **2024**, *31*, 3255–3286.
11. Wang, Y.; You, J.; Peng, J.; Di, Y. Production of Magnesium by Vacuum Aluminothermic Reduction with Magnesium Aluminate Spinel as a By-Product. *JOM* **2016**, *68*, 1728–1736.
12. Xu, J.; Zhang, T.; Li, X. Research on the Process, Energy Consumption and Carbon Emissions of Different Magnesium Refining Processes. *Materials* **2023**, *16*.
13. Ghali, E.; Revie, R. W. Corrosion and Its Control of Aluminum and Magnesium Alloys: Understanding, Engineering, and Performance; *ASM International*, **2020**.
14. Mathaudhu, S.; Luo, A.; Neelameggham, N.; Nyberg, E.; Sillekens, W. Essential Readings in Magnesium Technology; *Springer Cham*, 2016.
15. Hort, N.; Huang, Y.; Kainer, K. U. Intermetallics in Magnesium Alloys. *Adv. Eng. Mater.* **2006**, *8* (4), 235–240.
16. Chapman, G. R. Magnesium—Making Light of Resources. *Miner. Process. Extr. Metall.* **2002**, *111* (2), 49–52.
17. Skinner, H. *C. W.* The Web of Magnesium. *Int. Geol. Rev.* **2005**, *47* (11), 1111–1119.
18. Fridlyander, I. N. Aluminum Alloys: Promising Materials in the Automotive Industry. *Met. Sci. Heat Treat.* **2002**, *44*, 365–370.
19. Joost, W. J.; Krajewski, P. *E.* Towards Magnesium Alloys for High-Volume Automotive Applications. *Scripta Mater.* **2017**, *128*, 107–112.

20. Miller, W. Recent Development in Aluminum Alloys for the Automotive Industry. *Mater. Sci. Eng. A* **2000**, *280*, 37–49.
21. Kumar, D. S.; Sasanka, C. T.; Ravindra, K.; Suman, K. N. S. Magnesium, and Its Alloys in Automotive Applications – A Review. *Am. J. Mater. Sci. Technol.* **2015**.
22. Chapman, G. R. Magnesium—Making Light of Resources. *Mineral Process. Extr. Metall.* **2002**, *111* (2), 49–52.
23. Tan, J.; Ramakrishna, S. Applications of Magnesium and Its Alloys: A Review. *Appl. Sci.* **2021**, *11* (15), 6861.
24. Zhang, Y. Researching on the Dynamics and Parameters' Optimization of Smelting Magnesium by Silicon-Thermo-Reduction; *Changchun*, 2013.
25. Geological Survey. U.S. Geological Survey. *Mineral Commodity Summaries* **2024**.
26. Guo, T.; Geng, Y.; Song, X.; Rui, X. Tracing Magnesium Flows in China: A Dynamic Material Flow Analysis. *Resour. Policy,* **2023**, *83,* 103627.
27. Li, S.-S.; Yue, X.; Li, Q.-Y.; Peng, H.-L.; Dong, B.-X.; Liu, T.-S.; Yang, H.-Y.; Fan, J.; Shu, S.-L.; Qiu, F.; Jiang, Q.-C. Development and Applications of Aluminum Alloys for Aerospace. *J. Mater. Res. Technol.* **2023**, *27*, 944–983.
28. *Mineral Commodity Summaries* **2025**; US Geological Survey, 2025.
29. Schulz, P.; Berneder, J.; Uffelmann, D.; Zelger, C.; Melzer, C. Advanced 5xxx-, 6xxx- and 7xxx- Aluminium Alloys for Applications in Automotive and Consumer Electronics. *Mater. Sci. For.* **2011**, *690*, 451–454.
30. Dieringa, H.; Kainer, K. U. *Magnesium and Magnesium Alloys*. In Springer Handbook of Materials Data; Warlimont; Martienssen, H., Eds.; Springer: Cham, 2018.
31. Eugene Wong, W. L.; Gupta, M. High Performance Lightweight Magnesium Nanocomposites for Engineering and Biomedical Applications. *NanoWorld J.* **2016**, *2* (4).
32. Tian, Y. Analysis of Magnesia Carbothermic Reduction Process in Vacuum. *Mater. Trans. B,* **2014**, *45*, 1936–1941.
33. Kipouros, G. J.; Sadoway, D. *R.* Toward New Technologies for the Production of Magnesium. *JOM* **1998**, *50* (5), 22–24.
34. Lee, T. *H.* Development of a Novel Electrolytic Process for Producing-Purity Magnesium Metal from Magnesium Oxide Using a Liquid Cathode. *J. Magnes. Alloy* **2021**, *9*, 1644–1655.
35. Guo, J.; Li, X.; Zhang, T. Comparison of Extraction Behavior of Magnesium from Magnesite/Magnesia by Aluminothermic Process in Flowing Argon. *J. Sustain. Metall.* **2022**, *8*, 1756–1768.
36. Watson, E. B.; Price, J. D. Kinetics of the Reaction MgO + Al_2O_3 → $MgAl_2O_4$ and Al-Mg Interdiffusion in Spinel at 1200 to 2000 °C and 1.0 to 4.0 GPa. *Geochim. Cosmochim. Acta* **2002**, *66* (12), 2123–2138.
37. Takei, H. Epitaxial Growth of $MgAl_2O_4$ Spinel Crystals by Solid-State Reaction of MgO Crystal with Molten Al Metal. *Mater. Res. Bull.* **1976**, *11* (10), 1265–1272.
38. Ohya, Y.; Ishii, Y.; Ban, T. Reaction of Molten Aluminum with MgO and Formation of $MgAl_2O_4$ at 1000 °C. *Mater. Trans.* **2020**, *61* (2), 339–345.
39. Fujii, H.; Nakae, H. Three Wetting Phases in the Chemically Reactive MgO/Al System. *ISIJ Int.* **1990**, *30*, 1114–1118.
40. Matsushita, T.; Belov, I.; Siafakas, D. Interfacial Phenomena Between Molten Iron and Molten Slag-Effect of Nitrogen on the Marangoni Convection. *J. Mater. Sci.* **2021**, *56*, 7811–7822.
41. Tekuchev, V. V.; Kalinkin, D. P.; Ivanova, I. *V.* Electrotransfer in Liquid Binary Aluminum Alloys. *Russ. J. Phys. Chem.* **2018**, *92*, 1435–1437.

42. Weirauch, D. *A.* Interfacial Phenomena Involving Liquid Metals and Solid Oxides in the Mg-Al-O System. *J. Mater. Res.* **1988**, *3*, 729–739.
43. Kammerer, C. C.; Fu, M.; Zhou, L.; Keiser, D. D.; Sohn, Y. *H.* Interdiffusion and Reaction Between Pure Magnesium and Aluminum 6061. *Defect Diffus. Forum* **2015**, *364*, 157–164.
44. Brown, J. A.; Pratt, J. N. The Thermodynamic Properties of Solid Al−Mg Alloys. *Metall. Trans.* **1970**, *1*, 2743–2750.
45. Li, R. B.; Zhang, S. J.; Guo, L. J.; Wei, J. J. Numerical Study of Magnesium (Mg) Production by the Pidgeon Process: Impact of Heat Transfer on Mg Reduction Process. *Metall. Mater. Trans. B* **2014**, *45*, 236–250.
46. Que, Z.; Mendis, C. *L*. Effects of Native AlN Particles on Heterogeneous Nucleation in an Al-3Fe Alloy. *Metall. Mater. Trans. A* **2021**, *52* (2), 553–559.
47. Que, Z.; Zhou, Y.; Wang, Y.; Mendis, C. L.; Fan, Z. Effects of Mg Addition on the Al6(Fe,Mn) Intermetallic Compounds and the Grain Refinement of α-Al in Al-Fe-Mn Alloys. *Mater. Charact.* **2021**, *171*, 110758.
48. Moser, Z.; Zakulski, W.; Rzyman, K.; Gasior, W.; Panek, Z.; Katayama, I.; Matsuda, T.; Fukuda, Y.; Iida, T.; Zajaczkowski, Z.; Botor, J. New Thermodynamic Data for Liquid Aluminum-Magnesium Alloys from emf, Vapor Pressures, and Calorimetric Studies. *J. Phase Equilib.* **1998**, *19* (1), 38–47.
49. Yu, Q. C.; Deng, Y.; Yin, S. B.; Li, Z. Y. Thermal Process for Magnesium Production with Al-Si-Fe from Coal Ash: Thermodynamics and Experimental Investigation. *J. Min. Metall. B* **2021**, *57* (3), 421–430.
50. Tiwari, B. *L.* Thermodynamic Properties of Liquid Al-Mg Alloys Measured by the Emf Method. Metall. *Trans.* **1987**, *18* (9), 1645–1651.
51. Georgatis, E.; Lekatou, A.; Karantzalis, A. E.; Petropoulos, H.; Katsamakis, S.; Poulia, A. Development of a Cast Al-Mg2Si-Si In Situ Composite: Microstructure, Heat Treatment, and Mechanical Properties. *J. Mater. Eng. Perform.* **2013**, *22* (3), 729–741.

APPENDIX A

EDS ANALYSIS IMAGES

In this appendix section, the EDS point ID analysis images and tables of all the experiments from resistance and tube furnace are given which show different elemental composition.

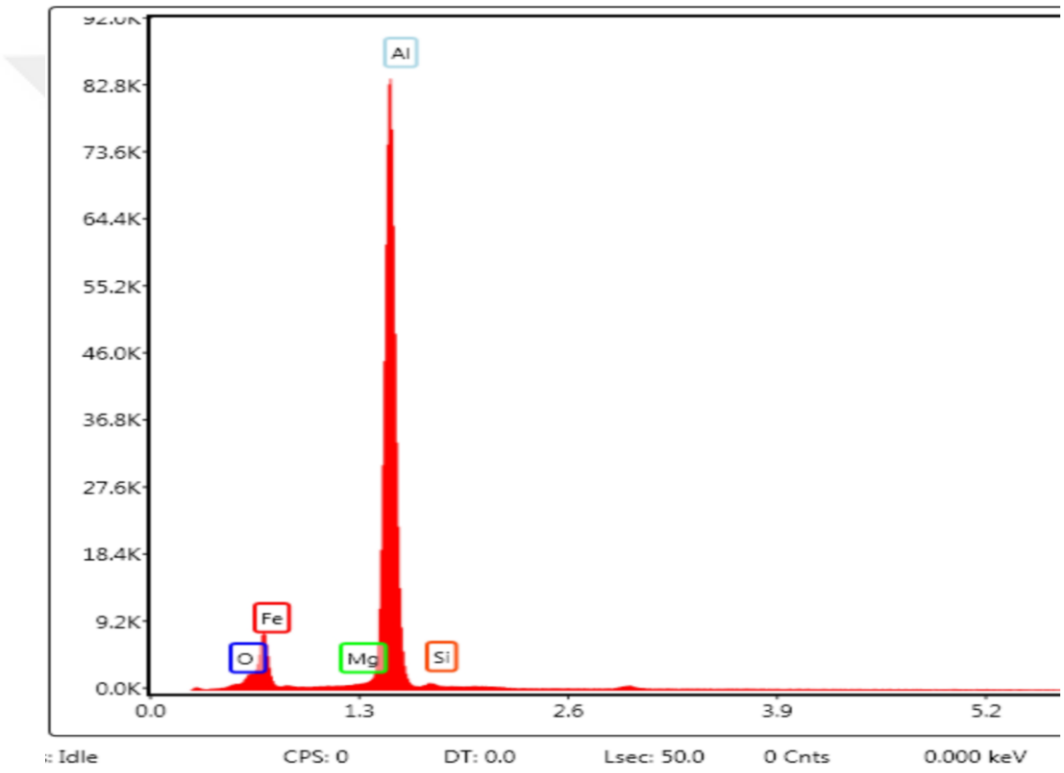

Figure A.1. EDS scans of point 1 experiment 1.

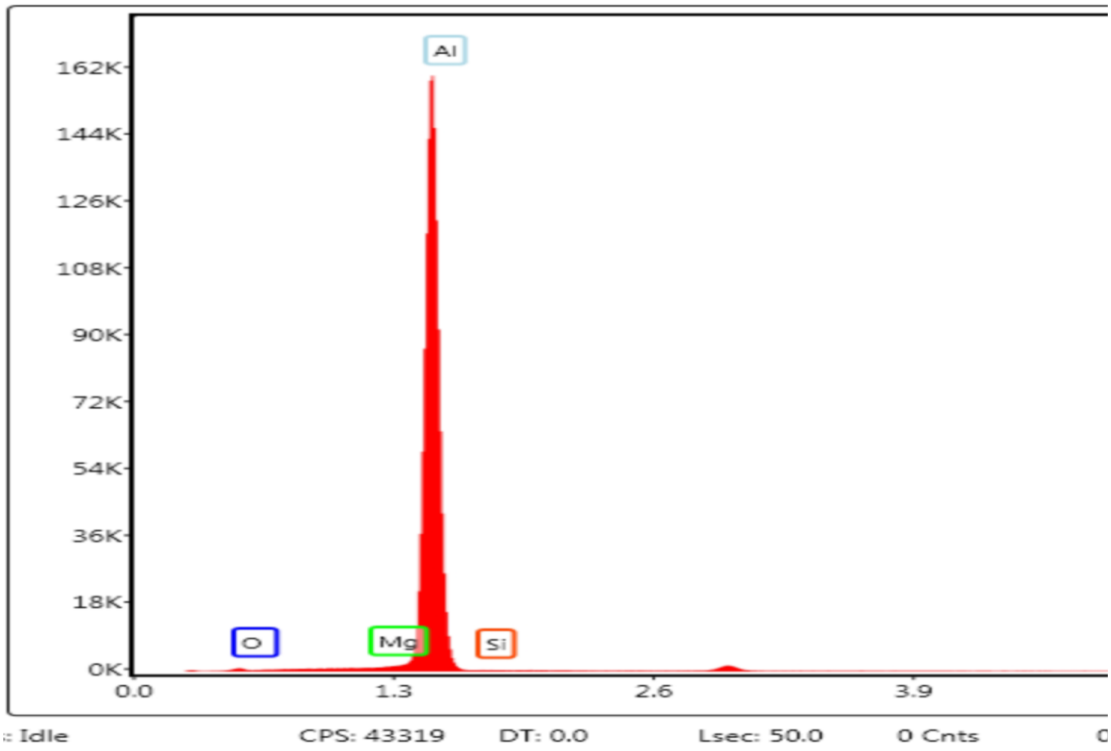

Figure A.2. EDS scans of point 2 experiment 1.

Table A.1. Concentration Measurement experiment 1.

Measurement	O%	Al %	Mg%	Si%
POINT 1	0.51	71.07	0.56	1.96
POINT 2	0.08	98.63	0.39	0.9

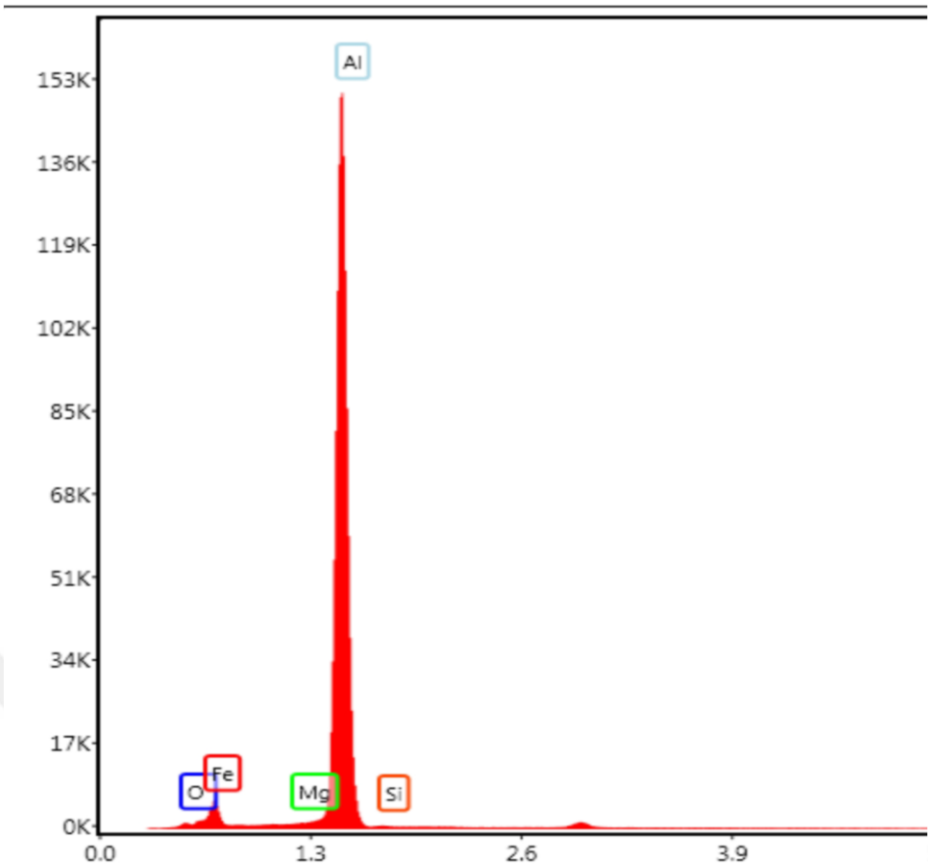

Figure A.3. EDS scans of point 1 experiment 2.

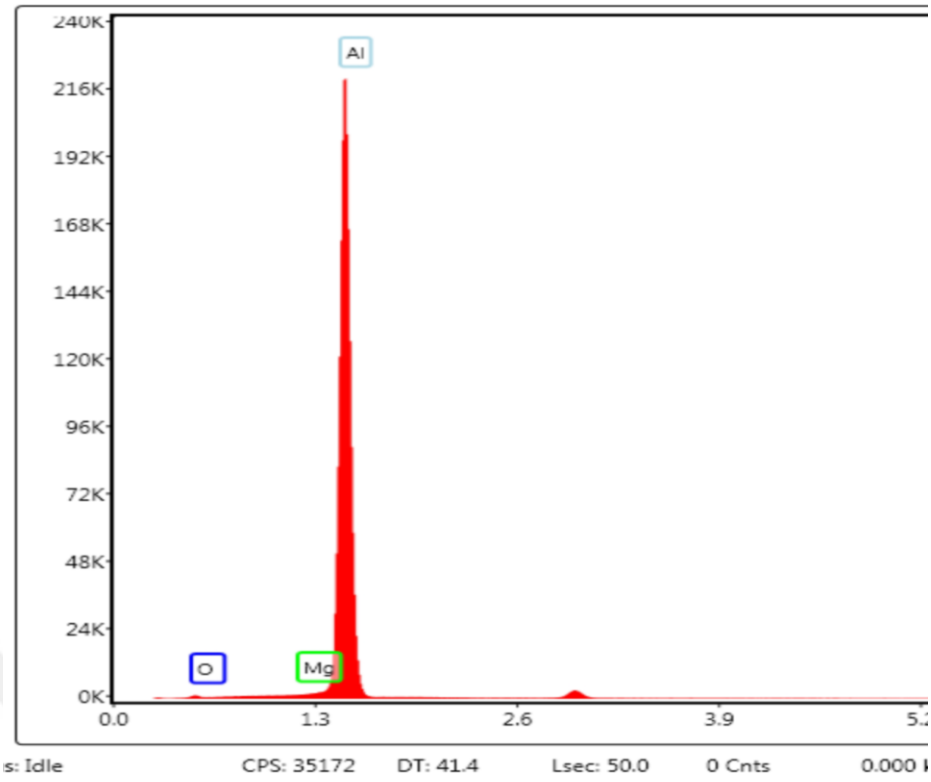

Figure A.3. EDS scans of point 2 experiment 2.

Table A.2. Concentration measurement experiment 2.

Measurement	O%	Al %	Mg%	Si%
POINT 1	0	81.98	0.20	0.64
POINT 2	0	100	0	0

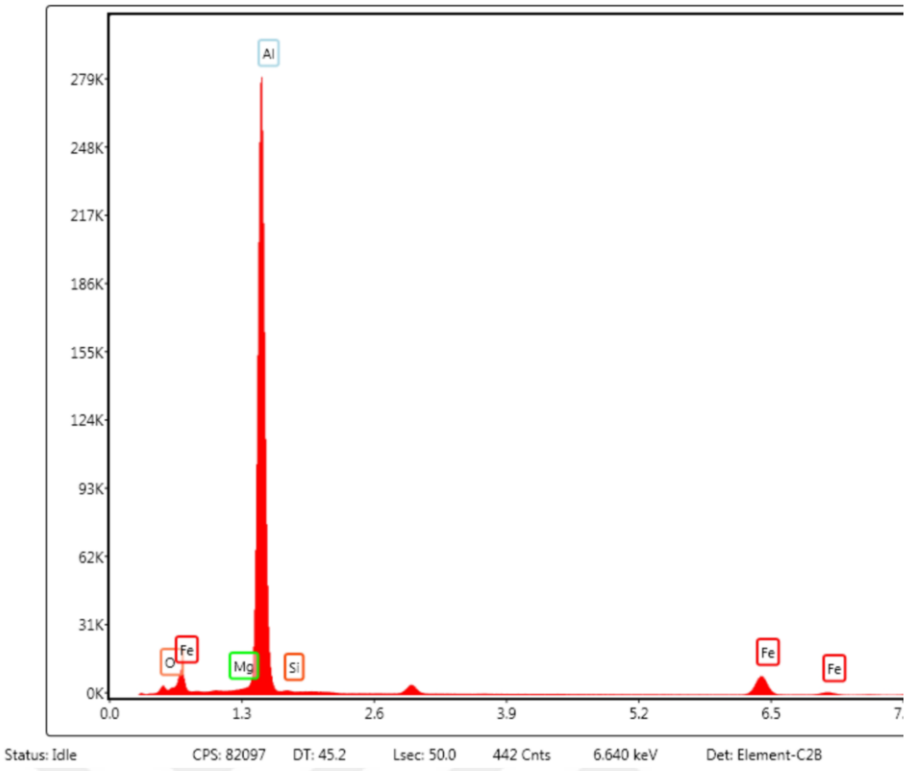

Figure A.4. EDS scans of point 1 experiment 5.

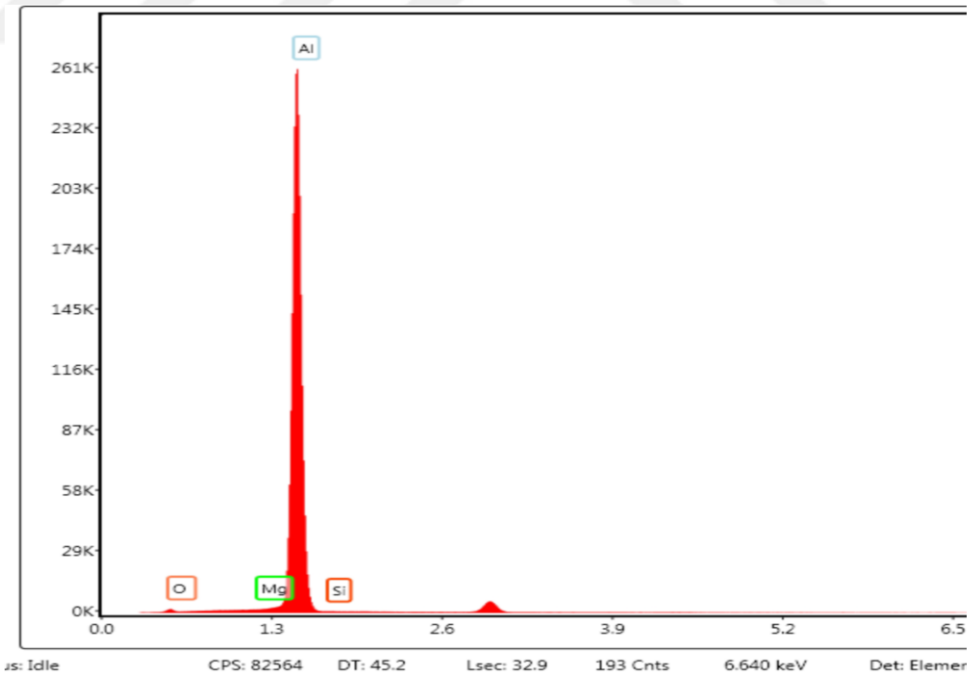

Figure A.5. EDS scans of point 2 experiment 5.

Table A.3. Concentration measurement experiment 5.

Measurement	O%	Al %	Mg%	Si%
POINT 1	1.16	81.81	0.11	1.69
POINT 2	0.32	98.15	0.32	1.22

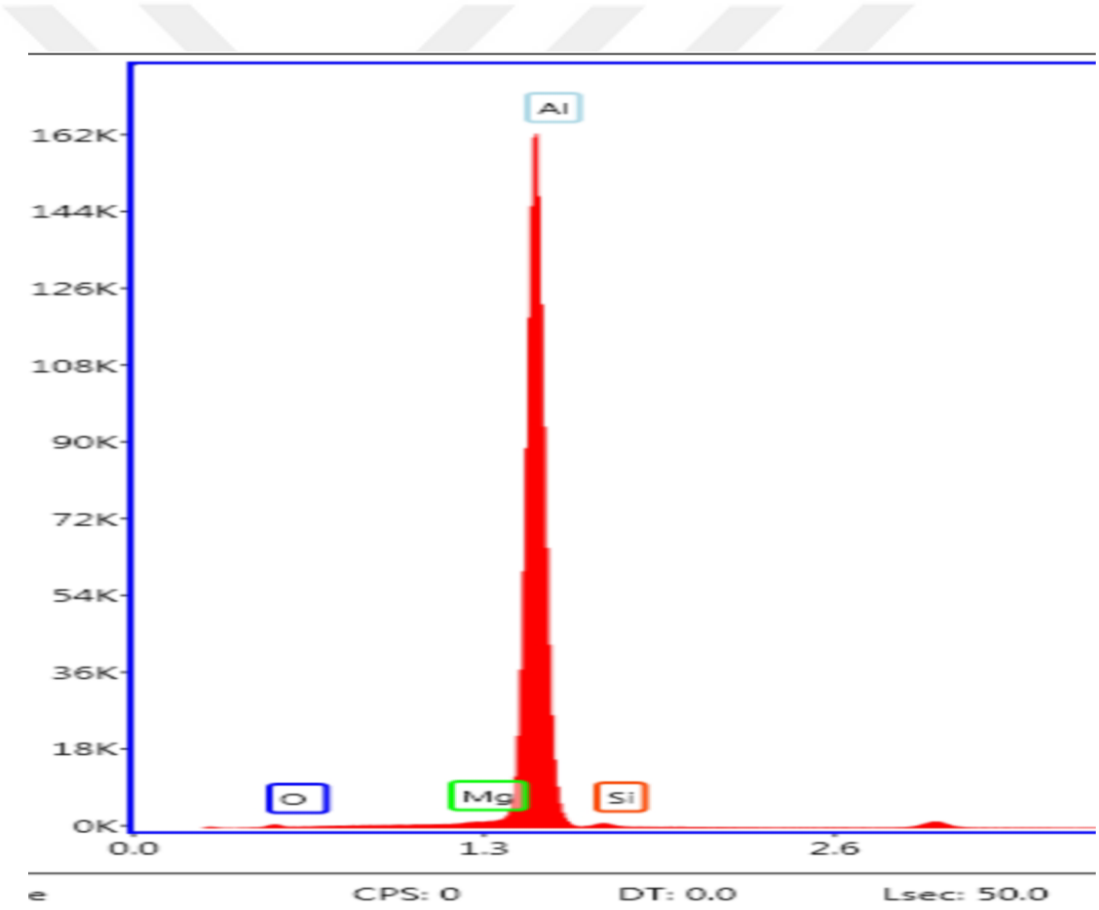

Figure A.6. EDS scans of point 1 experiment 3.

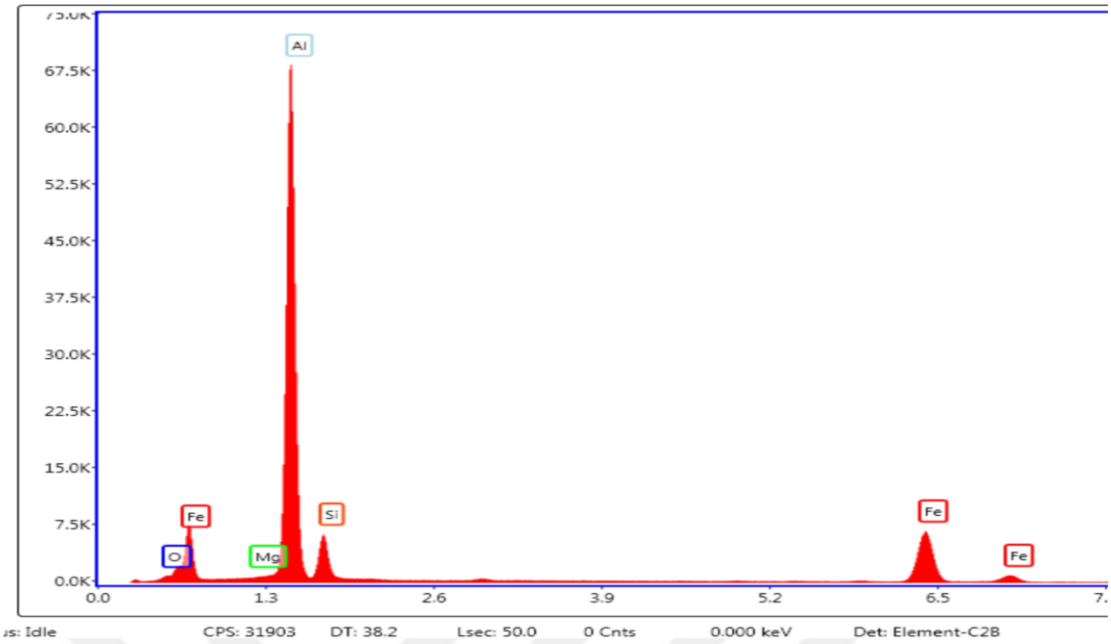

Figure A.7. EDS scans of point 2 experiment 3.

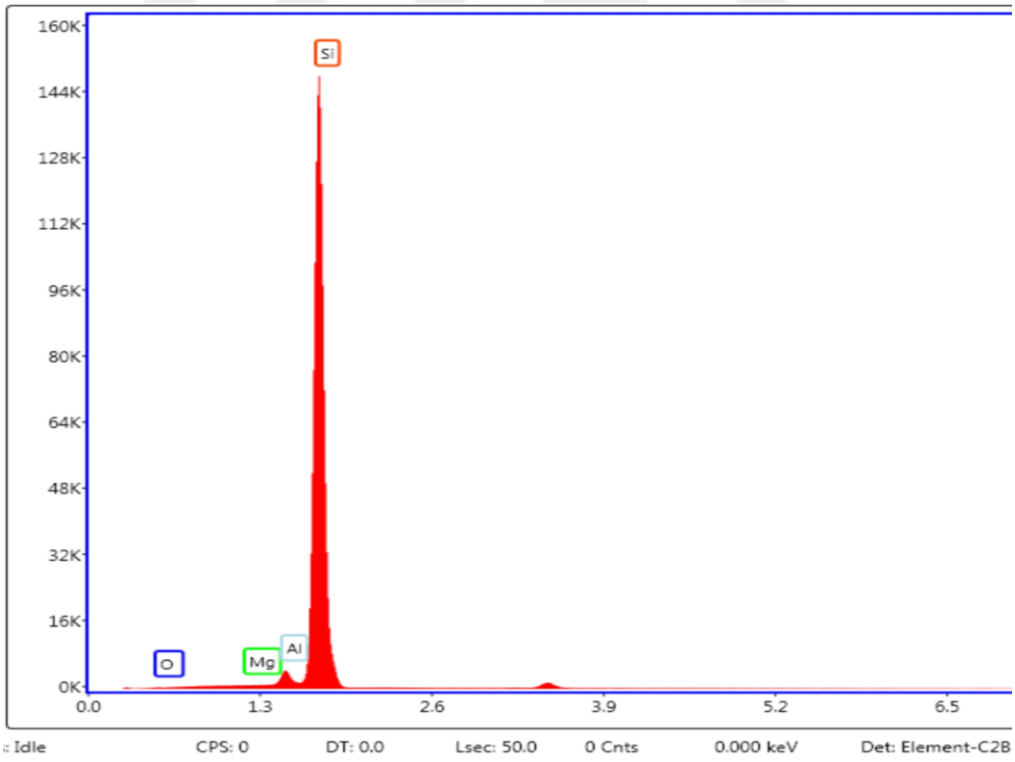

Figure A.8. EDS scans of point 3 experiment 3.

Table A.4. Concentration measurement experiment 3.

Measurement	O%	Al %	Mg%	Si%	Fe%
POINT 1	0.26	59.93	0.20	9.56	30
POINT 2	0.35	96.33	0.84	2.48	00
POINT 3	0	2.41	0.01	97.58	00

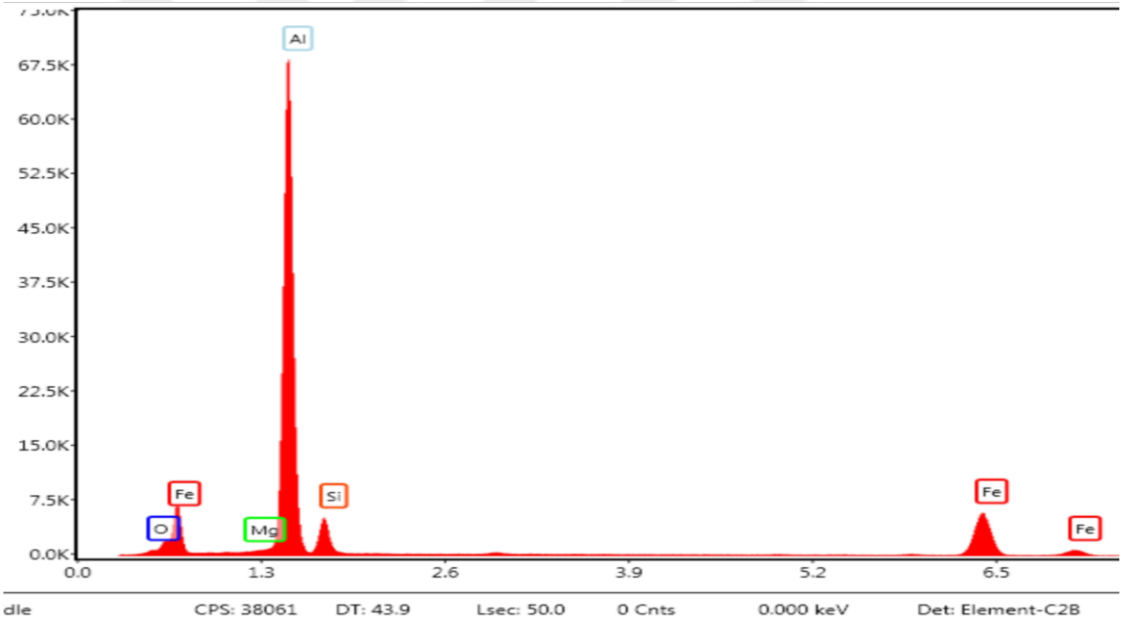

Figure A.8. EDS scans of point 3 experiment 3.

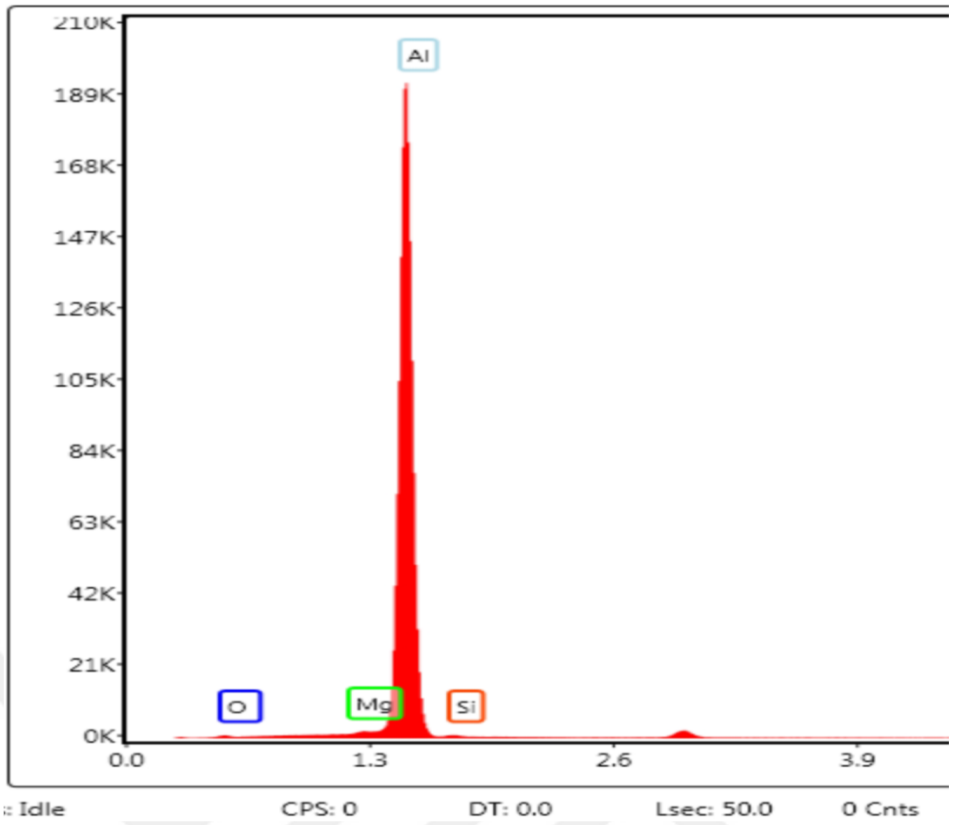

Figure A.9. EDS scans of point 1 experiment 4.

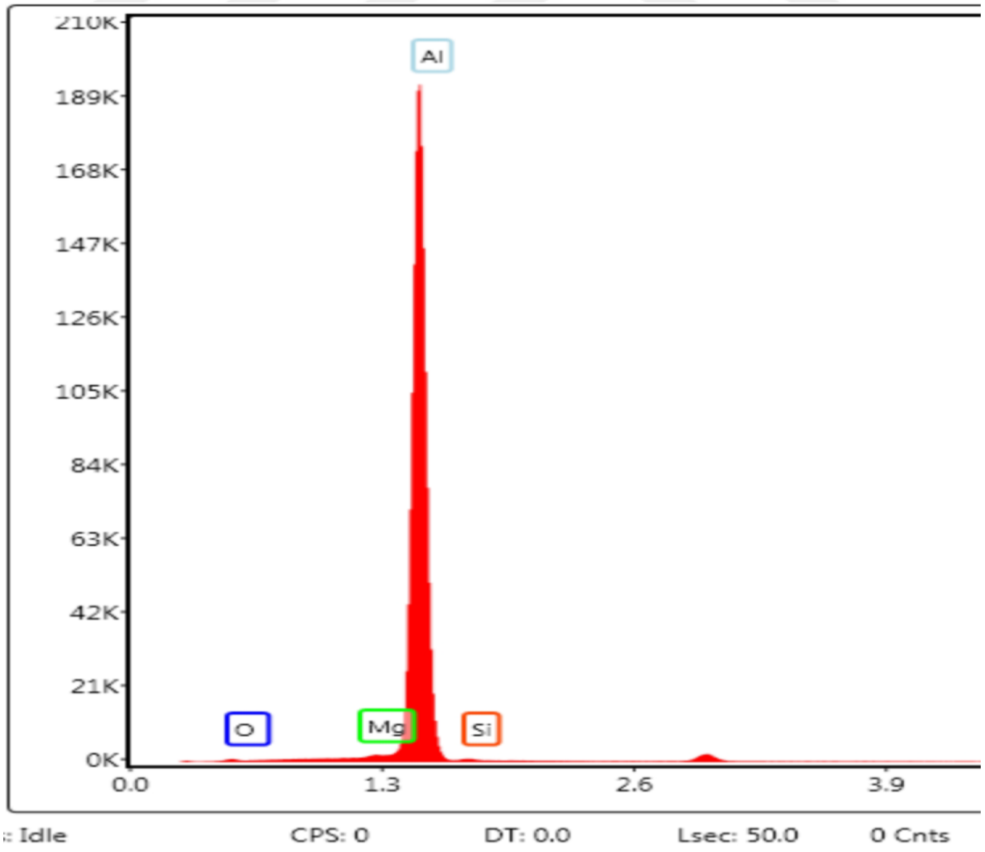

Figure A.10. EDS scans of point 2 experiment 4.

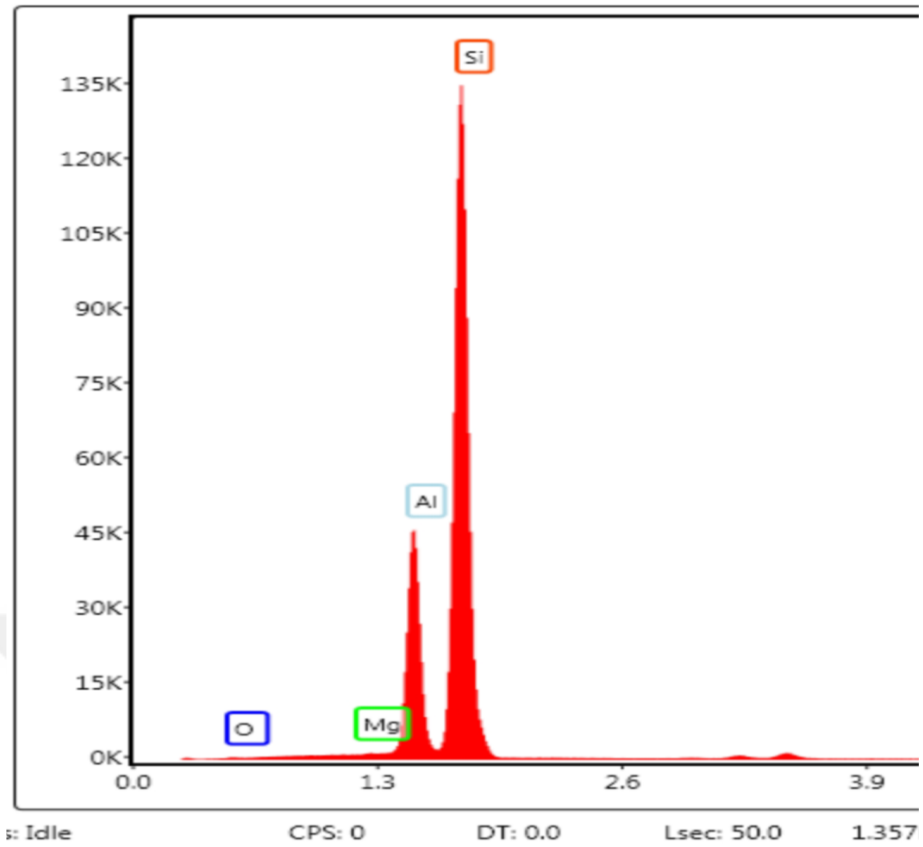

Figure A.11. EDS scans of point 3 experiment 4.

Table A.5. Concentration measurement experiment 4.

Measurement	O%	Al %	Mg%	Si%	Fe%
POINT 1	0.29	62.82	0.24	8.28	28.37
POINT 2	0	97.74	0.61	1.65	---
POINT 3	0	20.31	0.26	79.43	-----

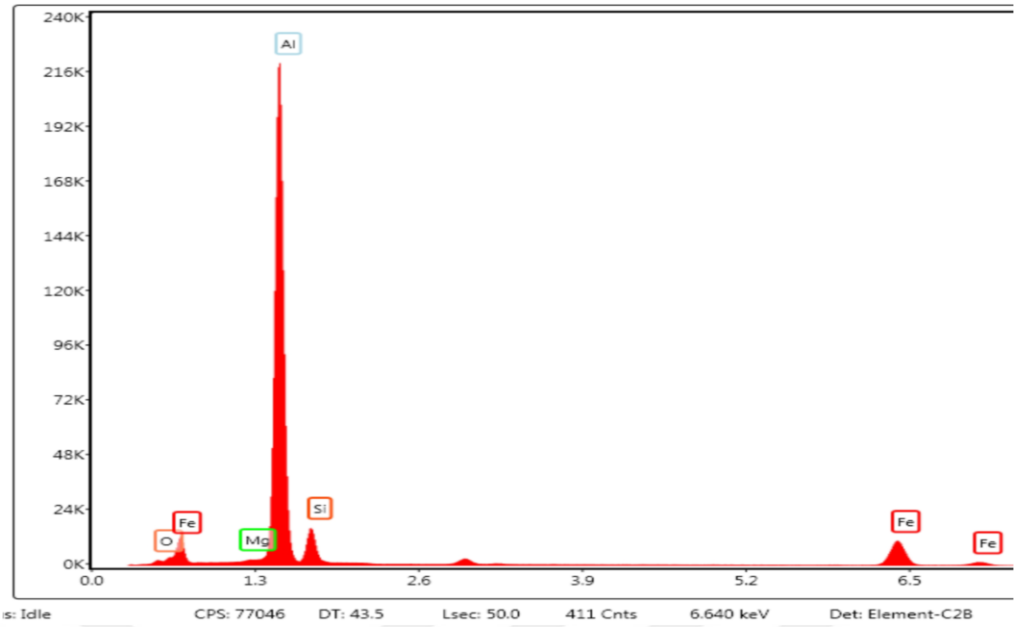

Figure A.12. EDS scans of point 1 experiment 6.

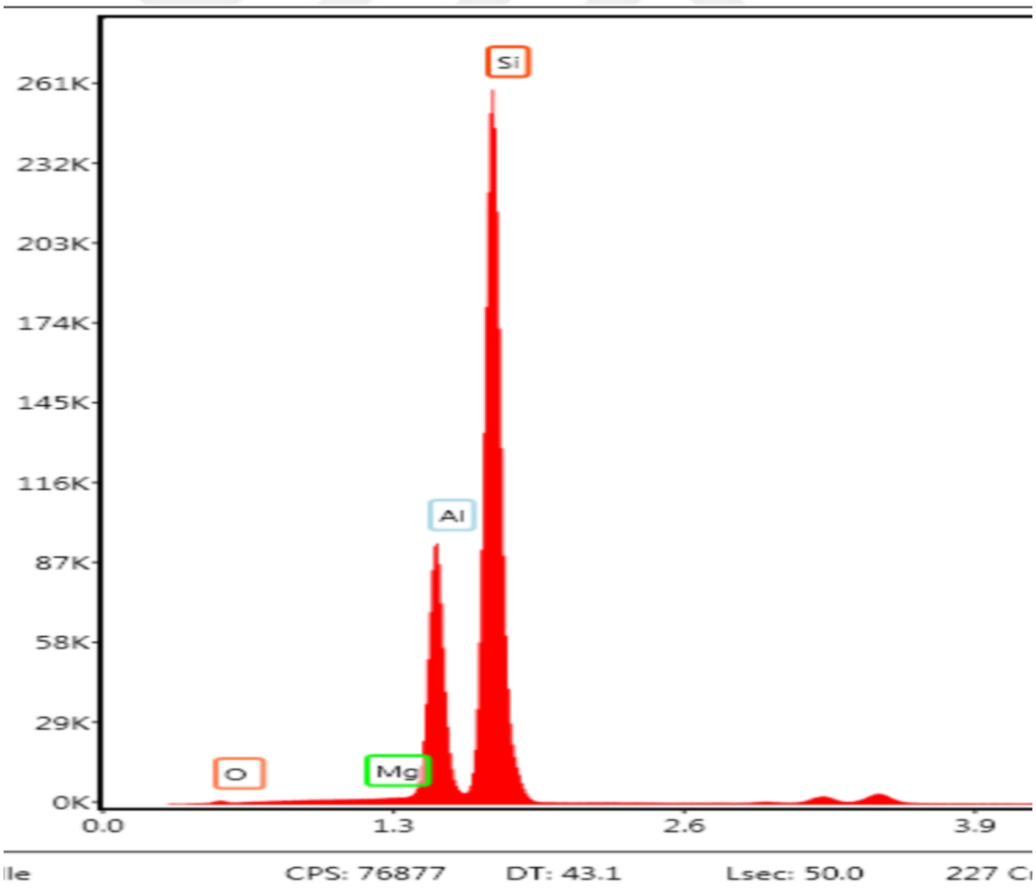

Figure A.13. EDS scans of point 2 experiment 6.

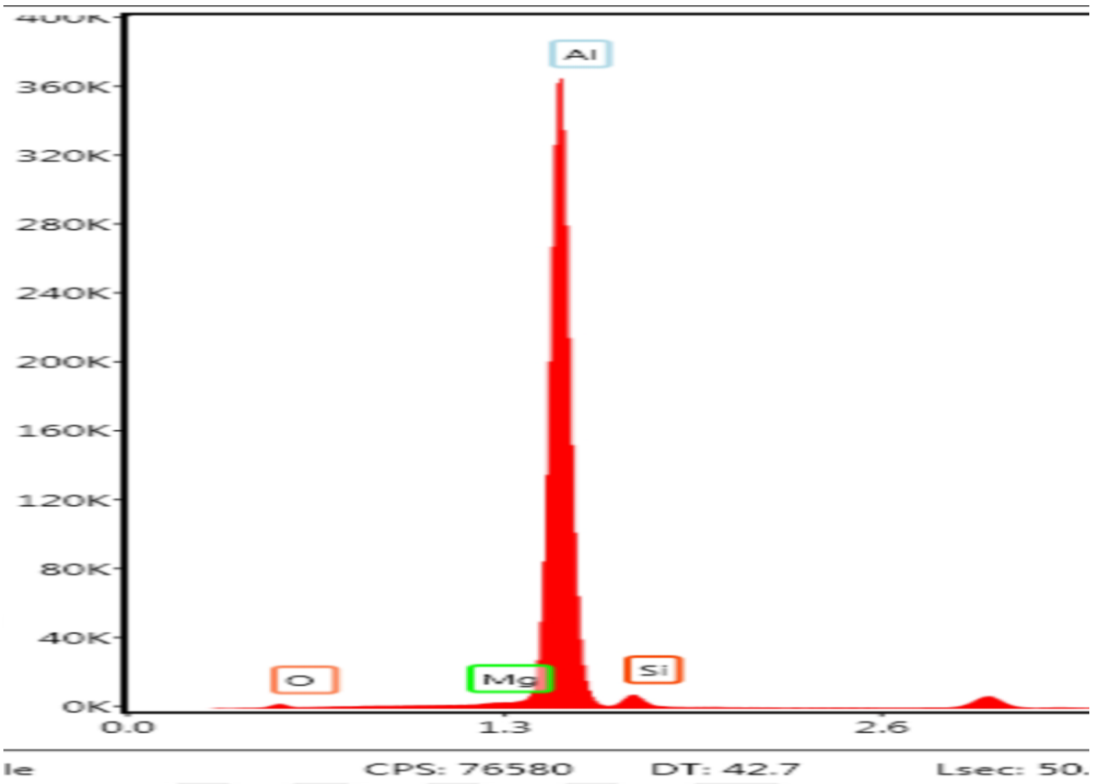

Figure A.14. EDS scans of point 3 experiment 6.

Table A.6. Concentration measurement experiment 6.

Measurement	O_2%	Al %	Mg%	Si%	Fe%
POINT 1	0.21	69.33	0.24	10.37	19.85
POINT 2	0.01	21.14	0.1	78.76	00
POINT 3	0.35	93.06	0.38	6.22	00

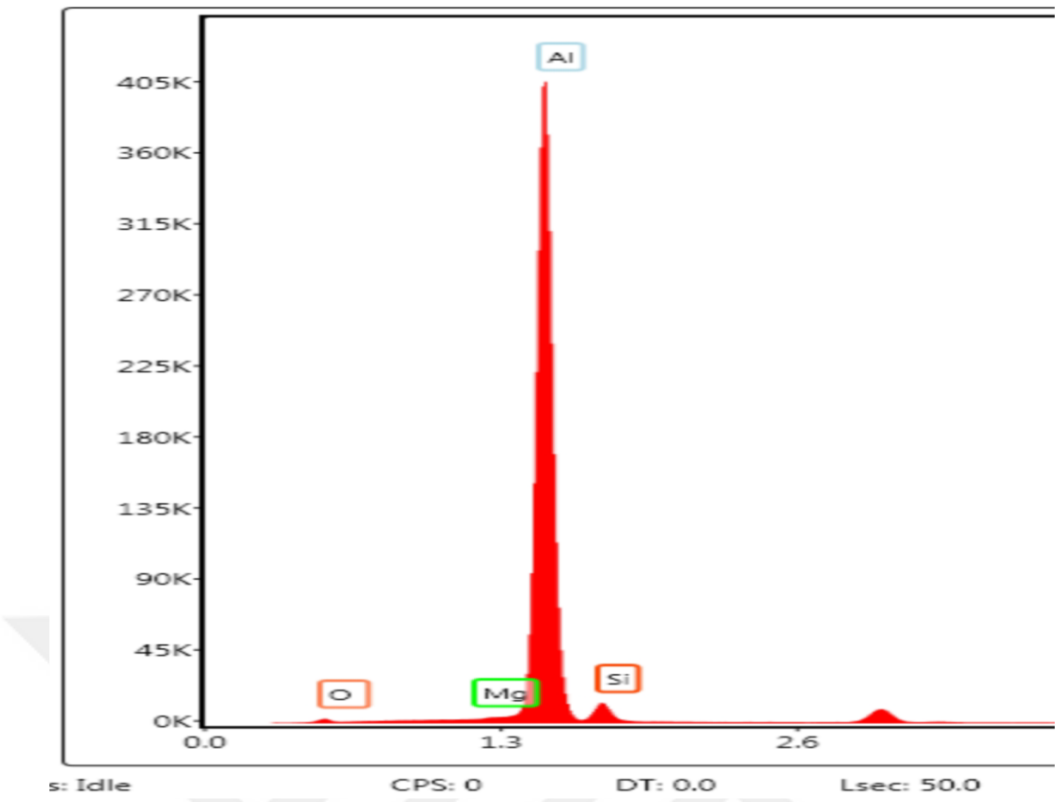

Figure A.15. EDS scans of point 1 experiment 7.

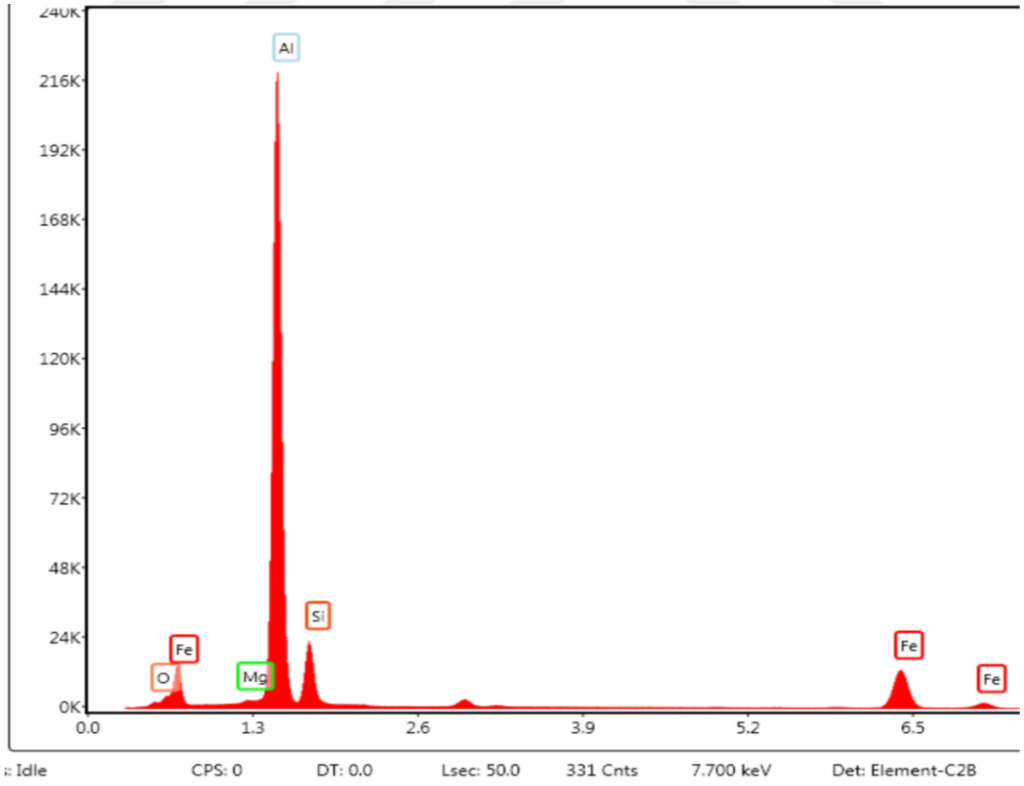

Figure A.16. EDS scans of point 2 experiment 7.

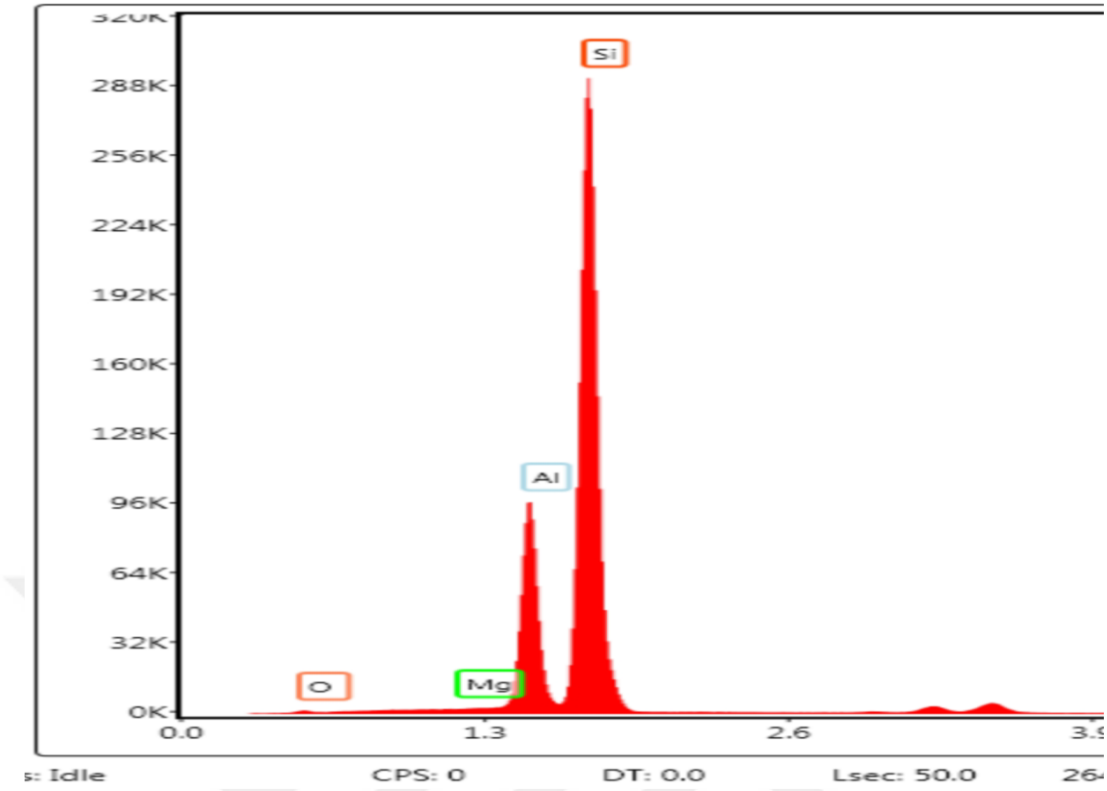

Figure A.17. EDS scans of point 3 experiment 7.

Table A.7. Concentration measurement experiment 7.

Measurement	O_2%	Al %	Mg%	Si%	Fe%
POINT 1	0.09	64.81	0.21	13.03	21.86
POINT 2	0.02	19.84	0.11	80.02	00
POINT 3	0.55	90.16	0.65	8.64	00

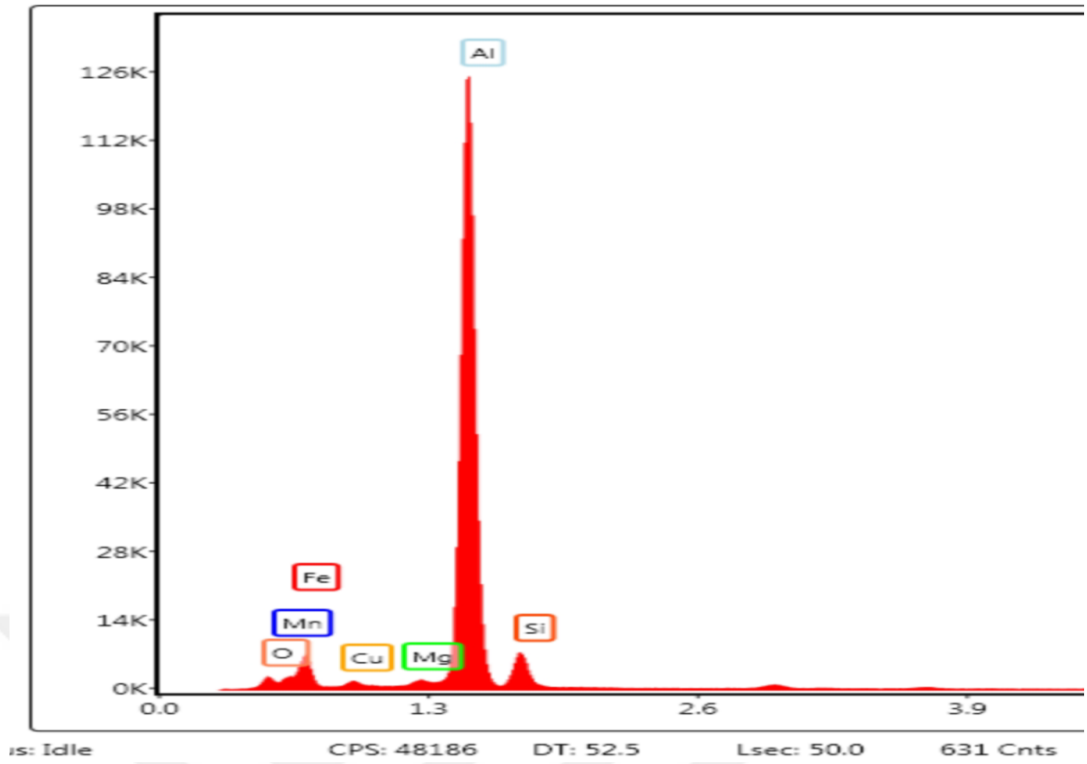

Figure A.18. EDS scans of point 1 experiment 8.

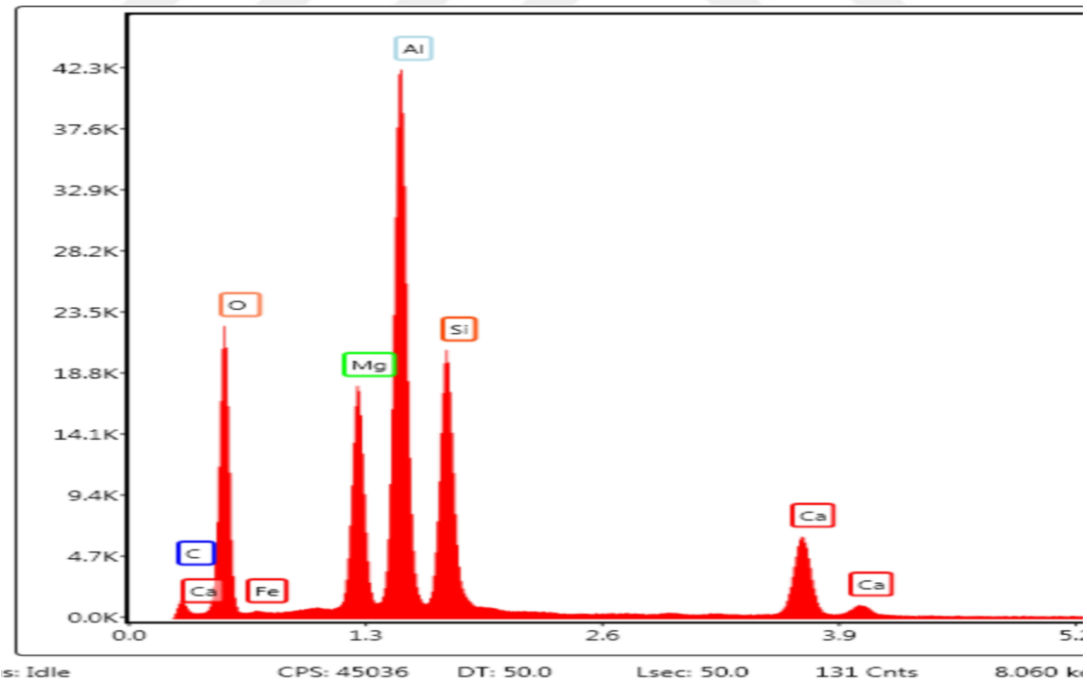

Figure A.19. EDS scans of point 2 experiment 8.

Table A.8. Concentration measurement experiment 8.

Measurement	O_2%	Al %	Mg%	Si%	Fe%
Point 1	1.74	65.36	0.77	7.52	10.94
Point 2	0.98	95.73	0.55	2.74	------ --

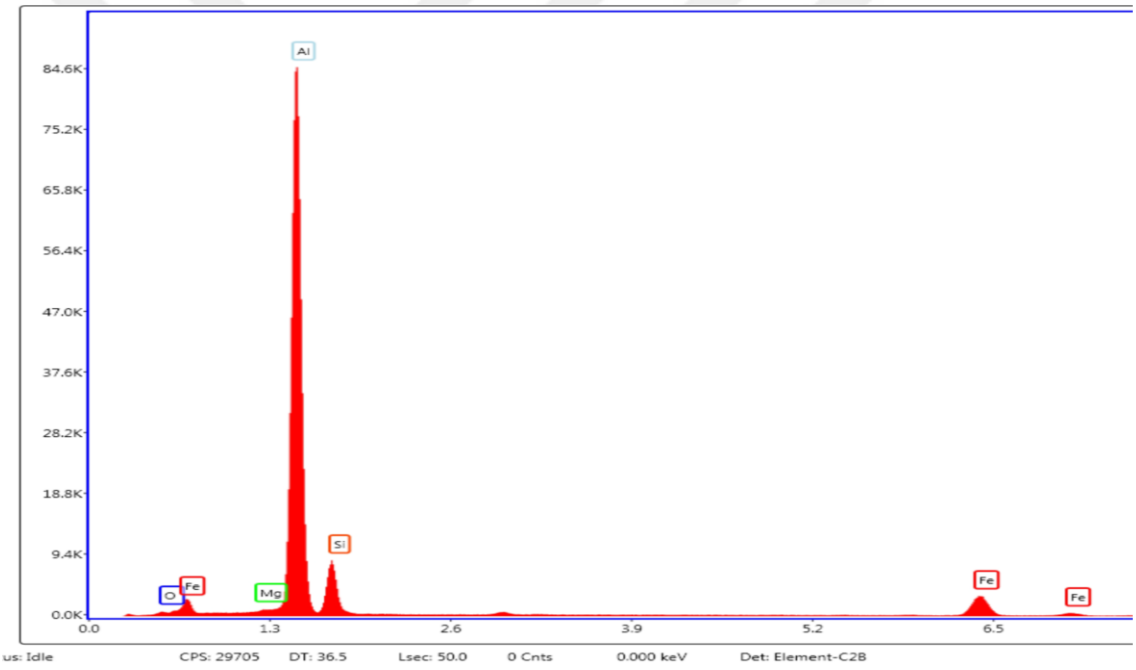

Figure A.20. EDS scans of point 1 experiment 10.

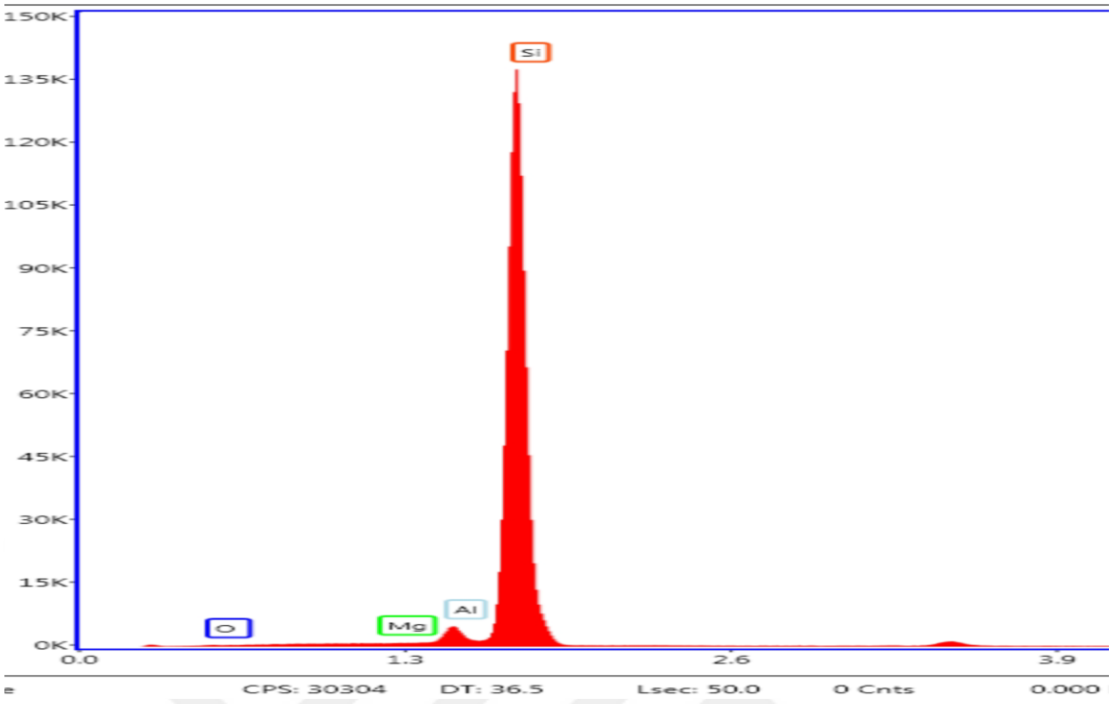

Figure A.21. EDS scans of point 2 experiment 10.

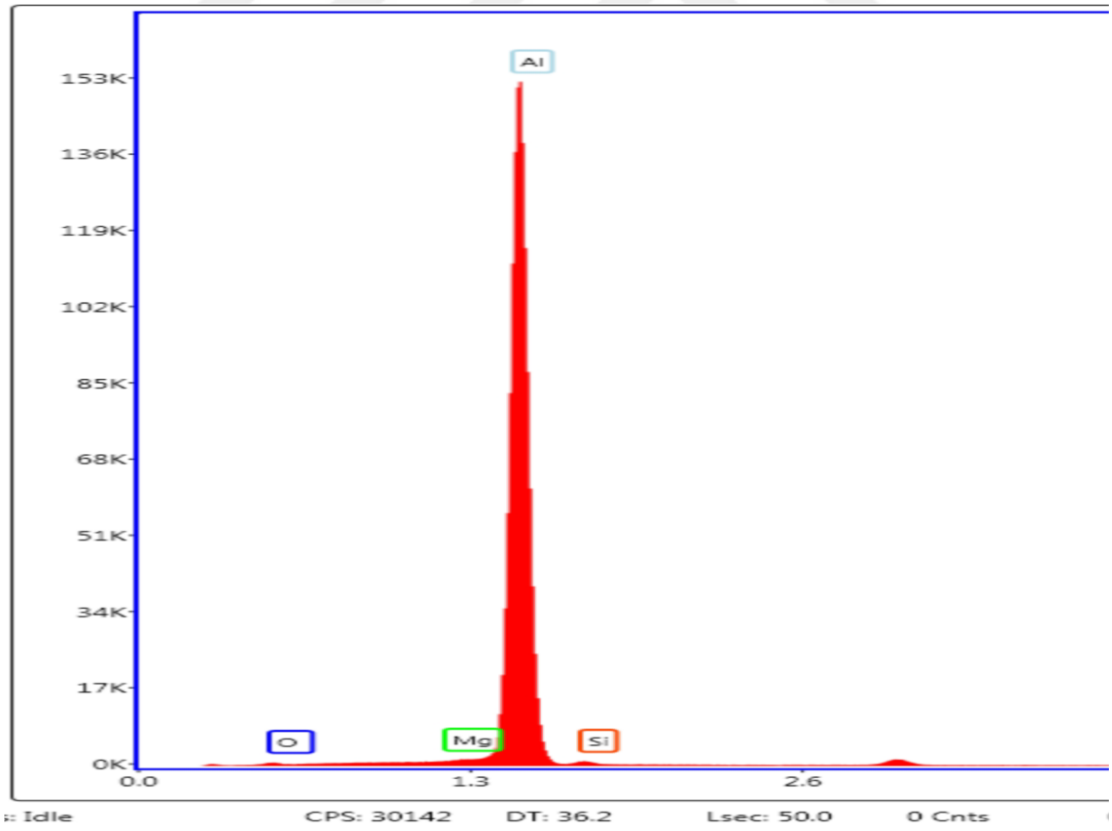

Figure A.22. EDS scans of point 3 experiment 10.

Table A.9. Concentration measurement experiment 10.

Measurement	O%	Al %	Mg%	Si%
POINT 1	0.03	69.67	0.35	14.28
POINT 2	0	2.9	0.03	97.07
POINT 3	0.11	96.83	0.84	2.22